POISSON-BOLTZMANN EQUATION WITH ELECTROSTATIC CORRELATION APPLIED TO EMULSIONS, ELECTROLYTE SOLUTIONS, AND IONIC LIQUIDS

Mirella Simões Santos

Tese de Doutorado apresentada ao Programa de Pós-graduação em Engenharia Química, COPPE, da Universidade Federal do Rio de Janeiro, como parte dos requisitos necessários à obtenção do título de Doutor em Engenharia Química.

Orientadores: Frederico Wanderley Tavares
Evaristo Chalbaud Biscaia Jr.

Rio de Janeiro
Dezembro de 2016

POISSON-BOLTZMANN EQUATION WITH ELECTROSTATIC CORRELATION APPLIED TO EMULSIONS, ELECTROLYTE SOLUTIONS, AND IONIC LIQUIDS

Mirella Simões Santos

TESE SUBMETIDA AO CORPO DOCENTE DO INSTITUTO ALBERTO LUIZ COIMBRA DE PÓS-GRADUAÇÃO E PESQUISA DE ENGENHARIA (COPPE) DA UNIVERSIDADE FEDERAL DO RIO DE JANEIRO COMO PARTE DOS REQUISITOS NECESSÁRIOS PARA A OBTENÇÃO DO GRAU DE DOUTOR EM CIÊNCIAS EM ENGENHARIA QUÍMICA.

Examinada por:

_____
Prof. Frederico Wanderley Tavares, D.Sc.

_____
Prof. Eduardo Rocha de Almeida Lima, D.Sc.

_____
Prof. Márcio Luis Lyra Paredes, D.Sc.

_____
Profª. Helen Conceição Ferraz, D.Sc.

_____
Prof. Amaro Gomes Barreto Jr., D.Sc.

RIO DE JANEIRO, RJ - BRASIL
DEZEMBRO DE 2016

Santos, Mirella Simões

Poisson-Boltzmann Equation with Electrostatic Correlation Applied to Emulsions, Electrolyte Solutions, and Ionic Liquids/ Mirella Simões Santos. – Rio de Janeiro: UFRJ/COPPE, 2016.

XVI, 154 p.: il.; 29,7 cm.

Orientadores: Frederico Wanderley Tavares

Evaristo Chalbaud Biscaia Jr.

Tese (doutorado) – UFRJ/ COPPE/ Programa de Engenharia Química, 2016.

Referências Bibliográficas: p. 16-21, 48-51, 74-76, 91-95.

1. Poisson-Boltzmann. 2. Emulsões. 3. Líquidos iônicos. I. Tavares, Frederico Wanderley *et al*. II. Universidade Federal do Rio de Janeiro, COPPE, Programa de Engenharia Química. III. Título.

To my parents and my brother,

with gratitude.

Acknowledgments

First of all, I would like to thank my beloved family for always encouraging me to follow my dreams regardless of how big they are. Thank you for giving me strength and motivating me in times of need, and also thanks for cheering me in every little victory in my life. Every accomplishment I have will always be dedicated to you all mom, dad, and brother. To my dear family Farina thank you for all the love my family got from you since the beginning.

Throughout my entire life I have had always encountered so many inspirational teachers and professors that made me admire this profession so much, and discover in myself the desire to be a part of that. My dear teachers Marister, Tânia, Cleiva, Mariângela, and Ana Laura, I am very thankful for everything I learned with you and for always inspiring me with your passion for spreading knowledge. My professor Renato for his engagement in science and my dear Prof. Walter for showing me that we always have to fight for a better world.

I am very thankful to have had the honor of being advised by these two great professors: Fred and Evaristo. I admire you both so much and I will carry all your valuable teachings through my entire professional and personal life. Your passion for science and spreading knowledge drives me and inspires me. I also would like to thank Prof. Bazant for receiving me in his research group at MIT. It was a pleasure to work with such a great group where I learned so much. I also would like to thanks Rahul for all our valuable discussions that contributed to the development of this thesis.

Throughout these four years, I also had the opportunity of meeting amazing people that had impacted my life in beautiful ways. My dear David for supporting me every day, with words of encouragement and care, and for making me happy in any skies, I thank you with all my heart. My great friend Marcela, thank you for being by my side since the very beginning of this thesis and for always being the sensate voice I need to hear. My dear friends Diana and Javier (and Sarinha) thank you for being my family away from home; you have a special place in my heart. Angela I thank you for the companionship in the easy and in the hard moments of life.

I cannot thank enough my long-time friends, Bruno, Carla, Tomás, Ellem, and Karine for our beautiful friendship and for always believing in me, and for always being there for me no matter how much time passes or where we were living. I also would like to thank my great friends and colleagues from G-130, who throughout the years brought joy and knowledge to my life. Thanks for the laughs, for the music, and for the serious talks; you all made that green lab always very welcoming. A special thanks to my friends from ATOMS. I am proud to be a part of such an amazing research group! Last but not least, I would like to thank Pedro Alijó who helped me and contributed to this work from the earliest stages. I am very thankful for your patience, promptness, and kindness for helping me even with the most fundamental questions.

Finally, I would like to thank the Brazilian agencies CNPq and CAPES for the financial support that made possible the elaboration of this work. Specifically, I would like to thank the Brazilian government that promoted the program Science Without Borders which made it possible for me to develop part of my doctoral research at MIT.

Resumo da Tese apresentada à COPPE/UFRJ como parte dos requisitos necessários para a obtenção do grau de Doutor em Ciências (D.Sc.)

EQUAÇÃO DE POISSON-BOLTZMANN COM CORRELAÇÃO ELETROSTÁTICA APLICADA A EMULSÕES, SOLUÇÕES ELETROLÍTICAS E LÍQUIDOS IÔNICOS

Mirella Simões Santos

Dezembro/2016

Orientadores: Frederico Wanderley Tavares
Evaristo Chalbaud Biscaia Jr.

Programa: Engenharia Química

Eletrólitos possuem papel fundamental em incontáveis processos e sistemas. Estão presentes em processos biológicos, na indústria do petróleo, no desenvolvimento de fármacos, entre outros. Apesar do grande esforço científico em melhorar a descrição do comportamento de eletrólitos, ainda existem desafios de ter uma boa descrição de propriedades de soluções de eletrólitos muito concentrados e/ou multivalentes e, principalmente, para os casos em que temos somente eletrólitos sem solventes como, por exemplo, líquidos iônicos e sais fundidos nos quais a modelagem é ainda mais complexa e os modelos existentes são incompletos e inadequados. Para esses casos, propõe-se incluir correlações iônicas eletrostáticas, não consideradas na equação de Poisson-Boltzmann original. Neste trabalho usamos uma modificação da equação de Poisson-Boltzmann com correlações eletrostáticas para descrever a micelização de surfactantes iônicos e zwitteriônicos, descrever a capacitância diferencial de líquidos iônicos e, também, a sua impedância eletroquímica. A abordagem proposta se mostrou capaz de predizer o comportamento observado experimentalmente e em simulações moleculares para sistemas em que correlações eletrostáticas são relevantes.

Abstract of Thesis presented to COPPE/UFRJ as a partial fulfillment of the requirements for the degree of Doctor of Science (D.Sc.)

POISSON-BOLTZMANN EQUATION WITH ELECTROSTATIC CORRELATION APPLIED TO EMULSIONS, ELECTROLYTE SOLUTIONS, AND IONIC LIQUIDS

Mirella Simões Santos

December/2016

Advisors: Frederico Wanderley Tavares
Evaristo Chalbaud Biscaia Jr.

Department: Chemical Engineering

Electrolytes play a major role in countless processes and systems. They are present in biological processes, in the petrochemical industry, and in the development of pharmaceutical products, among others. Although there has been a large scientific effort to better describe electrolytes, there are still challenges in describing properties of highly concentrated and/or multivalent electrolyte solutions. For electrolytes without solvents, *e.g.*, ionic liquids and molten salts, modeling is even more complex and the currently existing models are incomplete or inaccurate. Here, we used a modified Poisson-Boltzmann equation which takes into account ionic electrostatic correlations to describe the micellization phenomena of ionic and zwitterionic surfactants, in order to describe the differential capacitance of ionic liquids and their electrochemical impedance. The proposed approach has shown to be able to predict very well the behavior of those systems observed experimentally and in molecular simulations.

Content

Figures Index

Tables Index

Chapter 1: Introduction

1.1 Electrolytes and their behavior

Electrolytes play a major role in several fields, from biological systems to pharmaceutical products and to petrochemical processes. Even though there has been a large advance in the development of experiments and technologies in these areas, the theoretical description of biological, pharmaceutical, and petrochemical systems still needs more clarification regarding their physical and chemical nature and behavior. The search for a satisfactory theoretical approach is driven by the need of models that can be used as a tool for the development for new processes and products.

Inorganic salts are known to affect the stability of proteins, to influence the interactions between colloidal particles, and also to affect the aggregation between amphiphilic molecules such as surfactants (where the aggregates are known as micelles) (Goldsipe and Blankschtein, 2005). The influence of electrolytes in colloidal systems is due to the fact that, over charged surfaces, the binding and approximation of dissociated ions changes repulsive electrostatic forces. Furthermore, in systems where the adsorption of dissociated ions controls their charges, these ions are responsible for the interactions between colloidal particles (Leontidis *et al*., 2014).

Our attention now is not only focused on the development of theories for inorganic salts in aqueous solutions, but also on improving the description of ionic liquids, which can be seen as electrolyte solutions without the presence of a solvent. Ionic liquids have been the focus of numerous research efforts due to their unique electrochemical characteristics. They can be applied to supercapacitors, solar cells, batteries, membrane separation systems but until now there has been no simple theory able to describe their unique electrochemical behavior.

Most developments in describing electrolytes are now concentrated on the use of molecular and atomistic simulations, which are essential for the understanding of microscopic phenomena involved in systems containing electrolytes. Unfortunately, these approaches demand a very high computational cost and are time consuming, which make them unsuitable to model multiscale systems of complex processes. This

fact motivates us in improving mean field approaches like modified Poisson-Boltzmann equations, which encompass the fundamental effects on the interactions between charged surfaces and electrolytes, but at the same time require low computational cost and can be used to calculate properties in different scales and to describe much more complex processes.

Previous works performed in the research groups ATOMS (Applied Thermodynamics and Molecular Simulation) and LMSCP (Laboratory of Modeling, Simulation, and Process Control) of the Chemical Engineering program of COPPE – UFRJ (Moreira et al., 2007; Lima et al., 2007; Alijó et al. 2012; Alijó et al., 2015) verified the need to include modifications on the Poisson-Boltzmann equation, for a better description of electrochemical systems containing electrolytes. The recent boom in the research of micro-electromechanical devices and the tendency to miniaturize processes and systems make the improvement of electrochemical theories even more important.

1.2 Objectives

The main goal of this work is to improve the description of electrolyte systems by a modified Poisson-Boltzmann equation which takes into account effects of ionic electrostatic correlations. We apply this approach to the description of the micellization phenomena of ionic and zwitterionic surfactants, ionic liquids between charged electrodes (under alternating and continuous currents), and electrolyte solutions. For all these systems we validate the proposed approach by comparing the results obtained by the proposed model with experimental observations and data, as well as molecular simulation, and density functional theory data.

1.3 Thesis organization

This thesis is divided into six chapters and five appendixes. Chapter II presents a brief literature review of the systems studied in this work and the traditional approaches used to describe electrostatic interactions. The following chapters are each separated by the description of different systems, and are structured as individual scientific articles. Chapter III contains the proposed approach to describe the micellization phenomena of ionic and zwitterionic surfactants, where we compare our results to critical micelle

concentration and ionic binding experimental data. Chapter IV presents the application of the modified Poisson-Boltzmann equation to the description of the differential capacitance of ionic liquids. In this chapter we also propose an approach to consider the asymmetry in shape and size of ionic liquids. The model is validated by its comparison with experimental data and with molecular and DFT simulation results obtained from literature. Chapter V presents the development of an analytical expression for the description of the electrochemical impedance of electrolytes (both ionic liquids and solutions of electrolytes). This approach is able to predict the behavior of the impedance curve and explains the impact of electrostatic correlations in alternating current systems. Finally, Chapter VI lists the final remarks of this thesis and suggestions of future works and developments. There are also five appendices in this work. Appendix A presents the article "Molecular Thermodynamics of Micellization: Micelle Size Distributions and Geometry Transitions" published in the Brazilian Journal of Chemical Engineering. Appendix B presents the numerical and optimization approach for obtaining the critical micelle concentration when using the molecular thermodynamics approach. Appendix C presents the dynamics of electrolyte solutions considering ion size asymmetry and electrostatic correlation effects. Appendix D presents a numerical approach developed for solving the modified Poisson-Boltzmann equation with electrostatic correlation effects in bispherical coordinate systems. Finally, Appendix E reports an application of the modified Poisson-Boltzmann equation to predict the adsorption of proteins on different supports as a function of temperature, salt concentration, salt type, and pH.

Chapter 2: Literature Review

2.1 Electrical Double Layer

The behavior of electrolytes close to charged surfaces is a function of different forces. Mostly these forces are of short or long range, and their combined effects result in important consequences on the properties of colloidal solutions and electrochemical systems. The understanding of all the forces acting in these systems is crucial for a complete understanding of the behavior of electrolytes. For example, if van der Waals forces (which are attractive forces) were the only ones acting, we would expect that all particles – dispersed in solution and at low temperature – would agglomerate. However, as we know, that is not what usually happens because there are opposing forces also acting. One main opposing force, for example, is the one that arises due to the fact that any particle dispersed in water (or other liquid of large dielectric constant) can develop a charged surface, leading to the rise of electrostatic repulsion forces (Israelachvili, 1995).

Any charged surface in contact with electrolyte solutions will have its charge balanced by a region of ions of opposed charge (counterions). Some ions (either counterions or coions) are bounded to the charged surface, and this region is known as the Stern layer. In the mean field behavior, other ions present fast thermal movement, known as the diffuse layer. Figure 1 is an example of the organization of the electrical double layer close to a negatively charged surface.

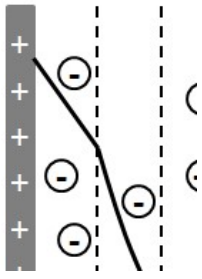

Figure 1 – Representation of the electrical double layer close to a positively charged surface.

The structure of the electrical double layer is a function not only of the charge or potential over the surface, but it is also intrinsically related to the nature of the ions (either in solution or as ionic liquids). Because of that, it is essential to consider the particularities of each electrolyte when we are modeling these kinds of systems. In the following sections we present a brief introduction of ionic specificity effects, steric effects and ionic electrostatic correlations and how they can be coupled to a mean-field approach by the use of the Poisson-Boltzmann equation.

2.2 Ionic Specificity Effects

Ionic specificity effects were first described at the end of the 19th century by the work of Hofmeister. This work described the effects of different salts in the solubility of albumin protein (Kunz *et al*., 2004). The observations from Hofmeister yielded the classification of ions according to their impact on a variety of biological and physicochemical systems, and it created a series, now known as the Hofmeister or lyotropic series. In Table 1 we present the Hofmeister series of cations and anions. However it is important to point out that this series might not always be followed (Bostrom *et al*., 2005), or, in some cases, it might be incomplete (especially due to the fact that most ions listed in the Hofmeister series are monovalent anions) (Leontidis *et al*., 2014). Ionic specificity effects have a major role in several applications. One important example is the chromatography separation of proteins, which is directly affected by the differences in solubility of different ions (Nfor *et al*., 2011; Lezin *et al*., 2011; Tavares *et al*., 2005). In this case, the ions are affected by both the hydrophobic and the electrostatic interactions in the medium. Also, Abezgauz *et al*. (2010) observed that when different salts are added to a surfactant (cetylpyridinium bromide) aqueous solution, the effect of the counterion on the critical micelle concentration and on the micelle growth follows the Hofmeister series.

Table 1 – Classical Hofmeister series of cations and anions

Anions	$F^- \; SO_4^{2-} > HPO_4^{2-} > acetate > Cl^- > NO_3^- > Br^- > ClO_3^- > I^- > ClO_4^- > SCN^-$
Cations	$NH_4^+ > K^+ > Na^+ > Li^+ > Mg^{2+} > Ca^{2+}$

It is important to emphasize that the effects of electrolytes on colloidal and electrochemical systems is not only a function of the kind of electrolyte used; it is also a

function of electrolyte concentration and the characteristics of the medium and of the charged surface. One important contribution to the free energy that arises at high electrolyte concentrations, high applied potential, or in ionic liquids, is that of the electrostatic correlation. In these systems, one ion affects the behavior of other ions in its surroundings in a nonlinear way. Furthermore, due to spatial restrictions on the area of electrical double layer, there are steric effects that arise from the fact that each ion has a defined volume (free volume effect). These three terms of electrolyte free energy, ion specificity contributions, free volume and electrostatic correlations are described on Item 2.3.2 of this chapter.

2.3 Poisson-Boltzmann Equation

As discussed in Item 2.1, ions close to a charged surface are rearranged, with ions of opposite charge (counterions) being attracted, and the ones with the same charge as the surface (coions) being repelled. The distribution of these ions can be described by the Boltzmann distribution and it is a function of the electric potential and the temperature. The Boltzmann distribution can be expressed in terms of concentration in the following form:

$$c_i = c_{i,\infty} \exp\left(-\frac{z_i e \psi}{kT}\right) \tag{2.1}$$

where c_i is the concentration of ion i, $c_{i,\infty}$ the concentration of ion i in the bulk, z_i the valence of species i, e the elementary charge of the electron, ψ the electrostatic potential, k the Boltzmann constant, and T the temperature.

The Poisson equation is an elliptical partial differential equation, and it can be used to describe the behavior of the electrostatic potential (ψ). It is a function of the volumetric charge density (ρ), and can be written as follows:

$$\varepsilon_0 \nabla(\varepsilon \nabla \psi) = -\rho \tag{2.2}$$

where ε_0 is the vacuum electric permittivity, and ε is the dielectric constant of the medium.

The volumetric charge density ($\rho = e\sum_i z_i\, c_i$) can now be coupled with the Boltzmann distribution, and then inserted in the Poisson equation, resulting in the Poisson-Boltzmann equation.

$$\varepsilon_0 \nabla(\varepsilon \nabla\psi) = -e\sum_i z_i\, c_{i,\infty} \exp\left(-\frac{z_i e\psi}{kT}\right) \tag{2.3}$$

This equation characterizes a boundary value problem, which requires two boundary conditions. These boundary conditions can be of three kinds: specified electric potential at the surface, specified charge density at the surface, and of charge regulation.

For specified electric potential at the surface:

$$\psi|_{surf} = \psi_0 \tag{2.4}$$

For specified charge density (γ) at the surface:

$$\varepsilon(\nabla\psi)|_{surf} = -\frac{\gamma}{\varepsilon_0} \tag{2.5}$$

Charge regulation boundary condition is used when the charged surface has ionizable groups, which makes the resulting charge of this surface a function of the conditions of the medium, such as pH, and temperature. Ninham and Parsegian (1971) presented a charge regulation model where the influence of pH on the surface charge is considered. In this approach, the boundary condition on the surface is:

$$\varepsilon(\nabla\psi)|_{surf} = \frac{4\pi e\alpha}{\varepsilon_0} \tag{2.6}$$

where α is the fraction of ionizable groups on the surface. This parameter is obtained from the dissociation constant of the groups on the surface (Z) and the concentration of H^+ ions (H^+):

$$Z = \frac{[H^+]_S[A^-]}{[AH]} = [H^+]_S \frac{\alpha}{1-\alpha} \tag{2.7}$$

and from the concentration of hydrogen in the solution:

$$[H^+]_S = H \exp\left(-\frac{e\psi}{kT}\right) \tag{2.8}$$

This kind of boundary condition is widely used for modeling interactions between proteins. Examples of its application can be found in the works of Boström *et al*. (2005), Lima *et al*. (2008), Deniz and Parsons (2013), and in the work presented in Appendix E.

When we are modeling only one charged surface in an electrolyte solution we also consider that the electrostatic potential in the bulk tends to zero.

$$\psi|_{bulk} = 0 \tag{2.9}$$

The Poisson-Boltzmann equation in its classical form considers that the ions are punctual charges, no excluded volumes are taken into account. Furthermore, no van der Waals (dispersion) interactions between ions and surface are included. Because of that, the classical Poisson-Boltzmann equation is only able to describe well the behavior of diluted electrolyte solutions, and monovalent electrolytes. This leaded to the development of modifications of the Poisson-Boltzmann equation in order to have a better description of a larger spectrum of electrolytes systems. Item 2.3.1 of this chapter presents several modifications on the Poisson-Boltzmann equation that make it more suitable to describe concentrated electrolyte solutions, multivalent electrolytes, and ionic liquids.

2.3.1 Modifications of the Poisson-Boltzmann approach

As mentioned before, approaches which describe ions as punctual charges that neglect free volume effects tend to fail at high concentrations, high voltages, or due to electrostatic correlation interactions. This is an indication that those effects should not be ignored. There are modifications on the Poisson-Boltzmann equation that aim to describe several physical observations such as dielectric relaxation, electrostatic ionic correlation, and ionic volume restrictions. In the group of Applied Thermodynamics and Molecular Simulation (ATOMS) there was a series of works carried out in order to improve the Poisson-Boltzmann equation. First, Moreira *et al*. (2007) considered dispersion interaction ion-colloid and colloid-surface. Lima *et al*. (2007) extended the approach proposed by Moreira by taking into account the shape of proteins, which resulted on a very effective approach to describe the interactions between proteins

immersed on different electrolytes solutions. Later, Alijó *et al*. (2012) considered ionic size exclusion effects on aqueous solutions, which showed to be especially relevant for the high electrolyte concentrations. Afterwards, Alijó *et al*. (2015) also considered electrostatic correlations and their effect on dynamic behavior. All these works represent a great contribution for the description of the behavior of electrolytes in aqueous solutions but still there are gaps to be filled, especially regarding the description of ionic liquids and concentrated electrolyte solutions.

The next sections in this chapter describe how the effects of dispersion, ionic sizes and electrostatic correlations can be included in the Poisson-Boltzmann equation.

Effects of dispersion and polarizability of ions

On an aqueous electrolyte solution, the mean field potential close to a charged surface is affected not only by the size and charge of the ion but also by its polarizability. Traditional models cannot explain why salts with the same valence and size impact in such a diverse manner in protein and colloidal systems (Tavares *et al*., 2004). Ninham and collaborators emphasized in their works that some behaviors caused by the ionic specificity can be described theoretically by the inclusion of ion-ion and ion-macroion dispersion forces (Boström *et al.* (2005), Moreira *et al.* (2006), Moreira *et al.* (2007), Mitchell *et al.* (1975), Fortini *et al.* (2004)).

The equivalence between electrostatic and dispersion forces is defined by taking the potential of interaction between an ion i and a surface (Lukanov and Firoozabadi, 2014):

$$U = U_i^{electrostatic} + U_i^{dispersion} \tag{2.10}$$

The electrostatic contribution is defined as $U_i^{electrostatic} = z_i e\psi$ and the dispersion energy of an ion at a distance r of a charged surface can be obtained using the Lifshitz theory as follows:

$$U_i^{dispersion} = -\frac{B_i}{r^3} h_i(r) \tag{2.11}$$

The term $h_i(r)$ is a factor of shape and it considers that the ions have a finite size. This factor can be defined as (Lukanov and Firoozabadi, 2014):

$$h_i(r) = 1 + \frac{2r}{\sqrt{\pi}a_i}\left[\frac{2r^2}{a_i^2} - 1\right]\exp\left(-\frac{r^2}{a_i^2}\right) - \left[1 + \frac{4r^4}{a_i^4}\right]\mathrm{erfc}\left(\frac{r}{a_i}\right) \quad (2.12)$$

Where a_i is the Gaussian radius of the ion. The values of this radius can be found in Parsons and Ninham (2009).

The dispersion coefficient (B_i) can be obtained by the dynamic polarizability of the ions and it includes dipolar contributions of all electromagnetic frequencies. This coefficient can be positive (repulsion) or negative (attraction) and it is a function of the polarizability at different frequencies of the solvent, the surface and the ionic specimens. How to obtain the dispersion coefficient is well described elsewhere, *e.g.*, Lukanov and Firoozabadi (2014), Tavares *et al*. (2004) and Boström *et al*. (2002).

Inclusion of the effects of ionic sizes

Bikermann (1942) is widely known as a pioneer to consider steric effects between ions. His approach was one of the first to treat ions as hard bodies with a delimited volume. However, in a review paper by Bazant *et al*. (2009) it is revealed that a description of steric effects – very similar to the one presented by Bikermann (1942) - was previously presented on the remarkable work of Stern (1924). In that work, Stern introduces the concept of a compact layer of molecules, which is a monomolecular layer that separates the electrode and the electrolytes diffuse layer. In that article Stern also considered the volume of the ions on the electrolyte phase, and the expression he obtained for the ratio between charge and voltage is very similar to the one obtained by Bikermann (1942) twenty years later.

In Bikermann's work, the first modification of the Poisson-Boltzmann equation was obtained, and the expression for the residual chemical potential of an ion i is:

$$\frac{\mu_i^{res,Bik}}{kT} = -\ln(1-\phi) \quad (2.13)$$

where $\phi = \sum_i c_i\sigma_i^3$ the volume fraction occupied by the ions with diameter σ and concentration c_i. Even though this approach was an important step on the improvement of the Poisson-Boltzmann equation, it has some limitations, such as, for example, the

fact that both anion and cation must have the same size. We can find a large number of works that obtained a good description of physical and biological systems, for example electrolyte solutions with large ions or large biological molecules, (Wiegel and Strating (2007), Boeukhov and Andelman (1997)), polyelectrolytes (Biesheuvel (2004), Israels (1994), González-Amezcua and Hernándes-Contreras (2004)), polymeric electrolytes (Van Soestbergen and Biesheuvel (2008)), electrophoreses of colloidal particles (López-Garca *et al.* (2007)), among others.

Carnahan-Starling (CS) equation of state for liquids consisting of monodisperse hard spheres can also be used to describe steric effects of electrolyte solutions. The residual chemical potential obtained with this methodology is presented below (Carnahan and Starling, 1969):

$$\frac{\mu_i^{res,CS}}{kT} = \frac{\phi(8 - 9\phi + 3\phi^2)}{(1-\phi)^3} \tag{2.14}$$

Even though the Bikermann and Carnahan-Starling models are able to give important information on free volume of different electrolyte solutions, there are several systems where the asymmetry on the size of electrolytes can't be neglected. One way to consider the asymmetry of ion sizes was presented by Alijó *et al*. (2012) where they used the Boublik-Mansoori-Carnahan-Starling-Leland (BMCSL) equation of state, and obtained the following residual chemical potential for an ion i:

$$\begin{aligned}\frac{\mu_i^{res,BMCSL}}{k_B T} = &\frac{\left(\xi_0 - \frac{\xi_2^3}{\xi_3^2}\right)\sigma_i^3 + 3\xi_2\sigma_i + 3\xi_1\sigma_i}{1-\xi_3} + \frac{2\xi_2^3\sigma_i^3}{\xi_3(1-\xi_3)^3} \\ &+ \frac{3\xi_1\xi_2\sigma_i^3 + \frac{3\xi_2^2\sigma_i^2}{\xi_3} + \frac{3\xi_2^3\sigma_i^3}{\xi_3^2}}{(1-\xi_3^2)} \\ &+ \left(-1 + \frac{3\xi_2^2\sigma_i^2}{\xi_3^2} + \frac{2\xi_2^3\sigma_i^3}{\xi_3^2}\right)\ln(1-\xi_3)\end{aligned} \tag{2.15}$$

where $\xi_n = \frac{\pi}{6}\sum_i c_i\sigma_i^n$, $n = 1 \text{ or } 2, \text{and } \xi_3 = \frac{\pi}{6}\phi$ is the packing fraction. This approach has the advantage of treating different ions with different sizes, but it also presents large deviations when modeling one-dimensional systems, making it still necessary for more improvements on the description of asymmetric electrolytes.

All the approaches presented here take into account the specific ion diameter. It is important to notice that the solvated diameter is not directly related to its atomic radius. For example, the diameter of an ion can depend on the solvent due to its degree of solvation (Bazant et al., 2009). Data of specific diameter of solvated ions can be found in the work of Nightingale Jr. (1959).

Ionic Electrostatic correlations: Bazant-Storey-Kornyshev model (BSK model)

Electrostatic correlation effects are relevant and cannot be neglected on a wide variety of systems, *e.g.,* concentrated electrolyte solutions, solutions containing multivalent ions (which are especially important for biological systems), and ionic liquids. Storey and Bazant (2012) observed that when electrodes are placed directly in contact with a fluid, very high charges on the surface are observed, which are not predicted by the classical theories. Besides that, classical theories cannot describe ionic liquids and molten salts.

Effects of ionic electrostatic correlations can lead to overscreening, which consists of the first layer of ions close to the charged surface being formed in a way that it has an excess countercharge in relation to the surface, then the net charge difference would lead to the formation of another layer of ions in order to balance this difference, and thus successively until neutrality is obtained. Aiming to develop a simple and phenomenological theory that is able to take into account electrostatic correlations, Bazant *et al*. (2011) proposed the following functional to describe the Gibbs energy of the system:

$$G = \int dr \left\{ g + \rho\psi - \frac{\varepsilon}{2}\left[|\nabla\psi|^2 + l_c^2(\nabla^2\psi)^2\right] \right\} + \oint dr q_s \psi \qquad (2.16)$$

where g is the enthalpy density which is a function of the ions concentration, ρ is the charge density in the volume V, q_s is the superficial charge density on a metallic surface S, and ψ is the mean field electrostatic potential. The self-energy of the electric field is $-(\varepsilon/2)|\nabla\psi|^2$.

The modification proposed by Bazant *et al*. (2011) was to include a potential gradient term:

$$-\frac{\varepsilon}{2} l_c^2 (\nabla^2 \psi)^2 \tag{2.17}$$

where l_c is the electrostatic correlation length. Bazant and collaborators comment that the electrostatic correlation length for punctual charges is around the Bjerrum length, $l_B = (ze)^2/4\pi\varepsilon kT$. For ionic liquids, their dielectric constants make the Bjerrum length several times longer than the ion diameter, and for these cases, it is assumed that the correlation length, l_c, is equal to the diameter of the ion. This last suggestion is also recommended by the work of Alijó *et al*. (2015).

The modified Poisson equation is known as the Bazant-Storey-Kornyshev modification, or simply the BSK model.

$$\varepsilon(l_c^2 \nabla^2 - 1)\nabla^2 \psi = \rho \tag{2.18}$$

In this approach, it is considered that the medium permissivity ($\hat{\varepsilon}$), due to the electrostatic correlations, is a linear differential operator $\hat{\varepsilon} = \varepsilon(1 - l_c^2 \nabla^2)$. The equation returns to the Poisson equation when the electrostatic correlation length is equal to zero.

The BSK equation is a fourth order differential equation, and for that, it demands four boundary conditions. The first two are the same used for the classical Poisson equation, for which the surface can be of specified charge, specified potential, or charge regulation. The extra boundary conditions arise from the consideration that there are no correlation effects over the charged surface, then:

$$\hat{n}\nabla(\nabla^2 \psi)|_{surf} = 0 \tag{2.19}$$

This equation is able to predict overscreening and overcharging due to short range correlations. Bazant *et al.* (2010) applied this approach to charged electrodes and was able to reproduce data obtained by molecular dynamics simulation for multivalent salts.

2.4 Ionic Liquids

Even though the theoretical description of aqueous dilute electrolyte solutions has been thoroughly developed, there are still a lot of gaps in the description of multivalent ions and ionic liquids and their unique behavior. Furthermore, the properties of the electrical double layer of ionic liquids are extremely relevant for the

understanding and description of systems of energy storage, such as, for example, batteries, supercapacitors, solar cells, and electroactuators (Ujjain *et al*., 2015; Bettini *et al*., 2015; Cowell *et al*., 2015; Appetecchi *et al*., 2011; Nakamoto *et al*., 2013; Kakibe *et al*., 2012). Ionic liquids are also used as solvents for organic systems, as well as extraction liquids (Kornyshev, 2007; Ferreira et al., 2016; Soares *et al*., 2016). The wide range of applications of ionic liquids is due to their very particular properties, such as their high charge density, electrochemical stability, and very low volatility. Furthermore, ionic liquids can be seen as electrolyte solutions without solvent, which is very convenient when aiming to reduce the size of electrochemical devices. Another important characteristic is that ionic liquids can be combined in order to achieve desired and specific properties. In this case, a simple model that can easily predict the behavior of ionic liquids would be a key tool on the design of new ionic liquids and different applications.

The efforts to model ionic liquids have been mostly carried out by molecular simulations (Fedorov and Kornyshev, 2008; Vatamanu *et al*., 2010; Kirchner *et al*., 2013). Most of these works have focused on understanding the behavior of the electrical double layer of ionic liquids close to charged surfaces. One feature observed by several works was that the overscreening effect observed in ionic liquids was related to the short-range ionic correlation interactions. They observed that the length of the tail of the ions might act as a solvent, which could explain some few similarities of the behavior of ionic liquids and diluted electrolyte solutions (Henderson *et al*., 2013; Gebbie *et al*., 2013).

Even though several relevant observations on the behavior of ionic liquids close to charged surfaces were obtained through molecular dynamics, its high computational cost limits its use on the description of those systems. Because of that, the mean-field theory with modified Poisson-Boltzmann equations is promising to adequately describe ionic liquids with low computational cost – so it can be employed to describe complex processes where ionic liquids are important. On the Chapters 4 and 5 a modified Poisson-Boltzmann equation is proposed to describe differential capacitance and the electrochemical impedance of ionic liquids.

2.5 Surfactant Systems

The aggregation of surfactants is extremely relevant to several chemical and biological processes. When salts are present in surfactant solutions, the formation of surfactant aggregates (known as micelles) is drastically changed by the specific kind of salt used (Lukanov and Firoozabadi, 2014). Ionic and zwitterionic surfactants are widely used in industry on detergents, pharmaceutical and personal care products, coating and lubrication, among others. The increase of the ionic strength on surfactant solutions reduces the critical micelle concentration (CMC) of ionic and zwitterionic surfactants, and also leads to larger micelles being formed and can cause their shape transition – from smaller and spherical micelles to larger and elongated ones. This effect is associated with the reduction of the electrostatic repulsion between the surfactant heads. Because of that, the addition of salts into surfactant solutions is subject of several experimental studies, important for their commercial application. It is experimentally observed that the micellar properties are not only influenced by the concentration of salt added but also and mostly by the specific kind of counterion (Srinivasan and Blankschtein, 2003).

Multivalent counterions, such as Al^{3+} and Ca^{2+}, are known for being much better micelle growth promoters than monovalent ions at the same ionic strength. For that, the development of a theory that can correctly predict the behavior of surfactant solutions with multivalent ions is of great interest for the selection of surfactant and salts to be applied to a certain process. Besides that, this theory must be able to predict properties of the micellization process that can be directly related to practical properties of surfactant solutions, such as solubility capacity and rheological behavior. This would reduce the time and cost of the trial and error experimentation processes.

In the literature, there are no models for the micellization phenomena that include electrostatic correlation effects, even though these effects are very important when describing multivalent counterion type and solutions with multivalent electrolyte and/or high concentrated electrolyte solutions. In this thesis, Chapter 3 presents the inclusion of electrostatic correlation effects on the micellization phenomena for solutions of both ionic and zwitterionic surfactants that contain monovalent and multivalent ions.

References

[1] Goldsipe, A., Blankschtein, D., (2005) Modeling counterion binding in ionic-nonionic and ionic-zwitterionic binary surfactant mixtures. *Langmuir*, *21*, 9850–9865.

[2] Leontidis, E. *et al*. (2014) The ion-lipid battle for hydration water and interfacial sites at soft-matter interfaces. *Current Opinion in Colloid & Interface Science*, *19*, (1), 2–8.

[3] Israelachvili, J., 1995, *Intermolecular and Surface Forces*, San Diego, Academic Press, Inc.

[4] Hiemenz, P.C., *Principles of Colloid and Surface Chemistry*, Marcel Dekker, New York, 1977.

[5] Kunz, W., Henle, J., Ninham, B. W. (2004) Zur Lehre von der Wirkung der Salze" (about the science of the effect of salts): Franz Hofmeister's historical papers", *Current Opinion in Colloid & Interface Science*, *9* (1-2), 19–37.

[6] Boström, M., Tavares, F. W., Finet, S., Skouri-Panet, F., Tardieu, A., & Ninham, B. W. (2005). Why forces between proteins follow different Hofmeister series for pH above and below pI. *Biophysical Chemistry*, *117*(3), 217–24.

[7] Nfor, B. K., Hylkema, N. N., Wiedhaup, K. R., Verhaert, P. D. E. M., van der Wielen, L. A. M., & Ottens, M. (2011). High-throughput protein precipitation and hydrophobic interaction chromatography: Salt effects and thermodynamic interrelation. *Journal of Chromatography A*, *1218*(49), 8958–8973.

[8] Lezin, G., Kuehn, M. R., & Brunelli, L. (2011). Hofmeister series salts enhance purification of plasmid DNA by non-ionic detergents. *Biotechnology and Bioengineering*, *108*(8), 1872–1882.

[9] Tavares, F. W., Bratko, D., & Prausnitz, J. M. (2004). The role of salt–macroion van der Waals interactions in the colloid–colloid potential of mean force. *Current Opinion in Colloid & Interface Science*, *9*(1–2), 81–86.

[10] Abezgauz, L., Kuperkar, K., Hassan, P. A., Ramon, O., Bahadur, P., & Danino, D. (2010). Effect of Hofmeister anions on micellization and micellar growth of the surfactant cetylpyridinium chloride. *Journal of Colloid and Interface Science*, *342*(1), 83–92.

[11] Ninham, B. W., Parsegian, V. A., (1971) Electrostatic potential between surfaces bearing ionizable groups in ionic equilibrium with physiologic saline solution. *Journal of Theoretical Biology*, *31* (3), 405–28.

[12] Lima, E. R. A., Tavares, F. W., & Biscaia Jr., E. C. (2008). Ion-Specific Potential of Mean Force Between two Aqueous Proteins. In *18th European Symposium on Computer Aided Process Engineering*.

[13] Deniz, V., & Parsons, D. F. (2013) Effect of nonelectrostatic ion interactions on surface forces involving ion adsorption equilibria. Journal of Physical Chemistry C, 117 (32), 16416–16428.

[14] Moreira, L. A. *et al*. (2007) Effect of the Ion-Protein Dispersion Interactions on the Protein-Surface and Protein-Protein Interactions, *Journal of Brazilian Chemical Society*, *18* (1), 223–230.

[15] Lima, E. R. A. *et al*., (2007) Osmotic Second Virial Coefficients and Phase Diagrams for Aqueous Proteins from a Much-Improved Poisson-Boltzmann Equation. *Journal of Physical Chemistry C*, *111*, 16055-16059.

[16] Alijó, P. H. R., Tavares, F. W., & Jr., E. C. B. (2012). Double layer interaction between charged parallel plates using a modified Poisson–Boltzmann equation to include size effects and ion specificity. *Colloids and Surfaces A: Physicochemical and Engineering Aspects*, *412*, 29–35.

[17] Alijó, P. H. R., Tavares, F. W., Biscaia Jr., E. C., & Secchi, A. R. (2015). Effects of electrostatic correlations on ion dynamics in alternating current voltages. *Electrochimica Acta*, *152*, 84–92.

[18] Tavares, F. W. *et al*., (2004) Ion-Specific Effects in the Colloid-Colloid or Protein-Protein Potential of Mean Force: Role of Salt Macroion van der Waals Interactions. *Journal of Physical Chemistry B*, *108*, 9228-9235.

[19] Moreira, L. A., Boström, M., Ninham, B. W., Biscaia Jr., E. C., & Tavares, F. W. (2006). Hofmeister effects: Why protein charge, pH titration and protein precipitation depend on the choice of background salt solution. *Colloids and Surfaces A: Physicochemical and Engineering Aspects*, *282–283*, 457–463.

[20] Mitchell, D. J. *et al.* (1976) Theory of Self-Assembly of Hydrocarbon Amphiphiles into Micelles and Bilayers. *Journal of the Chemical Society, Faraday Transactions 2: Molecular and Chemical Physics*, 1525–1568.

[21] Fortini, M. *et al*. (2004) Specific anion effects on the aggregation properties of anionic nucleolipids. *Current Opinion in Colloid & Interface Science*, *9* (1-2), 168–172.

[22] Lukanov, B., Firoozabadi, A., (2014) Specific Ion Effects on the Self-Assembly of Ionic Surfactants : A Molecular Thermodynamic Theory of Micellization with Dispersion Forces. *Langmuir*, *30* (10), 6373-6383.

[23] Parsons, D. F., Ninham, B. W. (2009) Ab initio molar volumes and Gaussian radii. *Journal of Physical Chemistry A*, *113*, 6, 1141-1150.

[25] Bikerman, J. (1942) Electrokinetic equations for gels and the absolute magnitude of electrokinetic poteintials. *Journal of Physical Chemistry*, *46,*724

[26] Bazant, M. Z. *et al*. (2009) Towards an understanding of induced-charge electrokinetics at large applied voltages in concentrated solutions. *Advances in Colloid And Interface Science*, *152* (1-2), 48–88.

[27] Stern, O., (1924) Zur theorie der electrolytischen doppelschicht. Z *Elektrochem*, *30*, 508–516.

[28] Wiegel, F.W., Strating, P., (1993) Distribution of electrolytes with excluded volume around a charged DNA molecule. *Modern Physics Letter B,* 7, 483–490

[29] Borukhov, I., Andelman, D., Orland, H., (1997) Steric effects in electrolytes: a modified Poisson–Boltzmann approach. *Physics Review Letter*, *79*, 435–438.

[30] Biesheuvel, P. M., (2004) Ionizable polyelectrolyte brushes: brush height and electrosteric interaction. *Journal Colloid Interface Science*, *275*, 97–106.

[31] Israëls, R., (1994) On the theory of grafted weak polyacids. *Macromolecules*, *27*, 3087.

[32] González-Amezcua, O., Hernández-Contreras, M., (2004) Phase evolution of lamellar cationic lipid-dna complex: steric effect of an electrolyte. *Journal of Chemical Physics*, *121*, 10742.

[33] Van Soestbergen, M. *et al*., (2008) Modified Poisson–Nernst–Planck theory for ion transport in polymeric electrolytes. *Journal of Electrostatics*, *66*, 567–573.

[34] López-Garca, J. *et al*., (2007) Electrical double layer around a spherical colloid particle: the excluded volume effect. *Journal of Colloid Interface Science*, *316*, 196–201.

[35] Carnahan, N. F., Starling, K. E., (1969) Equation of State for Nonattracting Rigid Sheres. *Journal of Chemical Physics*, *51*, 635-636.

[36] Nightingale Jr., E. R. (1959). Phenomenological Theory of Ion Solvation. Effective Radii of Hydrated Ions. *The Journal of Physical Chemistry*, *63*, 1381–1387.

[37] Storey, B. D., & Bazant, M. Z. (2012). Effects of electrostatic correlations on electrokinetic phenomena. *Physical Review E*, *86*, 56303.

[38] Bazant, M. Z., Storey, B. D., & Kornyshev, A. A. (2011). Double Layer in Ionic Liquids : Overscreening versus Crowding. *Physical Review Letters*, *106*, 46102.

[39] Ujjain, S. K., Sahu, V., Sharma, R. K., & Singh, G. (2015). High performance all solid state, flexible supercapacitor based on ionic liquid functionalized grapheme. *Electrochimica Acta*, *157*, 245–251.

[40] Bettini, L. G., Piseri, P., Giorgio, F. De, Arbizzani, C., Milani, P., & Soavi, F. (2015). Flexible, ionic liquid-based micro-supercapacitor produced by supersonic cluster beam deposition. *Electrochimica Acta*, *170*, 57–62.

[41] Cowell, M., Winslow, R., Zhang, Q., Ju, J., Evans, J., & Wright, P. (2014). Composite carbon-based ionic liquid supercapacitor for high-current micro devices. *Journal of Physics: Conference Series*, *557*(1), 12061.

[42] Appetecchi, G. B., Kim, G. T., Montanino, M., Alessandrini, F., & Passerini, S. (2011). Room temperature lithium polymer batteries based on ionic liquids. *Journal of Power Sources*, *196*(16), 6703–6709.

[43] Nakamoto, H., Suzuki, Y., Shiotsuki, T., & Mizuno, F. (2013). Ether-functionalized ionic liquid electrolytes for lithium-air batteries. *Journal of Power Sources*, *243*, 23–27.

[44] Kakibe, T., Hishii, J. Y., Yoshimoto, N., Egashira, M., & Morita, M. (2012). Binary ionic liquid electrolytes containing organo-magnesium complex for rechargeable magnesium batteries. *Journal of Power Sources*, *203*, 195–200.

[45] Kornyshev, A. A. (2007). Double-layer in ionic liquids: paradigm change? *The Journal of Physical Chemistry. B*, *111*(20), 5545–57.

[46] Ferreira, A. M., Faustino, V. F. M., Mondal, D., Coutinho, J. A. P., & Freire, M. G. (2016). Improving the extraction and purification of immunoglobulin G by the use of ionic liquids as adjuvants in aqueous biphasic systems. *Journal of Biotechnology*, *236*, 166–175.

[47] Soares, B., Passos, H., Freire, C. S. R., Coutinho, J. A. P., Silvestre, A. J. D., & Freire, M. G. (2016). Ionic liquids in chromatographic and electrophoretic techniques: toward additional improvements in the separation of natural compounds. *Green Chemistry*, *18*, 4582–4604.

[48] Fedorov, M. V., & Kornyshev, A. A. (2008). Ionic liquid near a charged wall: Structure and capacitance of electrical double layer. *Journal of Physical Chemistry B*, *112*(38), 11868–11872.

[49] Vatamanu, J., Borodin, O., & Smith, G. D. (2010). Molecular Insights into the Potential and Temperature Dependences of the Differential Capacitance of a Room-Temperature Ionic Liquid at Graphite Electrodes. *Journal of American Chemical Society*, *132*(Md), 14825–14833.

[50] Kirchner, K., Kirchner, T., Ivaništšev, V., & Fedorov, M. V. (2013). Electrical double layer in ionic liquids: Structural transitions from multilayer to monolayer structure at the interface. *Electrochimica Acta*, *110*, 762–771.

[51] Henderson, D., Lamperski, S., Bari Bhuiyan, L., & Wu, J. (2013). The tail effect on the shape of an electrical double layer differential capacitance curve. *Journal of Chemical Physics*, *138*(14), 1–4.

[52] Gebbie, M. A., Valtiner, M., Banquy, X., Fox, E. T., Henderson, W. A., & Israelachvili, J. N. (2013). Ionic liquids behave as dilute electrolyte solutions, *110*(24).

[53] Srinivasan, V., & Blankschtein, D. (2003). Effect of Counterion Binding on Micellar Solution Behavior: 1. Molecular−Thermodynamic Theory of Micellization of Ionic Surfactants. *Langmuir*, *19*(23), 9932–9945.

Chapter 3: Effect of electrostatic correlations on micelle formation

Micellization phenomena are fundamental to countless biological and chemical processes. Salts can dramatically change the micellization, depending on the kind of electrolyte and its concentration. Traditional approaches to model and describe these phenomena do not take into account electrostatic correlation interactions. Those interactions are essential when modeling surfactant solutions containing multivalent and/or highly concentrated electrolytes. Therefore, the development of a theory that is able to correctly predict the behavior of surfactant solutions with salts is a key to improve the application of surfactants in industrial processes. Here, we propose a simple methodology that uses a mean field approach to include electrostatic correlation effects and we coupled it with the well-established molecular thermodynamics approach to describe the micellization phenomena. From the proposed model, we can obtain the critical micelle concentration (CMC) of surfactant solutions and information about the size and shape of the micelles for ionic and zwitterionic surfactants. To validate the model we compared our results with experimental values of CMC and counterion binding for different surfactants. We obtained very good agreement with the experimental data with a completely predictive model.

Keywords: micellization, electrostatic correlations, molecular thermodynamics, surfactants, zwitterionic surfactants.

3.1 Introduction

Surfactant aggregation is a very important aspect of several chemical and biochemical processes. When salt is present in those processes, the formation of surfactant aggregates (also known as micelles) can be dramatically changed by the specific kind of electrolyte added [1]. An increase in the ionic strength of a surfactant solution causes the reduction of the critical micelle concentration (CMC), and may cause a transition in the shape of the micelles from spheres to elongated forms [2,3]. This effect is associated with the decrease of the electrostatic repulsion between the heads of the surfactants. Furthermore, the addition of salt to induce micelle growth is the subject of several studies, besides being exploited on commercial applications of

some surfactants. Moreover, the properties of micelles formed are strongly influenced by not only the counterion concentration but also by the specific kind of counterions present in the solution [2,4-8]. For example, Muller *et al*. [9] studied the impact of anions on different positions of the lyotropic series: one on the borderline, one kosmotropic, and one chaotropic. They verified that the different counterions would lead to different micelle shapes that are explained by how strongly the counterion interacts with the micelle. The anion with the strongest interaction would lead to a system with the more elongated micelles.

Also, multivalent counterions, such as Al^{3+} and Ca^{2+} are known for being great promoters of micelle growth when compared with monovalent counterions with the same ionic strength, as for example Na^{+} [10, 11]. In this way, the development of a theory that is able to correctly predict the behavior of surfactant solutions with multivalent and highly concentrated electrolytes is very important especially in the selection of the surfactant to be used for a certain application. Furthermore, such theory should be able to predict properties of the micellization phenomena that are directly related with practical properties (*e.g.* solubilization capacity and rheology). This would contribute to the reduction of the time and cost involved with the experimental process of trial and error when deciding which is the most suitable surfactant to be applied on a process.

When modeling the effect of salts on the micellization phenomena, the traditional approach uses a linearized form of the Poisson-Boltzmann equation to take into account the electrostatic repulsion of ionic surfactant heads. Some effort was done [1,12] in applying the full form of the Poisson-Boltzmann equation while also including ionic dispersion, which made it possible to observe the effects of ionic specification in the micellization phenomena. Even though the Poisson-Boltzmann equation is effective in describing different systems in different conditions, it is not adequate to describe solutions where the salt concentration is high or where are multivalent ions involved. For those systems, electrostatic correlation effects cannot be neglected.

In the literature, as far as we know there is no model available that considers the effects of electrostatic correlations on the micellization phenomena [2, 13-15]. Bazant *et al*. [16] proposed the so-called BSK model, a simple way to consider electrostatic correlations effects via a modified Poison-Boltzmann equation. The BSK model was

obtained through a gradient approximation for nonlocal electrostatics between different interacting ions. In this model, the permittivity is a differential operator that is a function of a correlation length (l_c). With this approach it is possible to capture the correct behavior of electrolytes close to charged surfaces obtained by molecular dynamics and, at the same time, be simple enough to be used on complex systems.

We present here the association of the traditional model for the micellization phenomena with the electrostatic free energy contribution using the BSK model in order to have a better description of the influence of different salts on surfactant solutions. With this model we obtain the thermodynamically stable state of the surfactant solution calculating the minimum of the total Gibbs energy which provides the amount of micelles formed, their size and shape, and the degree of binding over the micelle of electrolytes. Differently from what has been presented in the literature up to now, here we consider that not only ionic surfactants can have free ions binding to their micelle surface, but that also zwitterionic surfactants can have both anions and cations binding to their micelle surface. This is supported by several experimental observations [11, 17-19] which demonstrated how different kinds of electrolytes impact on the size and shape of zwitterionic micelles and on their critical micelle concentration.

All the systems analyzed here are on aqueous solutions and in the following sections, we discuss the equations and the methodology used to calculate the Gibbs energy and the BSK model used to calculate the electrostatic contribution.

3.2 Methodology

The model for the Gibbs energy of the micellization phenomena has been developed through the time by different authors, being a result mainly from Nagarajan and Ruckenstein [20], Moreira and Firoozabadi [12, 21], and Srinivasan and Blankschtein [4]. Given a global specification of temperature (T), pressure (P), total number of surfactant molecules (N_S) and the number of water molecules(N_w), the Gibbs energy (G) is calculated as the sum of two main contributions: the free energy of formation $\left(G_f\right)$ and the free energy of mixing (G_m).

$$G = G_f + G_m \tag{3.1}$$

Because we are analyzing only diluted surfactant solutions (around the critical micelle concentration) we neglect any interaction between micelles (supposing ideal mixture). The following expression for the Gibbs energy of formation (G_f) is obtained [20]:

$$G_f = N_w\mu_w^o + N_{1S}\mu_{1S}^o + \sum_{g=2}^{\infty} N_g\mu_g^0 + \sum_{i=2}^{\infty} N_i{}^{free}\mu_i^0 \tag{3.2}$$

where $N_w, N_{1S}, N_g,$ and N_i^{free} are respectively the number of water molecules, number of free surfactants, number of micelles containing g surfactant molecules, and number of free ions of the species i in solution. The parameters $\mu_w^0, \mu_{1S}^0, \mu_g^0,$ and μ_i^0 are the standard chemical potentials of the water, free surfactant, micelle with g surfactant molecules, and of the ion of specie i.

There are restrictions related to the mass balance of the components that must be respected.

$$N_S = N_{1S} + \sum_{g=2}^{\infty} gN_g \tag{3.3}$$

$$N_i = N_i^{free} + \sum_{g=2}^{\infty} g\beta_i N_g \tag{3.4}$$

where N_i is the number of ions of specie i in solution, β_i the degree of biding of the counterions of the specie i, which means the average fraction of counterions of specie i that are bounded to the surface of the micelle per surfactant unity.

Now considering the mass balances just presented, we can reorganize and rewrite Equation 3.2:

$$G_f = N_w\mu_w^0 + N_S\mu_{1S}^0 + \sum_{g=2}^{\infty} N_g g\Delta\mu_g^0 + \sum_i N_i\mu_i^0 \tag{3.5}$$

Where $g\Delta\mu_g^0 = \mu_g^0 - g\mu_1^0 - \sum_i g\beta_i\mu_i^0$ is the free energy of micellization, and N_S is the total number of surfactant molecules added to the solution.

With the considerations of ideal mixture of micelles, the free energy of mixing can be calculated as:

$$G_m = kT\left[N_w \ln X_w + N_{1S} \ln X_{1S} + \sum_{g=2}^{\infty} N_g \ln X_g + \sum_i N_i^{free} \ln X_i^{free}\right] \tag{3.6}$$

where X_a is the mole fraction of component a, and k is the Boltzmann constant. The mole fractions (X_a) are calculated as follows:

$$X_a = \frac{N_a}{N_w + N_{1S} + \sum_g N_g + \sum_i N_i^{free}} \qquad \forall\, a = w, 1s, g, i \tag{3.7}$$

And rewriting the equation for the free energy of micellization we obtain:

$$\begin{aligned} G = {} & N_w\mu_w^0 + N_S\mu_{1S}^0 + \sum_{g=2}^{\infty} N_g g\Delta\mu_g^0 + \sum_i N_i\mu_i^0 \\ & + kT\left[N_w \ln X_w + N_{1S} \ln X_{1S} + \sum_{g=2}^{\infty} N_g \ln X_g \right. \\ & \left. + \sum_i N_i^{free} \ln X_i^{free}\right] \end{aligned} \tag{3.8}$$

It is possible to reorganize the previous equation separating the terms that depend only on the fixed variables to the left hand side of the equation $(T, P, N_s, N_i, \text{and}, N_w)$ [21].

$$
\begin{aligned}
G' &= G - N_w\mu_w^0 - N_s\mu_1^0 - \sum_i N_i\mu_i^0 \\
&= \sum_{g=2}^{\infty} N_g g\Delta\mu_g^0 \\
&+ kT\left[N_w \ln X_w + N_{1S} \ln X_{1S} + \sum_{g=2}^{\infty} N_g \ln X_g \right. \\
&\left. + \sum_i N_i^{free} \ln X_i^{free}\right]
\end{aligned}
\tag{3.9}
$$

And dividing the expression by kT:

$$
\begin{aligned}
\frac{G'}{kT} &= \sum_{g=2}^{\infty} \frac{N_g g\Delta\mu_g^0}{kT} + N_w \ln X_w + N_{1S} \ln X_{1S} + \sum_{g=2}^{\infty} N_g \ln X_g \\
&+ \sum_i N_i^{free} \ln X_i^{free}
\end{aligned}
\tag{3.10}
$$

In Equations 3.8, 3.9 and 3.10 it is considered that there is a size distribution of micelles formed. However, some surfactants present a very narrow size distribution and for these cases we can approximate this distribution with the maximum term method. The applicability of this approximation for micelle formation was shown in [22]. Several authors used the same approximation [1, 12, 20, 21]. This method consists on considering that there is one representative micelle size that can describe all micelle size distributions. When we use this methodology the previous equation is reduced to, where g is the average number of surfactants in the micelles:

$$
\frac{G'}{kT} = \frac{N_g g\Delta\mu_g^0}{kT} + N_w \ln X_w + N_{1S} \ln X_{1S} + N_g \ln X_g + \sum_i N_i^{free} \ln X_i^{free} \tag{3.11}
$$

Equation 3.11 is then minimized to obtain the most stable state of the solution considering that we have a micelle size distribution, and 3.11 considering the maximum term methodology. We have shown that both methodologies are equivalent for low concentration of surfactant [22].

3.2.1 Free energy of micellization

The free energy of micellization is calculated as a sum of different contributions. The path we considered here starts with the break of the bond between the head and the tail of the surfactant. Next, the tail is transferred from the aqueous medium to a liquid hydrocarbon corresponding to the tail. After, the tails are reorganized on the micelle core. This happens because one of the ends of the surfactant tail must be located at the surface of the micelle. Following this rearrangement we are able to reconnect the heads to the tails located on the interface water-micelle interface. Because this interface is spatially limited, some effects due to repulsion between the surfactant heads occur. Those effects constitute the last step on the path to describe the micellization phenomena. The following infographic illustrates (Fig. 1) the steps on the path between the initial and final state of the micelle formation. Therefore, the free energy of micellization can be calculated by Eq. 3.12 [12, 20, 21].

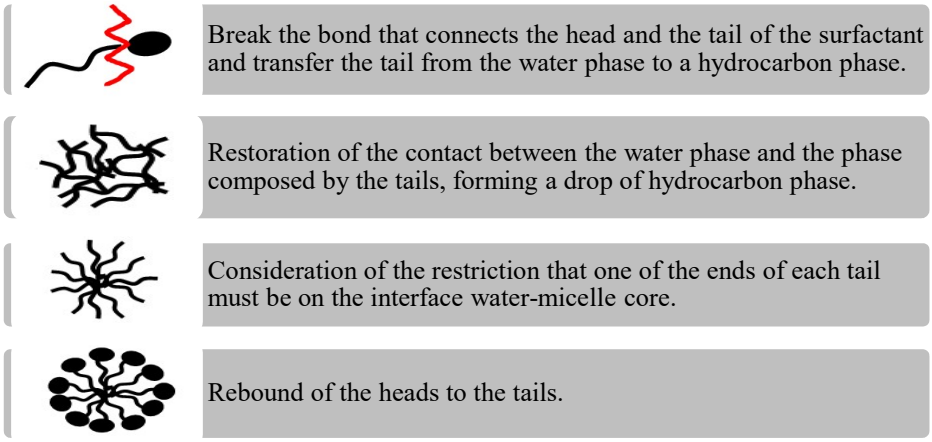

Figure 1 - Path defined to describe the micellization process, from free surfactant in solution to surfactant in micelle structure.

$$\left(\frac{\Delta\mu_g^0}{kT}\right) = \left(\frac{\Delta\mu_g^0}{kT}\right)_{trans} + \left(\frac{\Delta\mu_g^0}{kT}\right)_{def} + \left(\frac{\Delta\mu_g^0}{kT}\right)_{int} + \left(\frac{\Delta\mu_g^0}{kT}\right)_{steric} + \left(\frac{\Delta\mu_g^0}{kT}\right)_{ionic} \quad (3.12)$$

In this work our focus is on a better description of the ionic electrostatic interactions of the surfactants heads and its contribution to the free energy of micellization (subindex *ionic*). The *trans* contribution stands for the energy spent on the transfer of the surfactant tail from an aqueous environment to a hydrocarbon medium. A detailed description of this contribution can be obtained in Nagarajan and Ruckenstein

[20]. The *def* contribution takes into account the free energy on the deformation and packing of the tails of the surfactants in the hydrocarbon nucleus due to the imposed limitation that one of the ends of the tails must be located at interface of the nucleus. This contribution is calculated on a similar way as by Moreira e Firoozabadi [21]. The *int* contribution takes into account the energy lost in the formation of the interface between the water and the hydrocarbon micelle core. It is a function of the area and the interfacial tension of this new interface. For this contribution we used the approach presented by Moreira and Firoozabadi [22]. The *steric* contribution considers the steric effects that arise due to the restrictions of space on the interface of the micelle occupied by the surfactants head. For that we considered the approach proposed by Nagarajan and Ruckenstein [20].

Free energy of the electrostatic interactions between the heads $\left(\Delta\mu_g^0/kT\right)_{ionic}$

For ionic surfactants

Electrostatic interactions between the heads of surfactants become relevant when the surfactants in the solution are either ionic or zwitterionic. In this section we discuss the approach for ionic surfactants and in the next section for zwitterionic surfactants. The contribution of the ionic electrostatic interactions to the free energy of micellization was analyzed using the methodologies proposed by Lukanov and Firoozabadi [1] and Srinivasan and Blankschtein [4]. For ionic surfactants we consider that the counterions from surfactant head and from added electrolyte can bind to the charged surfaces of the micelles. This directly impacts on the ionic contribution to the micellization free energy $\left(\Delta\mu_g^0/kT\right)_{ionic}$ represents the amount of work performed to assemble the charged surface of the micelle and the electrical double layer on surrounding. Considering a reversible isothermal process, it can be calculated as follows:

$$\left(\frac{\Delta\mu_g^0}{kT}\right)_{ionic} = \frac{a_{ch}}{kT}\int_0^{\sigma}\psi_0(\sigma')d\,\sigma' \tag{3.13}$$

where σ is the final charge density on the surface per molecule of surfactant, ψ_0 is the electrostatic potential on the surface of the micelle per molecule of surfactant for a surface of charge (σ), and a_{ch} is the area per molecule of surfactant calculated as:

$$a_{ch} = \frac{4\pi R_{ch}^2}{g} \tag{3.14}$$

The radius R_{ch} is defined as a function of the equivalent radius of the micelle (R_{eq}) and the distance between the center of the micelle's nucleus and the surface of the micelle (d_{ch}). The last one is a tabled value available for some surfactants. And with this information we can calculate the charge density on the micelle's surface (σ).

$$R_{ch} = R_{eq} + d_{ch} \tag{3.15}$$

$$\sigma = \frac{e\left(z_A + \sum_j z_j \beta_j\right)}{a_{ch}} \tag{3.16}$$

Where z_A is the valence of the surfactant head, z_j is the valence of the counterions j, β_j is the degree of counterion binding on the micelle surface, and e is the elementary charge.

For zwitterionic surfactants

To model the electrostatic contribution to the free energy of micellization for an aqueous solution of zwitterionic surfactants and salts we adapted the model presented by Goldsipe and Blankschtein [23] and Moreira and Firoozabadi [12] as shown hereafter.

We first consider here that the anion of the salt added to the solution can bind to the positive part of the dipole, the same way the cation can bind to the negative pole. As presented on the previous item for ionic surfactants, the charging contribution is treated as the reversible work to charge the surface of the micelle as presented by Equation 3.13. However, this equation must be applied to each charged surface of the micelle (Fig. 2). For that, we need to know the charge structure of a micelle formed by zwitterionic surfactants. Figure 2 presents a scheme for the charged surfaces for a micelle formed by zwitterionic surfactant immersed in an electrolyte solution.

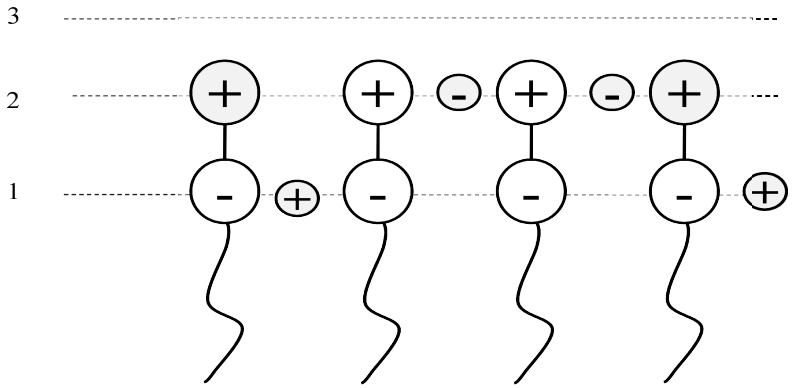

Figure 2 - Scheme of charging layers for zwitterionic surfactant immersed in an electrolyte solution.

In Figure 2, the layer number 3 represents the Stern surface of the micelle. The charge on surfaces 1 and 2 can be calculated as a function of the charge on the dipoles and the degree of binding of anions and cations. We need to calculate $\left(\frac{\Delta\mu_g^0}{kT}\right)_{ionic}$ for surfaces 1 and 2, and for that, the final charge on each of those surfaces (σ) can be calculated as follows:

$$\sigma_1 = \frac{e(z_{innerA} + \beta_+ z_+)}{a_{ch}} \tag{3.17}$$

$$\sigma_2 = \frac{e(z_{outerA} + \beta_- z_-)}{a_{ch}} \tag{3.18}$$

And the total $\left(\frac{\Delta\mu_g^0}{kT}\right)_{ionic}$ can be written as:

$$\left(\frac{\Delta\mu_g^0}{kT}\right)_{ionic} = \sum_{i=1}^{2} \int_0^{\sigma_i} \psi_{0i}(q)\, dq \tag{3.19}$$

In this equation and in Equation 3.13, ψ_{0i} is the electrostatic potential in the surface of charge i, and it is calculated through a modified version of the Poisson-Boltzmann equation where we include effects of ionic electrostatic correlations and ion-surface van der Waals interactions.

Aiming to have a better description of systems containing multivalent electrolytes and/or higher salt concentration we included the effects of ionic

electrostatic correlations by using the approach proposed by Bazant *et al*. [16]. Their mean field approach considers that the permittivity is a linear operator with a contribution for the ion-ion correlations. That consideration when coupled with the Poisson-Boltzmann equation leads to a fourth order differential equation.

We considered on this analysis that the micelles are charged flat plates. This consideration is based on the fact that the dimensions of micelles are much larger than the size of any ion in solution, and, from the point of view of an ion, the micelle can be seen as a sphere of infinite radii (a flat plane). For this case, the unidirectional Fourth order Poisson equation (BSK model) in Cartesian coordinates is written as:

$$l_c^2 \frac{d^4\psi}{dx^4} - \frac{d^2\psi}{dx^2} = \frac{\rho}{\varepsilon} \tag{3.20}$$

where l_c is the correlation length. Here we follow the definition for the correlation length proposed by Alijó *et al*. (2015) where l_c is the radii of the hydrated ion.

The boundary conditions of this problem are related to a specific charge (σ) on the surface that is a function of the number of surfactants on the micelle (g) and the degree of binding of counterions β_i, that can be calculate by Eq. 3.16, for ionic surfactants, and by Eqs. and 3.17 and 3.18 for zwitterionic surfactants. Then the boundary condition can be written as:

$$\left.\frac{d\psi}{dx}\right|_{x=0} = \frac{-\sigma}{\varepsilon} \tag{3.21}$$

The other boundary conditions are defined bellow, as suggested by Bazant *et al*. [16]:

$$\left.\frac{d^3\psi}{dx^3}\right|_{x=0} = 0 \tag{3.22}$$

$$\psi(\infty) = 0 \tag{3.23}$$

$$\left.\frac{d\psi}{dx}\right|_{x=\infty} = 0 \tag{3.24}$$

A new dependent variable is proposed to reduce the order of the differential equation to be solved.

$$\phi(x) = \frac{d^2\psi(x)}{dx^2} \tag{3.25}$$

Applying this to the previous equation and the boundary conditions we obtain:

$$l_c^2 \frac{d^2\phi}{dx^2} - \phi = \frac{\rho}{\varepsilon} \tag{3.26}$$

$$\left.\frac{d\psi}{dx}\right|_{x=0} = \frac{-\sigma}{\varepsilon} \tag{3.27}$$

$$\left.\frac{d\phi}{dx}\right|_{x=0} = 0 \tag{3.28}$$

$$\psi(\infty) = 0 \tag{3.29}$$

$$\phi(\infty) = 0 \tag{3.30}$$

And the fourth order differential equation to be solved is converted into a system of two second order differential equations. From the solution of this system we can obtain the profile of the electrostatic potential and the concentration profile of the ions as a function of the distance from the micelle surface. To enhance the numerical solution we expressed the independent variable x in terms of dimensionless variable ζ:

$$\zeta = 1 - \exp[-\kappa x] \tag{3.31}$$

The differential operators considering the new independent variable ζ are expressed for a generic dependent variable f:

$$\frac{df}{dx} = \kappa(1-\zeta)\frac{df}{d\zeta} \tag{3.32}$$

$$\frac{d^2f}{dx^2} = \kappa^2(1-\zeta)\left[(1-\zeta)\frac{d^2f}{d\zeta^2} - \frac{df}{dx}\right] \tag{3.33}$$

This change allows the independent variable, that before was defined from zero to infinite, to be now defined on a bounded finite interval $\zeta = [0,1]$. We also defined

the dimensionless electrostatic potential and ion concentration $y = e\psi/kT$ and $\chi_i = c_i/c_{i,0}$. The charge density ρ is $\rho = e\sum_i z_i c_i$, where e is the elementary charge, z_i and c_i are the valence and concentration of ion i. The dimensionless concentration of ion i can be written as $\chi_i = \exp(z_i y - U_i)$, where U_i is the nonelectrostatic nondimensional potential (van der Waals interaction between the ion i and the micelle surface).

$$U_i = -\frac{B_i}{x^3} \quad \text{for } x > r_i \tag{3.34}$$

The parameter B_i is the dispersion parameter of the ion i, and x is the perpendicular distance between the center of the ion i and the surface of the micelle. Details can be found in Lima *et al*. [24] and Tavares *et al*. [25].

The Debye length (κ) is defined as follows:

$$\kappa = \sqrt{\frac{2e^2 I}{\varepsilon\varepsilon_0 kT}} \tag{3.35}$$

where I is the ionic strength, defined as $I = \frac{1}{2}\sum_i z_i^2\, c_{i,0}$.

Applying all the variable changes proposed we obtain the system of differential equations to be solved here to calculate the electrostatic contribution to the free energy of micellization.

$$l_c^2(1-\zeta)\left[(1-\zeta)\frac{d^2\phi}{d\zeta^2} - \frac{d\phi}{d\zeta}\right] - \phi = \frac{e^2}{\varepsilon kT\kappa^2}\sum_i z_i c_{i,0}\chi_i \tag{3.36}$$

$$\phi = (1-\zeta)\left[(1-\zeta)\frac{d^2 y}{d\zeta^2} - \frac{dy}{d\zeta}\right] \tag{3.37}$$

And the boundary conditions:

$$\left.\frac{dy}{d\zeta}\right|_{\zeta=0} = \frac{-\sigma e}{\kappa\varepsilon kT} \tag{3.38}$$

$$\left.\frac{d\phi}{d\zeta}\right|_{\zeta=0} = 0 \tag{3.39}$$

$$y(1) = 0 \tag{3.40}$$

$$\phi(1) = 0 \tag{3.41}$$

3.3 Numerical strategy

To solve the system consisted by Eqs. 3.36 and 3.37 we applied the finite differences method with the central difference approximation to describe the derivatives. After obtaining the profile around the micelle of the electrostatic potential (ψ) considering the electrostatic correlation effect, we are able to calculate the contribution to the free energy of micellization due to the electrostatic interactions between the heads of the surfactants. For that, we need to solve Equation 3.13 (for ionic surfactants) or Equation 3.19 (for zwitterionic surfactants) -which accounts for the contribution due to the electrostatic interactions between surfactant heads -, and these equations contain an integral of the electrostatic potential at the micelle surface as a function of the surface potential. The Composite Simpson's Rule is used to obtain the numerical result of these integrals.

To calculate the most stable state of the surfactant + electrolyte aqueous solution, we minimize the expression for the free energy (Equation 3.11) with respect to some optimization parameters. Two sets of optimization variables were defined: one for solutions of surfactants and salts where it is not expected to obtain vesicular micelles, and the other for solutions of surfactants and salts where it is expected to obtain vesicular micelles. For the first ones we defined the optimization variables to be the number of micelles formed (N_g), the number of surfactants on each micelle formed or aggregation number (g) and the degree of biding (β_i) of ions to the surface of the micelle. For vesicular micelles, the set of optimization variables included the same ones defined above and also the number of surfactants on the intern layer of the vesicle (g_i) and the Radius of the outer part of the vesicle (R_o).

In this work we did not consider the size distribution of the micelles because we are interested in analyzing conditions close to the critical micelle concentration, at which narrow size distribution of the micelles are formed [22]. The optimization was performed with the deterministic algorithm *fmincon* from *Matlab* which is a constrained nonlinear optimizer based on the trust region reflective algorithm. The optimization parameters N_g and g were constrained to be only positive numbers, as we cannot have a negative number of micelles being formed or micelles with a negative number of surfactants. Also, by definition, the number of surfactants in the micelle should be bigger or equal to 2. The degree of binding of the ions (β_i) is constrained between 0 and 1. Regarding the optimization parameters g_i and g for vesicular micelles, there is a constraing due to the fact that the number of surfactants in the inner part of the micelle (g_i) cannot be greater than the total number of surfactants in the micelle (g). The proper definition of the optimization variables is a very important step when we are minimizing the Gibbs energy (if we over specify the number of parameters to be minimized we might obtain a sharp Gibbs energy function and erroneous interpretations of the results).

Each most stable state is obtained for a specified condition at fixed temperature, pressure, salt and surfactant concentrations. From this state we are able to obtain the number of micelles formed, their size and shape. To validate our model we compare the predictive calculations with critical micelle concentration (CMC) data. Experimentally, the critical micelle concentration (CMC) is defined as the concentration where there is an abrupt change on one property of the surfactant solution. The approach used here is the same proposed by Santos *et al*. [22] to calculate the critical micelle concentration from the minimization of the free energy of the surfactant solution. To obtain the CMC, we perform different simulations of a solution containing an increasing amount of surfactant. Then, for each solution with a different amount of surfactant added we performed the minimization of the Gibbs free energy. This procedure makes it possible to relate the total number of surfactant molecules added (N_S) with the number of free surfactant molecules in the solution (N_1). The CMC is then defined as the concentration of surfactant added (N_S) where an inflexion of the curve is observed. To obtain this point automatically, a regularization function is used which relates N_1 as a function of N_S, and it is presented in equation 4 of the Appendix A.

3.4 Results and discussions

First, to observe the impact of electrostatic correlations on the electrostatic contribution to the free energy of micellization $\left(\Delta\mu_g^0/kT\right)_{ionic}$ we fixed the optimization variables, temperature, surfactant and salt concentration and observed how the variation of the correlation length (l_c) impacts on this term. A higher correlation length represents a system where electrostatic correlation interactions are stronger. For the surfactant sodium dodecyl sulfate (SDS) we performed this analysis for a solution containing sodium chloride (NaCl) and one containing calcium chloride ($CaCl_2$) (Fig. 3). We can observe that increasing the electrostatic correlations length on the system, the electrostatic contribution to the micellization increases, increasing the electrostatic repulsion between the surfactant heads. It is important to notice that here we opted to consider the correlation length is equal to the mean hydrated radii of the ionic species as suggested elsewhere [26]. Therefore, larger ions will contribute to increase the $\left(\Delta\mu_g^0/kT\right)_{ionic}$ contribution.

To validate the proposed methodology we calculated the CMC for different surfactant aqueous solutions with different salts, both monovalent and multivalent, for a wide range of salt concentration. The ionic surfactants analyzed were sodium dodecyl sulfate (SDS) and dodecylpyridinium chloride (C_{12}PyCl), and the zwitterionic surfactants are dodecyl n-betaine (C_{12}-betaine), and decyl lecithin (C_{10}-lecithin). As the focus of this work is to obtain a better description of micellar solutions at elevated salt concentrations and/or in the presence of multivalent ions, we concentrated our analysis for two different salts: sodium chloride (NaCl) and calcium chloride ($CaCl_2$). For a specific analysis of the ionic specificity effects please refer to the work of Moreira and Firoozabadi [11]. The proposed methodology converges for values reported by the Moreira and Firoozabadi work when the electrostatic correlation is neglected (*i.e.*, $l_c = 0$).

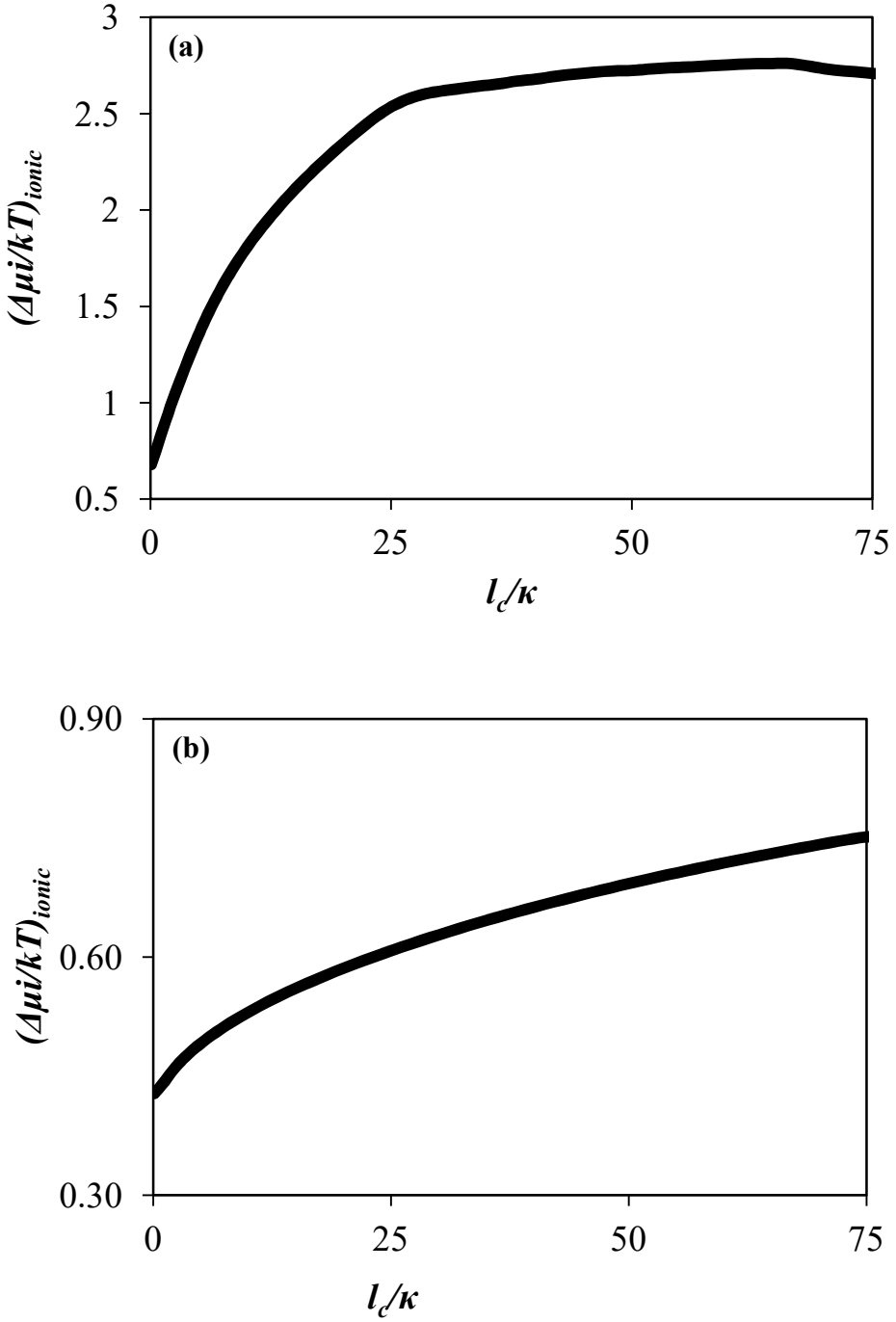

Figure 3 - Electrostatic contribution to the free energy of micellization as a function of the dimensionless correlation length for the systems SDS + NaCl (a), and (b) SDS + $CaCl_2$. The variables, the temperature, and the salt concentration and surfactant concentration were fixed. $\left(\boldsymbol{T = 25℃},\ \boldsymbol{c_0 = 0.5M},\ \boldsymbol{c_{surf} = CMC_{SDS}}\right)$

Figure 4 presents the critical micelle concentration (CMC) of SDS as a function of the salt concentration for NaCl (a) and $CaCl_2$ (b) compared to experimental data. Sodium dodecyl sulfate is an anionic surfactant and, when in aqueous solution, the

sodium ion unbinds from its head. In the event of the formation of a micelle, this unbound cation might reconnect again to the surfactant head present on the surface of the micelle. If there are different kinds of cations on the solution they also can bind to the surface of the micelle. As the final charge on the micelle surface is a function of the amount of those counterions bound to it. Therefore, the stability of the micelle formed is a function of which and how much counterions are bound on the micelle surface. In the first example, Na^+ is the counterion from the surfactant head and from the added electrolyte. In the second case, the counterion from the added electrolyte is calcium, a divalent ion. Their different charges impact on the amount of counterion binding to the micelle surface, and also on the critical micelle concentration. Furthermore, the increase of the aggregation number (g) as the salt concentration increases is observed for both cases as shown in Figure 5.

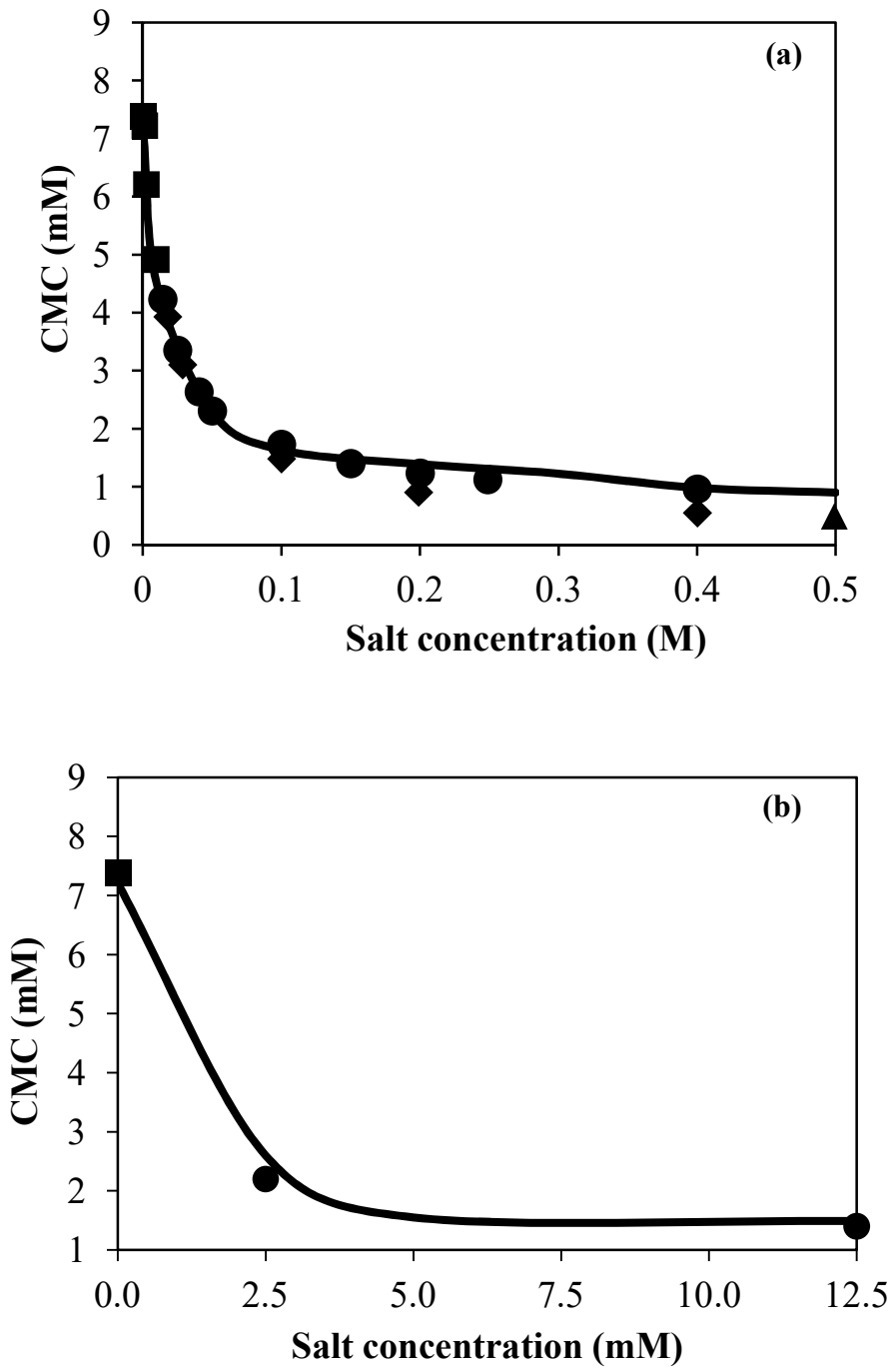

Figure 4 - Calculated (continuous line) and experimental critical micelle concentration for solutions containing (a) SDS and NaCl, and (b) SDS and $CaCl_2$ both at $\boldsymbol{T = 25}$℃. Points are experimental data from [27-30].

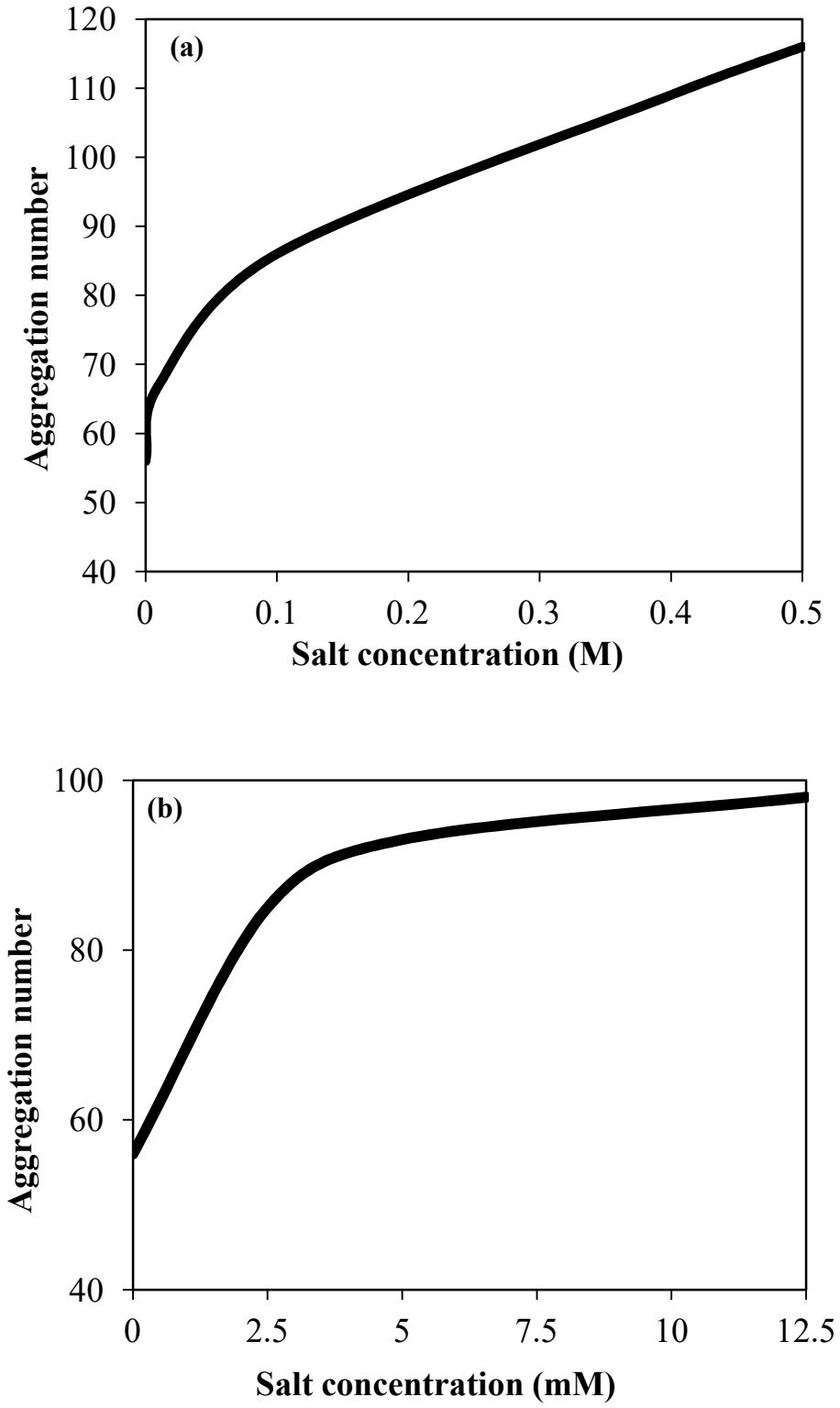

Figure 5 - Calculated aggregation number $(\boldsymbol{g})$ of micelles for the systems SDS and NaCl (a), and (b) SDS and $CaCl_2$ both at $\boldsymbol{T = 25}$℃.

These calculations predict the substitution of the counterion from the surfactant head with the bivalent ion from the added salt, as expected from experimental

observations. Lima *et al*. [3] observed experimentally that multivalent counterion caused a larger aggregation number (g) as the counterion concentration increased. The same was shown by Koroleva and Victorov [2] for monovalent ions and three different ionic surfactants. For both cases studied we verified the reduction of the critical micelle concentration with the increase of salt concentration, and that is a feature observed already experimentally. Besides that, it is also known that multivalent ions provide the formation of larger micelles [23], what is observed by our model.

The model also provides the degree of counterion biding on the surface of the micelle. For a solution containing the surfactant SDS and NaCl, both the counterion from the surfactant head and the counterion from the added salt are the same (sodium). Thereby, we expect that the degree of biding of the counterion from both sources have a similar value. For the solution with SDS and NaCl 4mM, the degree of binding for the counterion from the surfactant head was equal to 0.27 and for the counterion from the added salt was equal to 0.24, then the behavior was as expected. Now for the SDS solution with 12.5mM of $CaCl_2$ the degree of biding of ion sodium (from the surfactant head) was equal to 0.002 while for the ion calcium was 0.14. For the solution of SDS and 2.5mM of $CaCl_2$, the ion sodium presented a degree of binding equal to 0.004 and the ion calcium 0.22.

For a cationic surfactant, when NaCl and $CaCl_2$ are added, the counterion is for both cases the chloride ion. Therefore we expect that both salts would have similar effects on the micellization of cationic surfactants. From Figure 6 we can see that crititical micelle concentration (CMC) of the cationic surfactant dodecylpyridinium chloride (C_{12}PyCl) is slightly impacted on a higher way on the presence of multivalent electrolytes. This is explained by the fact that for the same salt concentration, the concentration of chloride ions is larger for the multivalent electrolyte than for the monovalent one. But the reduction on the CMC is on the same order of magnitude for both salts, which was not the case for the SDS example, where the NaCl concentration has to be much higher than the concentration of $CaCl_2$ in order to obtain the same reduction on the critical micelle concentration.

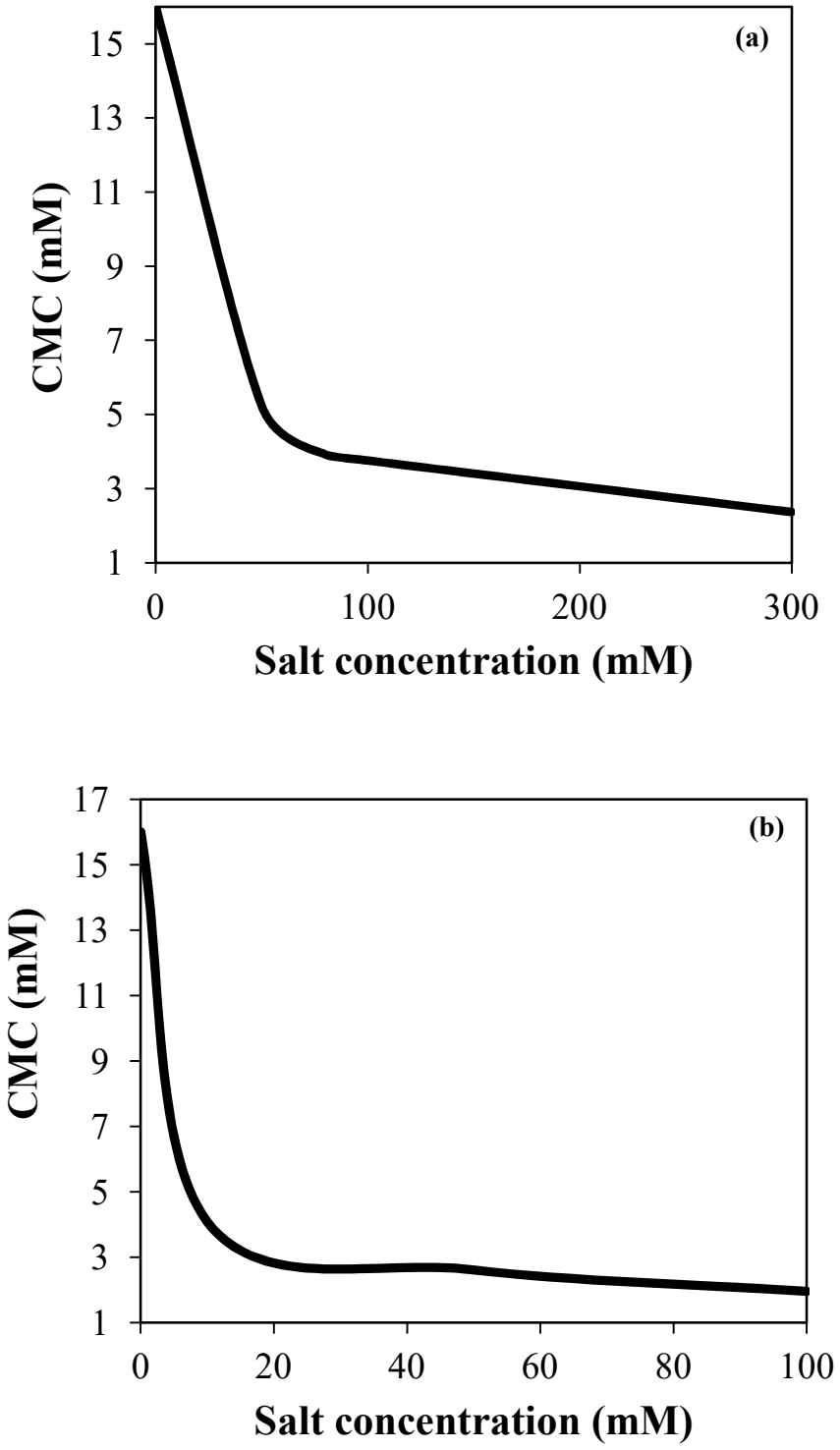

Figure 6 - Critical micelle concentration as a function of salt concentration for solutions containing (a) dodecylpyridinium chloride and NaCl, and (b) dodecylpyridinium chloride and $CaCl_2$.

To analyze aqueous solutions containing zwitterionic surfactants and electrolytes, we modeled surfactant solutions of C_{12}-lecithin and C_n-n-betaines. It is important to notice that C_n-lecithins are known for forming vesicular micelles, so it is important to consider on the model the geometrical restrictions of this kind of micelle. The full geometrical relations for vesicular micelles can be found elsewhere [31-32]. Another important consideration when modeling C_n-lecithins is that these surfactants present a double tail, thus demanding small alterations on the contributions to the micellization free energy [33]. In the other hand, C_n-n-betaines tend to form smaller and spherical micelles as can be observed in Table 2.

Table 2 shows how the addition of NaCl and the increase in the surfactant concentration influences on the size of the formed micelles. As it is observed from our calculations and from experimental data [34], the aggregation number (g) shows a very small change when electrolytes and surfactants are added to the solution on the same proportion.

Table 2 - Effects of the increase of the surfactant and salt concentration on the aggregation number $(\boldsymbol{g})$ for $\boldsymbol{T = 25°C}$ for the surfactant the surfactant dodecyl n-betaine.

C_{12}-n-betaine [M]	NaCl [M]	g (model)	g (experiment) [34]
0.197	0	63	80
0.194	0.194	70	85
0.467	0.467	69	82

As observed by different experimental works [17, 34] and also predicted by our model (Figure 7), ions from the added salt do bind to the surface of the micelle formed by zwitterionic surfactants. Because they are more polarizable, anions tend to have a degree of biding (β) higher than the cations. As we can see, comparing Figures 7(a) and 7(b), the degree of binding of the anion for the multivalent salt is higher than the one for the monovalent ion and again can be related to the larger concentration of chloride ions in the $CaCl_2$ salt, when compared to the same salt concentration of NaCl.

Furthermore, Priebe *et. al*. [35] observed that regardless the order of the charges on the dipole of the zwitterionic surfactant, micelles are preferentially associated to anions than to cations, leading to negative zeta potentials. Our model showed to be able to predict this trend, as the surfactants n-betaine and lecithin have opposite order of their dipole charges and both of them presented a larger degree of binding for the anions, as it can be seeing in Table 3 where we present the results for the C_{12}-lecithin surfactant and NaCl.

Table 3 - Degree of counterion binding to micelles of C_{12}-lecithin surfactant at different NaCl concentrations at T = 25ºC.

C_{12}-lecithin [M]	NaCl [M]	β_{Na}	β_{Cl}
0.016	0.007	0.13	0.31
0.008	0.1	0.095	0.28
0.008	0.4	0.084	0.27

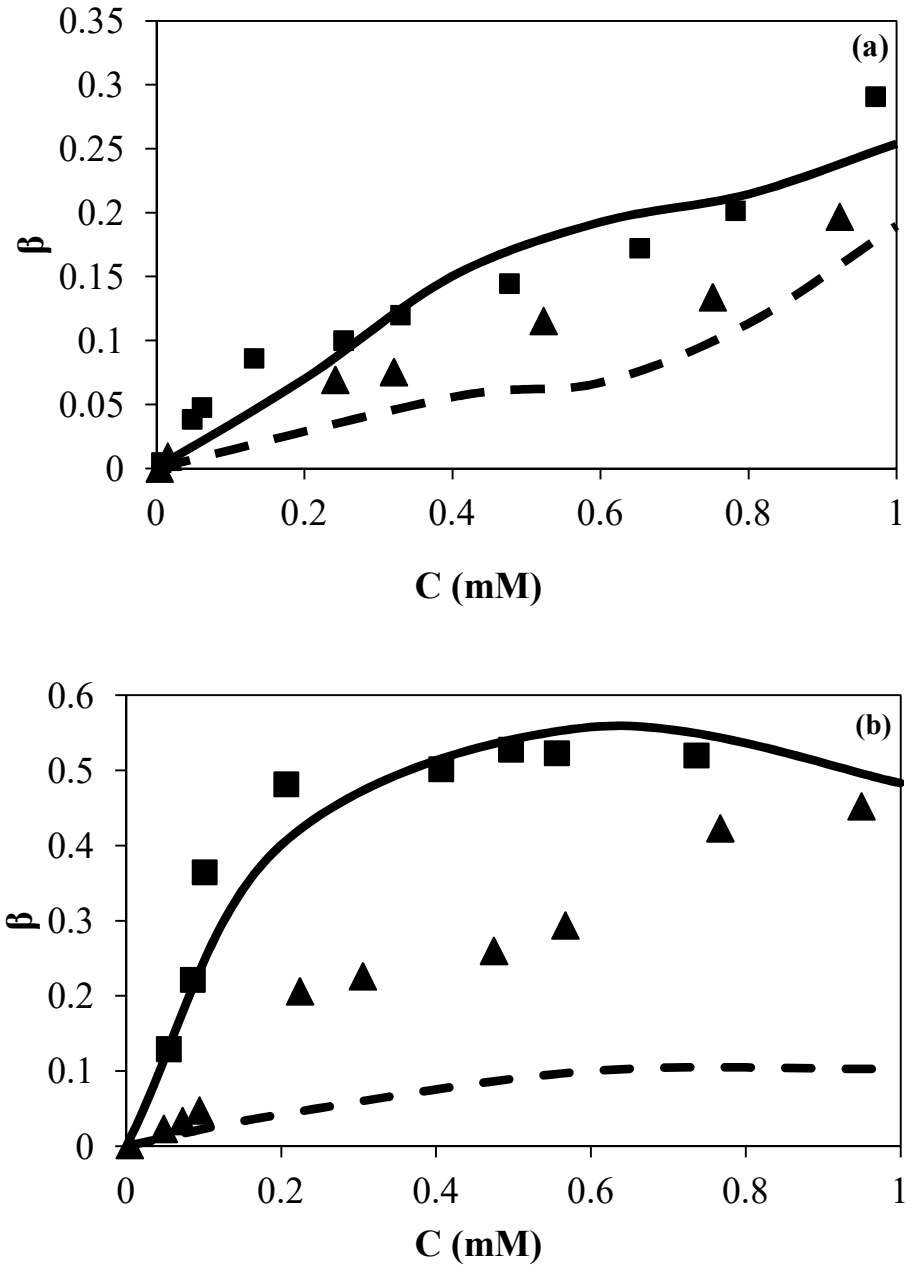

Figure 7 - Degree of ion binding ($\boldsymbol{\beta}$) on the surface for the surfactant C_{12}-n-betaine. (a) with NaCl, where the continuous line is the model prediction of $\boldsymbol{\beta}$ for the chloride ion, the dashed line is the prediction of $\boldsymbol{\beta}$ for the sodium ion, the squares are experimental data for chloride, and the triangles experimental data for sodium. (b) with $CaCl_2$, where the continuous line is the model prediction of $\boldsymbol{\beta}$ for the chloride ion, the dashed line is the prediction of $\boldsymbol{\beta}$ for the calcium ion, the squares are experimental data for chloride, and the triangles experimental data for calcium. All the experimental data was obtained from the work of [34].

Finally, in Figure 8 we observe that the model is also able to predict that the degree of ion binding in the surface of a zwitterionic surfactant reduces as the length of the surfactant tail increases. This behavior was experimentally observed by Okano *et al*. [36]. The authors suggested that a larger alkyl group near the head of the surfactant reduces the Coulombic repulsions between the surfactant heads.

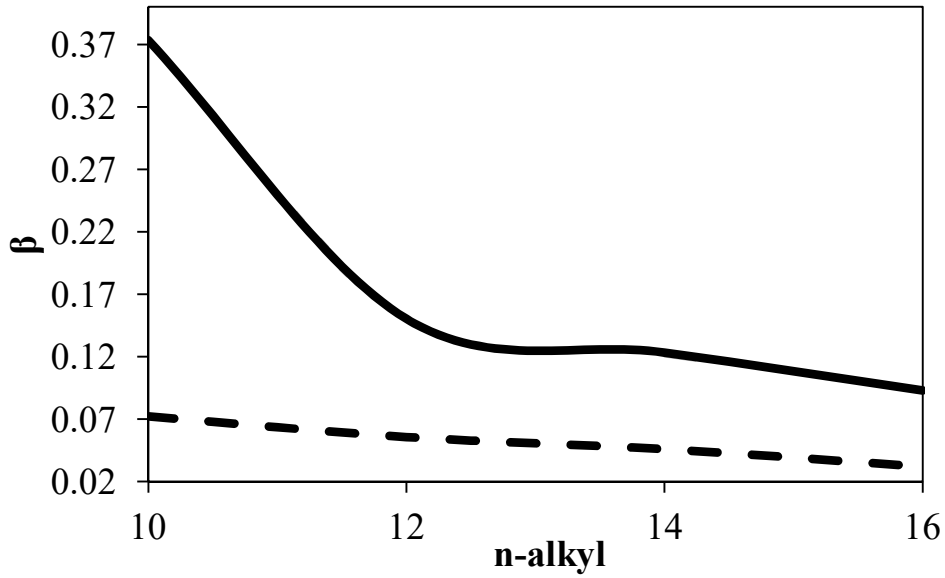

Figure 8 - Degree of ionic binding ($\boldsymbol{\beta}$) on a system containing NaCl (0.4M) and C_n-n-betaine at the critical micelle concentration, as a function of the length of the surfactant tail. The continuous line represents $\boldsymbol{\beta}$ for the chloride ion and the dashed line for sodium ion.

3.5 Final Remarks

Here we analyzed the effects of electrostatic correlation on the micellization phenomena. We improved the classical molecular thermodynamics approach by considering a modified version of the Poisson-Boltzmann equation (BSK model) to better calculate the electrostatic contributions. Electrostatic correlations had shown to increase the electrostatic contribution to the micellization. This effect is particularly relevant for solutions containing concentrated and/or multivalent electrolytes. The proposed model showed to be able to predict experimental data of critical micelle

concentration (CMC) for a large range of salt concentrations. Furthermore, we were able to predict the tendency of ion binding on the surface of zwitterionic micelles supported by experimental data, which reassures the model assumptions and contributes to its validation.

All the analyses presented here confirm the importance of ionic electrostatic correlations for micelle formation and that the micellization phenomena can be calculated by the completely predictive model proposed here. This approach can be extended for microemulsions and may be useful for the design of surfactants.

References

[1] B. Lukanov, A. Firoozabadi, Specific ion effects on the self-assembly of ionic surfactants: a molecular thermodynamic theory of micellization with dispersion forces, Langmuir, 2014, 30:10: 6373-6383.

[2] S. V. Koroleva, A. I. Victorov, Modeling of the effects of ion specificity on the onset and growth of ionic micelles in a solution of simple salts, Langmuir, 2014, *30*:12:3387–3396.

[3] F. S. Lima, I. M. Cuccovia, D. Horinek, L. Q. Amaral, K. A. Riske, S. Schreier, *et al*., Effect of counterions on the shape, hydration, and degree of order at the interface of cationic micelles: The triflate case, Langmuir, 2013, *29*:13: 4193–4203.

[4] V. Srinivasan, D. Blankschtein, Effect of counterion binding on micellar solution behavior: 1. Molecular−thermodynamic theory of micellization of ionic surfactants, Langmuir, 2003, 19:23: 9932–9945.

[5] Anacker, E W; Ghose, H. M. (1963). Counterions and Micelle Size. I. Light Scattering By Solutions of Dodecyltrimethylammonium Salts1. *The Journal of Physical Chemistry*, *594*(14).

[6] Anacker, E. W., & Ghose, H. M. (1968). Counterion and Micelle Size. II. Light Scattering by Solutions of Cetylpyridinium Salts. *Journal of the American Chemical Society*, *90*(12), 3161–3166.

[7] Preiss, U. P., Eiden, P., Luczak, J., & Jungnickel, C. (2013). Modeling the influence of salts on the critical micelle concentration of ionic surfactants. *Journal of Colloid and Interface Science*, *412*, 13–6.

[8] Chevalier, Y., Kamenka, N., Chorro, M., & Zana, R. (1995). Aqueous Solutions of Zwitterionic Surfactants with Varying Carbon Number of the Intercharge Group. 1. Micelle Aggregation Numbers. *Langmuir*, *11*(1), 4234–4240.

[9] W. Muller, C. Déjugnat, T. Zemb, J. F. Dufrêche, O. Diat, How do anions affect self-assembly and solubility of cetylpyridinium surfactants in water, Journal of Physical Chemistry B, 2013, 117:5:1345–1356.

[10] Alargova, R. G., Danov, K. D., Petkov, J. T., Kralchevsky, P. A., Broze, G., & Mehreteab, A. (1997). Sphere-to-Rod Transition in the Shape of Anionic Surfactant Micelles Determined by Surface Tension Measurements. *Langmuir*, *13*(14), 5544–5551.

[11] Alargova, R. G., Danov, K. D., Kralchevsky, P. a, Broze, G., & Mehreteab, a. (1998). Growth of giant rodlike micelles of ionic surfactant in the presence of Al 3+ counterions. *Langmuir*, *14*(15), 4036–4049.

[12] L. A. Moreira, A. Firoozabadi, Molecular thermodynamic modeling of specific ion effects on micellization of ionic surfactants, Langmuir, 2010, 26: 19:15177–15191.

[13] L. S. Hao, Y. T. Deng, L. S. Zhou, H. Ye, Y. Q. Nan, P. Hu, Mixed micellization and the dissociated Margules model for cationic/anionic surfactant systems, Journal of Physical Chemistry B, 2012,116:17:5213–5225.

[14] Y. Zhu, M. L. Free, Evaluation of ion effects on surfactant aggregation from improved molecular thermodynamic modeling. Industrial & Engineering Chemistry Research, 2015, 54:36:9052–9056.

[15] A. Khoshnood, B. Lukanov, A. Firoozabadi, Temperature effect on micelle formation: molecular thermodynamic model revisited, Langmuir, 2016, 32:2175−2183.

[16] M. Z. Bazant, B. D. Storey, A. A. Kornyshev, Double layer in ionic liquids: Overscreening vs. crowding, Physical Review Letters, 2010, 106: 3–6.

[17] Drinkel, E., Souza, F. D., Fiedler, H. D., & Nome, F. (2013). The chameleon effect in zwitterionic micelles: Binding of anions and cations and use as nanoparticle stabilizing agents. *Current Opinion in Colloid & Interface Science*, *18*(1), 26–34.

[18] Priebe, J. P., Souza, F. D., Silva, M., Tondo, D. W., Priebe, J. M., Micke, G. A., Nome, F. (2012). The chameleon-like nature of zwitterionic micelles: Effect of cation binding. *Langmuir*, *28*(3), 1758–1764.

[19] Chevalier, Y., Kamenka, N., Chorro, M., & Zana, R. (1995). Aqueous Solutions of Zwitterionic Surfactants with Varying Carbon Number of the Intercharge Group. 2. Ion binding by the micelles. *Langmuir*, *11*(1), 4234–4240.

[20] R. Nagarajan, R., E. Ruckenstein, Theory of surfactant self-assembly: a predictive molecular thermodynamic approach, Langmuir, 1991, 7: 3: 2934–2969.

[21] L. A. Moreira, A. Firoozabadi, Thermodynamic modeling of the duality of linear 1-alcohols as cosurfactants and cosolvents in self-assembly of surfactant molecules, 2009, Langmuir, 25:20: 12101–13.

[22] M. S. Santos, E. C. Biscaia Jr., F. W. Tavares, Molecular Thermodynamics of Micellization: Micelle Size Distributions and Geometry Transitions, Brazilian Journal of Chemical Engineering, 2016, 33 (03), 515-523.

[23] A. Goldsipe, D. Blankschtein, Modeling counterion binding in ionic-nonionic and ionic-zwitterionic binary surfactant mixtures, Langmuir, 2005, 21:9850–65.

[24] [15] Lima, E. R. A. *et al*., (2007) Osmotic Second Virial Coefficients and Phase Diagrams for Aqueous Proteins from a Much-Improved Poisson-Boltzmann Equation. *Journal of Physical Chemistry C*, *111*, 16055-16059.

[25] Tavares, F. W., Bratko, D., & Prausnitz, J. M. (2004). The role of salt–macroion van der Waals interactions in the colloid–colloid potential of mean force. *Current Opinion in Colloid & Interface Science*, *9*(1–2), 81–86.

[26] Alijó, P. H. R., Tavares, F. W., Biscaia Jr., E. C., & Secchi, A. R. (2015). Effects of electrostatic correlations on ion dynamics in alternating current voltages. *Electrochimica Acta*, *152*, 84–92.

[27] de la Ossa, E. M.; Flores, V. (1987) Effect of temperature and electrolyte on C.M.C. *Tenside Surfactants Detergents,* 24, 38–41.

[28] Dutkiewicz, E.; Jakubowska, A. (2002) Effect of electrolytes on the physicochemical behaviour of sodium dodecyl sulphate micelles. *Colloid Polymer Science*, 280, 1009–1014.

[29] Williams, R. J.; Phillips, J. N.; Mysels, K. J. (1955) The critical micelle concentration of sodium lauryl sulfate at 25℃. *Transactions of the Faraday Society*, 51, 728–737.

[30] Mysels, K. J.; Princen, L. H. (1959) Light scattering by some lauryl sulfate solutions. *Journal of Physical Chemistry*, 63, 1696–1700.

[31] Israelachvili, J. N., Mitchell, D. J., & Ninham, W. (1976). Theory of Self-Assembly of Hydrocarbon Amphiphiles into Micelles and Bilayers. *J. Chem. Soc.,* Faraday Trans. *2, 72*, 1525–1568.

[32] Nagarajan, R. Self-Assembly: The Neglected Role of the Surfactant Tail, Langmuir, 2002, *18*(01), 31–38.

[33] R. Nagarajan, Theory of Micelle Formation: Quantitative Approach to Predicting Micellar Properties from Surfactant Molecular Structure, Surfactant Science and Technology: Retrospects and Prospects, Taylor & Francis Group, 2003.

[34] Chorro, M.; Kamenka, N.; Faucompre, B.; Partyka, S.; Lindheimer, M.; Zana, R. (1996). Micellization and adsorption of a zwitterionic surfactant: N-dodecyl betaine - effect of salt. *Colloids and Surfaces A*, *110*, 249–261.

[35] Priebe, J. P., Souza, F. D., Silva, M., Tondo, D. W., Priebe, J. M., Micke, G. A., (2012). The chameleon-like nature of zwitterionic micelles: Effect of cation binding. *Langmuir*, *28*(3), 1758–1764.

[36] Okano, T., Tamura, T., Nakano, T. Y., Ueda, S. I., Lee, S., & Sugihara, G. (2000). Effects of side chain length and degree of counterion binding on micellization of sodium salts of α-myristic acid alkyl esters in water: A thermodynamic study. *Langmuir*, *16*(8), 3777–3783.

Chapter 4: Effects of electrostatic correlations and asymmetric ion sizes on the differential capacitance

4.1. Introduction

Differential capacitance (C_D) is essential information of electrochemical systems and it is used as an aid to understand the characteristics and behavior of the electrical double layer of a particular system. It shows how the structure of the electrical double layer (EDL) behaves as a function of the applied potential over an electrode. This structure acts contributing or preventing the transport of electrons to the surface of the electrode and, consequently, impacts on the kinetics of electrochemical reactions in the system (e.g. electrosynthesis, corrosion and charging/discharging of batteries) [1]. Because of that, the performance of these systems depends mostly on the electrical double layer close to the electrodes.

The dependence of the differential capacitance with the voltage, $C_d(U)$, quantifies the response of a capacitor of varying capacitance to the variation of the applied voltage. The shape of the differential capacitance curve varies depending on the kind of electrolyte used. For example, the differential capacitance of diluted electrolyte aqueous solutions usually is a camel shaped $C_D(U)$ curve. For highly concentrated electrolyte solutions, bell shaped differential capacitance curves are observed. Following these facts, it would be expected that ionic liquids (liquid electrolytes with no solvent) would present a differential capacitance curve tending to a bell shape – just as a very concentrated electrolyte solution. Nonetheless, what is observed is that ionic liquids actually present a camel shape on their differential capacitance curve. The reason for this behavior is still controversial. Most authors [2] support that the humps on the differential capacitance curve arise from the effect of neutral tails of one of the ions, which would behave as a solvent on an electrolyte solution, while other authors [3] affirm that the camel shape is due to the loss of the effect of van der Waals attractions near a charged electrode.

Another observation obtained from C_D data is that the width of the electrical double layer increases as function of the applied potential for high values of the surface charge. When trying to model this behavior, the classical Poisson-Boltzmann equation is not able to predict it, nor the camel shape of differential capacitance curves, unless steric effects are considered [4].

The objective of this work is to obtain an approach for modeling the differential capacitance of ionic liquids where the asymmetry of the ions (shape and size) is considered together with ionic electrostatic correlations. The model is validated by comparing our results with differential capacitance data from experiments, molecular simulations, and density functional theory (DFT) simulations.

4.2 Differential capacitance of ionic liquids

As mentioned before, the $C_d(U)$ curve for ionic liquids has been reported to have a camel shape, thus containing two asymmetrical peaks. From experiments with ionic liquids, it was observed that the difference between both peaks of the differential capacitance is associated with size difference of both ions. For example, a higher value of C_D close to the positive electrode can be attributed to the smaller size of anions that are able to pack more closely to the electrode surface, creating a stronger structure of the electrical double layer. One aspect observed by Li *et al*. [5] for two ionic liquids, with the same anion but with different alkyl chain length of the cation, is that the electrical double layer is more structured for the longer cation chain. This can be explained by the fact that a longer alkyl chain would increase solvophobic interactions, and for consequence the organization near the electrode. Costa *et al*. [6] also observed that, by increasing the alkyl chain of cations, the width of the electrical double layer also increases, suggesting that there is a multilayer of interpenetrating layers of cations and anions on the interface of the electrode. These multilayering and packing observed in systems containing ionic liquids indicate that ionic electrostatic correlation effects do play an important role and cannot be neglected.

4.2.1 Modeling the Differential Capacitance

The majority of the attempts to describe the behavior of ionic liquids rely on molecular simulations and density functional theory (DFT) approaches [7-10]. Although they have enabled us to understand several peculiarities of ionic liquids, their elevated computational cost is a drawback and causes difficulties to use them as simple methodologies to describe and design systems and processes containing ionic liquids. Furthermore, they are not recommended when trying to describe the impact of several parameters and conditions, nor for large and complex systems. In order to fulfill this gap on the description of ionic liquids, the mean field theory approach with a adequate modified Poisson-Boltzmann equation can be an alternative of low computational cost. In this case, data obtained from molecular and DFT simulations can be used to validate and refine mean field theory models.

In the following items we describe some of the most important observations obtained by different methodologies to model the differential capacitance of ionic liquids.

Modeling of ionic liquids by molecular dynamics

As ionic liquids are very large molecules, an usual approach is to model them as charged hard spheres. Fedorov and Kornishev [11] used this approach in molecular dynamics to simulate an ionic liquid placed between two charged plates. The cation and anion were modeled as hard spheres of different sizes. In this work they observed that short-range ionic correlations were responsible for the overscreening effect, which cannot be predicted by the fundamental mean field theory. They also observed that size asymmetry of ions resulted on the characteristic asymmetric camel shape of the differential capacitance curve. Later, Kornishev *et al*. [12] expanded their previous analysis and considered that anions and cations would differ in sizes and charge densities. The cations, composed by two hard spheres, one uncharged and one charged sphere – would have the alkyl chain usually present in the cation of ionic liquids represented by the uncharged sphere. This study brought the attention to the effect of a neutral tail to the behavior of ionic liquids, which was later studied thoroughly by Henderson *et al*. (2013). These authors observed that the neutral tail of ionic liquids behave the same way as the solvent on an electrolyte solution, and this would explain

why ionic liquids have differential capacitance curves similar in shape to the aqueous electrolyte solutions.

Breitsprecher *et al*. [8] modeled an ionic liquid between two charged electrodes using the coarse grained technique. They considered the ions as soft spheres, which could be of different sizes and valences. Their work made possible to reproduce qualitatively the behavior of the differential capacitance, as a function of both size and valence of the ions. Furthermore, the authors were able to predict a transition between the shapes of the $C_D(U)$ curve, from camel to bell shape by just changing the density of the ionic liquid. This might indicate that the free volume of an ionic liquid is a relevant parameter when considering the position of each peak of the differential capacitance curve. These peaks would be located closer to each other for ionic liquids with a very low free volume, with the extreme case being the one where both peaks are so close together that they merge to form a bell shaped differential capacitance curve – the same shape observed on the differential capacitance curve of highly concentrated aqueous electrolyte solutions. On their following work, Breitsprecher *et al*. [9] considered that the cation had a triangular geometry. This made possible to observe that the distribution of charges over a complexly shaped cation impacts on the cation orientation close to the charged surface. This structure close to the electrode showed to strongly influence the behavior of the differential capacitance. Merlet *et al*. [14] also observed through molecular dynamics simulations of ionic liquids that the orientation of the ions close to the charged surface impacts on the electrical double layer structure, and then on the differential capacitance.

Besides the characteristic of the ionic liquids being analyzed, the electrode might also play an important role on the behavior of the differential capacitance. Vatamanu *et al*. [15] used atomist simulations to predict the differential capacitance of the ionic liquid [$C_n$mim][TFSI] between flat and rough electrode surfaces. The same way as experimentally observed [1,16] Vatamanu *et al*. [15] observed that the structure of the electrode surface (if it is smooth or rough) also affects the values of differential capacitance, but not the shape of the $C_D(U)$ curve. Here, we opted to consider that the ionic liquid is placed between flat blocking electrodes in order to observe just the influence the differential capacitance in ionic liquids.

Modeling of ionic liquids by density functional theory

Density functional theory (DFT) had also being applied to describe the differential capacitance of ionic liquids. The same way as molecular simulations, the DFT approach was able to predict the transition between the camel and bell shape of the differential capacitance curve. Furthermore, Liang *et al*. [17] and Ma *et al*. [7] predicted the formation of alternating layers of anions and cations close to the electrode surfaces, which is not predicted by the Classical Poisson-Boltzmann approach, but that it can be predicted by the inclusion of the electrostatic correlations on the modified Poisson-Boltzmann equation.

Modeling of ionic liquids by Poisson-Boltzmann equation

When using the Gouy-Chapman simplification of the Poisson-Boltzmann equation, the curve of differential capacitance as a function of the electrode potential diverges for high voltages, which leads to a U-shaped curve. Furthermore, it neglects free volume effect by considering ions as point-like charges, which makes it unsuitable to be used to describe any electrolyte solution that is not diluted. In order to overcome the restrictions of the Gouy-Chapman approach, Kornyshev [18] took into account the effects of the ion sizes. Instead of the U-shaped differential capacitance curve, Kornyshev [18] observed a differential capacitance curve with its maximum located close to the potential of zero charge, *i.e.*, a bell-shaped curve. This approach was derived from a mean-field lattice-gas description of a concentrated electrolyte and the observed bell-shape of the differential capacitance is the same as the one predicted by the Bikerman-Freise model for an aqueous electrolyte solution when the solvent concentration is zero [11]. If we consider that an ionic liquid is incompressible with no free volume, this would be the expected behavior of its differential capacitance. However, the camel shaped curve is experimentally observed, and cannot be described by their approaches.

4.3 Theoretical formulation

Here, we coupled the modified Poisson-Boltzmann equation that takes into account electrostatic correlations together with a lattice model to account for free-

volume and ionic size asymmetry on the ions of ionic liquids. To consider the steric effects we modified the approach developed by Han *et al.* [19].

In this approach [19], the Helmholtz free energy of the system can be defined as:

$$F = e\phi(N_+ - N_-) - kT \ln \Omega \tag{4.1}$$

Where N_+ and N_- denote the number of cations and anions respectively, ϕ is the mean-field electrostatic potential, e is the elementary charge, T is the temperature, k the Boltzmann constant and Ω is the number of possible different configurations of the ions in the lattice. Following Han *et al.* (2014), we computed $\Omega = \Omega_+\Omega_-$. We also considered that the anions are hard spheres of radius r_- and the cations are chains of tangent α hard spheres with radius r_+ each as illustrated on Figure 9.

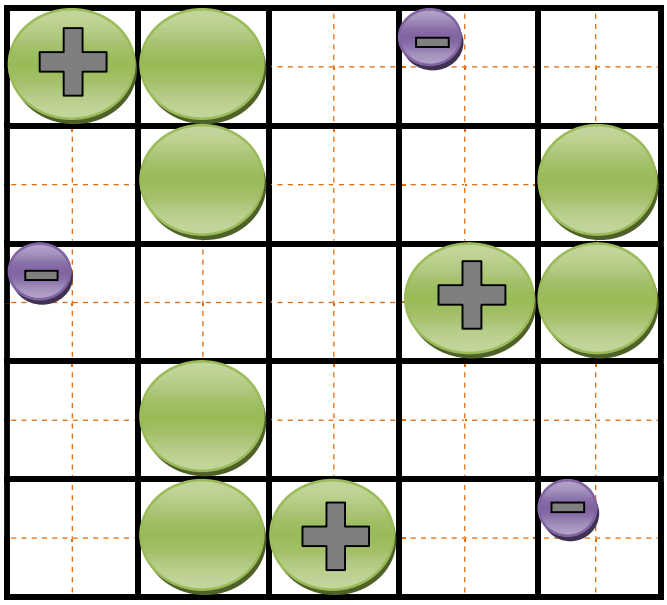

Figure 9 - Schematic 2D representation of the lattice model for ionic liquids considering that cations are larger than anions.

Regarding the consideration of spaces on the lattice, molecular simulations have predicted large free volume (cavities) inside ionic liquids justifying that some sites of the lattice may not be occupied by any ion [20].

We can calculate Ω_+ following Han *et al.* (2014) as:

$$\Omega_+ = \frac{N!}{\alpha N_+!\,(N - \alpha N_+)!} \tag{4.2}$$

It is convenient to define a parameter that describes the degree of asymmetry between the cation and the anion. Then we can define the parameter ξ as the ratio between the anion and cation volumes.

$$\xi = \frac{V_-}{V_+} = \frac{r_-^3}{\alpha\, r_+^3} \tag{4.3}$$

For a large number of ionic liquids it is expected that ξ varies from 0 to 1. Thus, the number of vacancies in the lattices left for the anions is $[(N - \alpha N_+)/\xi]$, where the brackets denote the integer part of this number. Then Ω_- is given by:

$$\Omega_- = \frac{[(N - \alpha N_+)/\xi]!}{N_-!\,([(N - \alpha N_+)/\xi] - N_-)!} \tag{4.4}$$

And the total number of configurations is:

$$\Omega = \frac{N!}{\alpha N_+!\,(N - \alpha N_+)!}\,\frac{[(N - \alpha N_+)/\xi]!}{N_-!\,([(N - \alpha N_+)/\xi] - N_-)!} \tag{4.5}$$

Using the Stirling approximation, is (for $N \gg 1$)

$$\ln N! \approx N \ln N - N \tag{4.6}$$

the partition function Ω can be rewritten:

$$\begin{aligned} \ln \Omega = {} & N \ln N + [(N - \alpha N_+)/\xi] \ln[(N - \alpha N_+)/\xi] - \alpha N_+ \ln \alpha N_+ \\ & - (N - \alpha N_+) \ln(N - \alpha N_+) - N_- \ln N_- \\ & + \{[(N - \alpha N_+)/\xi] - N_-\} \ln\{[(N - \alpha N_+)/\xi] - N_-\} \end{aligned} \tag{4.7}$$

From Eqs. (4.1) and (4.7), we can express the chemical potential of each ion:

$$\mu_+ = \frac{\partial F}{\partial N_+} \tag{4.8}$$

$$\mu_+ = e\phi - kT\left\{-\frac{\alpha}{\xi}\ln\left[\frac{N-\alpha N_+}{\xi}\right] - \alpha\ln\alpha N_+ + \alpha\ln(N-\alpha N_+) + \frac{\alpha}{\xi}\ln\left(\frac{N-\alpha N_+}{\xi} - N_-\right)\right\} \tag{4.9}$$

$$\mu_- = \frac{\partial F}{\partial N_-} \tag{4.10}$$

$$\mu_- = -e\phi - kT\left\{\ln\left(\left[\frac{N-\alpha N_+}{\xi}\right] - N_-\right) - \ln N_-\right\} \tag{4.11}$$

For the ions in the bulk, far from the charged electrode, we have $\phi = 0$ and $N_+ = N_- = N_0$ and their chemical potentials are:

$$\mu_{+0} = -kT\left\{-\frac{\alpha}{\xi}\ln\left[\frac{N-\alpha N_0}{\xi}\right] - \alpha\ln\alpha N_0 + \alpha\ln(N-\alpha N_0) + \frac{\alpha}{\xi}\ln\left(\frac{N-\alpha N_0}{\xi} - N_0\right)\right\} \tag{4.12}$$

$$\mu_{-0} = -kT\left\{\ln\left(\left[\frac{N-\alpha N_0}{\xi}\right] - N_0\right) - \ln N_0\right\} \tag{4.13}$$

Considering the local chemical equilibrium states, the chemical potential of each component is the same anywhere. With this we can write the following equalities:

$$\mu_+ - \mu_{+0} = 0 = e\phi - kT\left\{-\frac{\alpha}{\xi}\ln\left[\frac{N-\alpha N_+}{N-\alpha N_0}\right] - \alpha\ln\frac{N_+}{N_0} + \alpha\ln\left(\frac{N-\alpha N_+}{N-\alpha N_0}\right) + \frac{\alpha}{\xi}\ln\left(\frac{N-\alpha N_+ - \xi N_-}{N-\alpha N_0 - \xi N_0}\right)\right\} \tag{4.14}$$

$$\mu_- - \mu_{-0} = 0 = -e\phi - kT\left\{\ln\left(\frac{N-\alpha N_+ - \xi N_-}{N-\alpha N_0 - \xi N_0}\right) - \ln\frac{N_-}{N_0}\right\} \tag{4.15}$$

Using the auxiliary parameters of porosity (γ) and compressibility (η):

$$\gamma = \frac{2N_0}{N} \tag{4.16}$$

$$\eta = \frac{2}{\gamma} - \alpha - \xi \tag{4.17}$$

and rewriting equations 4.16 and 4.17 in terms of concentrations, we obtain:

$$\exp\left(-\frac{e\phi}{kT}\right) - \frac{1}{\eta}\left[\frac{2}{\gamma} - \alpha\frac{c_+}{c_0} - \xi\frac{c_-}{c_0}\right] + \frac{c_-}{c_0} = 0 \tag{4.18}$$

$$\exp\left(\frac{e\phi}{kT}\right) - \left(\frac{1}{\eta}\left[\frac{2}{\gamma} - \alpha\frac{c_+}{c_0} - \xi\frac{c_-}{c_0}\right]\right)^{\frac{1}{\xi}} + \frac{c_+}{c_0} + \left(\frac{1}{\eta}\left[\frac{2}{\gamma} - \alpha\frac{c_+}{c_0}\right]\right)^{\frac{1-\xi}{\xi}} = 0 \tag{4.19}$$

When $\alpha = 1$, equations 4.18 and 4.19 recover the model proposed by Han *et al*. (2014).

4.3.1 Differential capacitance model

From its definition, the differential capacitance (C_D) is a parameter that relates the dependence of the charge (σ) of an electrode surface as a function of the applied potential (ϕ) for a given condition (considering constant $\mu, T,$ and P). Then we have:

$$C_D = \left(\frac{\partial\sigma}{\sigma\psi}\right)_{\mu,T,P} \tag{4.20}$$

To predict the differential capacitance of ionic liquids using the mean field approach, we consider that the electrostatic potential (ϕ) can be described using the fourth order Poisson equation (BKS model) [21] – where the electrostatic correlations are taken into account, and the charge density expression (ρ) includes the effects of the size asymmetry of anion and cation. Both expressions are presented below, where l_c is the electrostatic correlation length.

$$\varepsilon(l_c^2\,\nabla^4\psi - \nabla^2\psi) = \rho \tag{4.21}$$

$$\rho = e(c_+ - c_-) \tag{4.22}$$

For a better mathematical treatment of these expressions we defined dimensionless variables, as follows:

$$\tilde{l}_c = \frac{l_c}{\lambda_D} \tag{4.23}$$

$$y = \frac{e\phi}{kT} \tag{4.24}$$

$$\tilde{x} = \frac{x}{\lambda_D} \tag{4.25}$$

$$\tilde{\rho} = \frac{\rho}{ec_0} \tag{4.26}$$

Where the square of the Debye length (λ_D^2) is:

$$\lambda_D^2 = \frac{\varepsilon kT}{2e^2 c_0} \tag{4.27}$$

Then on the dimensionless form we have:

$$\tilde{l}_c^2 \, \nabla^4 y - \nabla^2 y = \tilde{\rho} \tag{4.28}$$

To study the differential capacitance of ionic liquids in blocking electrode, we consider flat electrode and a one-dimensional problem:

$$\tilde{l}_c^2 \, \frac{d^4 y}{d\tilde{x}^4} - \frac{d^2 y}{d\tilde{x}^2} = \tilde{\rho}(\tilde{x}) \tag{4.29}$$

To solve it using the solver for boundary value problem *bvp4c* on *Matlab*, we need to transform the previous fourth order differential equation into four first order differential equations. For that, we define the following group of auxiliary variables.

$$u = \frac{d^2 y}{d\tilde{x}^2} \tag{4.30}$$

$$\phi_1 = \frac{dy}{d\tilde{x}} \tag{4.31}$$

$$u_1 = \frac{du}{d\tilde{x}} \tag{4.32}$$

Then the resulting set of equations is:

$$\frac{du_1}{d\tilde{x}} = \frac{1}{\tilde{l}_c^2}\,\tilde{\rho}(\tilde{x}) + u \tag{4.33}$$

$$\frac{dy_1}{d\tilde{x}} = u \tag{4.34}$$

$$\frac{du}{d\tilde{x}} = u_1 \tag{4.35}$$

$$\frac{dy}{d\tilde{x}} = y_1 \tag{4.36}$$

The boundary conditions are defined at the surface of the electrode ($\tilde{x} = 0$) and on the bulk of the electrolyte solution $\tilde{x} \to \infty$. The boundary conditions are defined as:

$$y|_{\tilde{x}=0} = y_0 \tag{4.37}$$

$$y|_{\tilde{x}=\infty} = 0 \tag{4.38}$$

$$\left.\frac{d^3y}{d\tilde{x}^3}\right|_{\tilde{x}=0} = 0 \tag{4.39}$$

$$\left.\frac{d^2y}{d\tilde{x}^2}\right|_{\tilde{x}=\infty} = 0 \tag{4.40}$$

When using the auxiliary variables from Eqs. 4.30 to 4.32, the resulting set of boundary conditions used to solve the set of first order differential equations 4.33 to 4.36 becames:

$$y|_{\tilde{x}=0} = y_0 \tag{4.41}$$

$$y|_{\tilde{x}=\infty} = 0 \tag{4.42}$$

$$u_1|_{\tilde{x}=0} = 0 \tag{4.43}$$

$$u|_{\tilde{x}=\infty} = 0 \tag{4.44}$$

After obtaining the profile of the electrostatic potential we can calculate the differential capacitance (C_D) for a certain applied potential to the surface (y_0). From Equation 4.20, we can express the capacitance relative to the Debye-Huckel capacitance $(C_{DH} = \varepsilon/\lambda_D)$ as follows (Storey and Bazant, 2012):

$$\frac{C}{C_{DH}} = -\frac{1}{y(0)}\frac{dy}{d\tilde{x}} \tag{4.45}$$

And considering the capacitance of the Stern layer C_{stern}, we will arrive on the final expression for the differential capacitance(C_D):

$$\frac{1}{C_D} = \frac{1}{C} + \frac{1}{C_{stern}} \tag{4.46}$$

In this work we considered the C_{Stern} to be a constant. The capacitance of the electrode (C_{El}) is not taken into account because, for metallic electrodes or glassy carbon electrodes, C_{El} is usually very high and would not have a significant contribution for the measured differential capacitance (Lockett *et al.*, 2010). If the electrodes are composed by semiconductors, C_{El} must be considered.

4.3.2 Numerical strategy

The resulting set of partial differential equations was solved using the solver *bvp4c* of Matlab. This solver uses the collocation method for the boundary value problems. One of its requirements is a good initial guess. Taking into account that this problem must be solved several times, we used the result of former electrostatic potential as a better initial guess for a higher potential. To describe one curve of the differential capacitance we usually have its value calculated for different electrostatic potentials on a range $[-V, V]$. Then on this approach we start with a positive and very small value of electrostatic potential applied (ϕ_0) and the numerical result of the system of differential equations would be the initial guess for the next simulation considering a

small increase $(\phi_0 + \delta)$ on the surface potential. The same procedure is repeated to cover the full range $[-V, V]$.

As the model presented here has three parameters that define the structure of double layer in ionic liquids (compressibility γ, ionic size ration ξ, and correlation length l_c) these parameters were analyzed and results obtained here were compared to experimental, molecular simulation, and DFT data. For each set of data we defined the parameters to be fitted and for the parameter fitting we performed the optimization by using the *lsqnonlin* optimizer from Matlab, which is suitable for nonlinear data-fitting problems. This tool searches for the parameters that lead to the minimum of the sum of the difference between the differential capacitance obtained by our model and the one from experiments (or molecular/DFT simulation), *i.e.* the objective function is $F_{obj} = \sum_i \left(C_D|_{model} - C_D|_{experimental}\right)^2$.

4.4 Results and discussion

To better understand the impact of ionic electrostatic correlations on the differential capacitance of ionic liquids, we first analyzed how the correlation length affects the $C_D(U)$ curve. For that, we fixed all other parameters of this model and considered a hypothetical ionic liquid that has a cation larger than the anion. In this work we follow the definition of the correlation length proposed by Alijó *et al*. [23] where the correlation length is defined as a function of the radius of the electrolyte ions. Because of that, the size of the electrolytes and the correlation length are directly related. From Figure 10 we can observe that while increasing the correlation length, the dimensionless differential capacitance reduces significantly. This can be related to the modification on the permittivity of the electrical double layer due to electrostatic correlations effect. This is particularly important when describing differential capacitance with mean-field approaches because they tend to overestimate the value of C_D , and attempts to fit them to experimental data might lead to a super estimation of steric effects on the system, resulting on the prediction of larger ions than they really are [22].

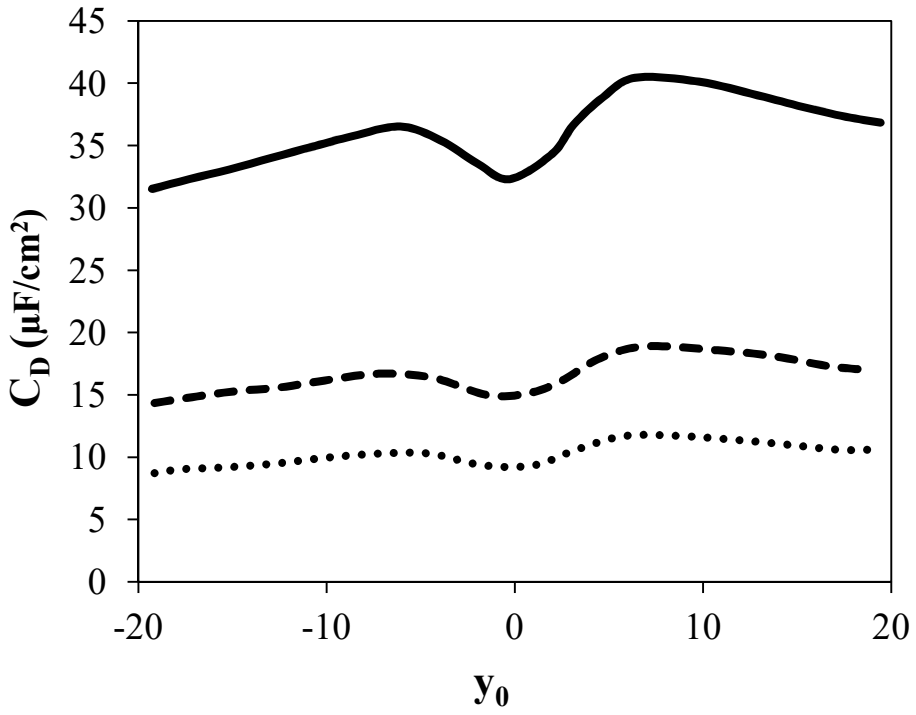

Figure 10 – Differential capacitance ($\boldsymbol{C_D}$) of ionic liquids obtained from the proposed model as a function of the dimensionless applied potential ($\boldsymbol{y_0}$). The continuous line is for the correlation length ($\boldsymbol{l_c}$) equal to 5 $\boldsymbol{Å}$, the dashed line represents $\boldsymbol{l_c = 10\,Å}$, and the dotted line $\boldsymbol{l_c = 15\,Å}$. We fixed $\boldsymbol{T = 25°C}$, $\boldsymbol{\gamma = 0.1}$, and $\boldsymbol{\xi = 0.5}$. We also fixed $\boldsymbol{C_{stern} = 125, \varepsilon = 5}$ and $\boldsymbol{T = 25}$°C.

We also analyzed the impact caused by the ionic liquid compressibility (γ) on the differential capacitance calculated by the proposed model. The way the compressibility is defined here reflects the magnitude of the amount of free volume present in the ionic liquid. A small compressibility parameter γ means that there is a small amount of ions occupying a certain volume of ionic liquid, which implies that there is a large amount of voids in this ionic liquid. From Figure 11, we can observe that as we increase the value of γ, the peaks of the differential capacitance curve tend to get closer. In the limit of this behavior, larger γ, the model converges to a bell-shaped capacitance curve as observed using DFT and molecular simulations by, respectively, Jiang *et al*. [17] and Fedorov & Kornyshev [11].

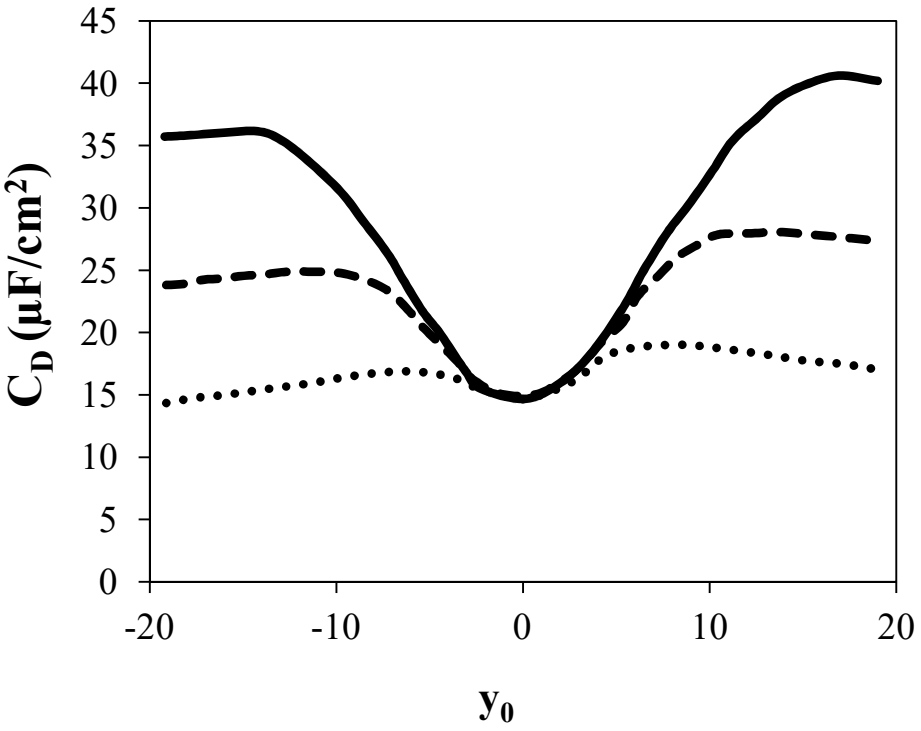

Figure 11 - Differential capacitance ($\boldsymbol{C_D}$) of ionic liquids obtained from the proposed model as a function of the dimensionless applied potential ($\boldsymbol{y_0}$). The continuous line is for the compressibility parameter ($\boldsymbol{\gamma}$) equal to 0.001, the dashed line represents $\boldsymbol{\gamma = 0.01}$, and the dotted line $\boldsymbol{\gamma = 0.1}$. We fixed $\boldsymbol{T = 25°C}$, $\boldsymbol{l_c = 10\,Å}$, and $\boldsymbol{\xi = 0.5}$. We also fixed $\boldsymbol{C_{stern} = 125, \varepsilon = 5}$ and $\boldsymbol{T = 25°C}$.

We analyzed the impact of the size asymmetry of the ions in the differential capacitance curve. For that, we considered three cases: the cation is ten times larger than the anion ($\xi = 0.1$), the cation is two times larger than the anion ($\xi = 0.5$) and the cation and the anion have the same size($\xi = 1$). As we can observe from Figure 12, as we change the ratio between the anion and the cation size (ξ), the difference of the peaks of the capacitance curve starts to increase, and the largest asymmetry of those peaks is observed for the biggest difference between the size of the anions. This is explained by the fact that the smaller ion (in these cases the anion) is able to pack more close to the charged electrode, increasing the differential capacitance for positive values of potential applied to the electrode.

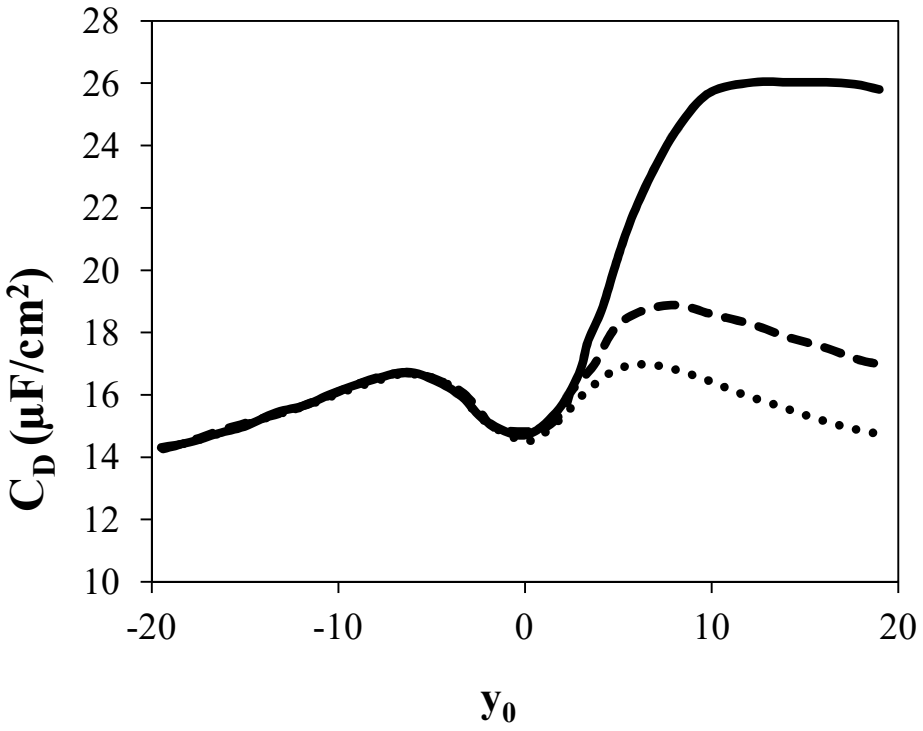

Figure 12 - Differential capacitance ($\boldsymbol{C_D}$) of ionic liquids obtained from the proposed model as a function of the dimensionless applied potential ($\boldsymbol{y_0}$). The continuous line is for the size ratio between the anion and the cation $\boldsymbol{\xi}$ equal to 0.1, the dashed line represents $\boldsymbol{\xi = 0.5}$, and the dotted line $\boldsymbol{\xi = 1}$. We fixed $\boldsymbol{T = 25}$℃, $\boldsymbol{l_c = 10}$ Å , and $\boldsymbol{\gamma = 0.1}$.

4.4.1 Correlate differential capacitance data (parameter estimation)

In order to test the proposed model for describing differential capacitance of different ionic liquids, we compared it to different sets of data, from experiments, molecular simulations and from density functional theory approaches. As this model considers some parameters that are not straight forward to be obtained because they are related to the structural characteristics of the ionic liquids (compressibility, size ratio of the ions, and correlation length), we performed a parameter fitting for each set of data. The validation of the model is related with physical meaning of the parameters obtained for each system.

The first set of data is from Kornyshev *et al*. (2008). In order to analyze the effects of ion size asymmetries, Kornyshev *et al*. performed a Monte Carlo simulation

of asymmetric ionic liquids, considering that the cation is represented by a different number of beads. We first compare results from the proposed model to the results presented by Kornyshev *et al*. [11] for an ionic liquid where the cation is represented by two beads. In Figure 13 we can observe that our model (continous line) is able to describe the same qualitative behavior obtained by the Kornyshev model (dashed line). The very small value for the compressibility parameter (γ) is associated with high free volume expected for mixtures of dimmers and monomers. The same is observed for the second case (Figure 14) where a cation is described by three beads. Again we obtain a good description of the differential capacitance when compared to Kornyshev *et al.* [11]. In this analysis we opted for also adjusting the correlation length (l_c). For both sets of data we obtained $l_c = 21.484$ Å and $l_c = 25.554$ Å. These values are very close to the radius of the beads used in the molecular simulations performed by Kornyshev *et al*. [11] $(25\,\text{Å})$, which helps to reinforce the methodology adopted by Alijó *et al*. [23] where they define the correlation length as the radius of the ions in solution, and suggests that the parameters obtained are physical and reasonable.

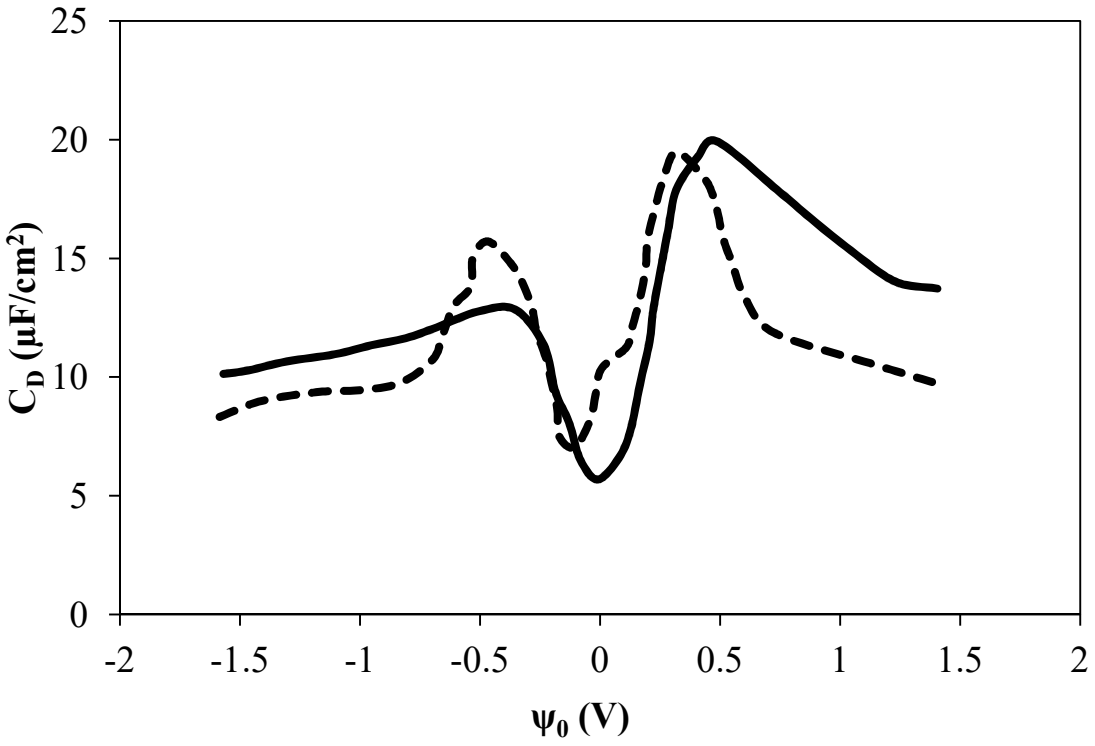

Figure 13 – Comparison of the proposed model to the results obtained by Kornyshev *et al*. [11] (dashed line) with two-bead cation and one-bead anion model for an ionic liquid of $\boldsymbol{\varepsilon = 5}$ at $\mathbf{100}$℃. The parameters are $\boldsymbol{l_c = 21.484}$ Å, $\boldsymbol{\gamma = 0.0034}$, $\boldsymbol{\xi = 0.13}$ and we fixed $\boldsymbol{C_{stern} = 125}$.

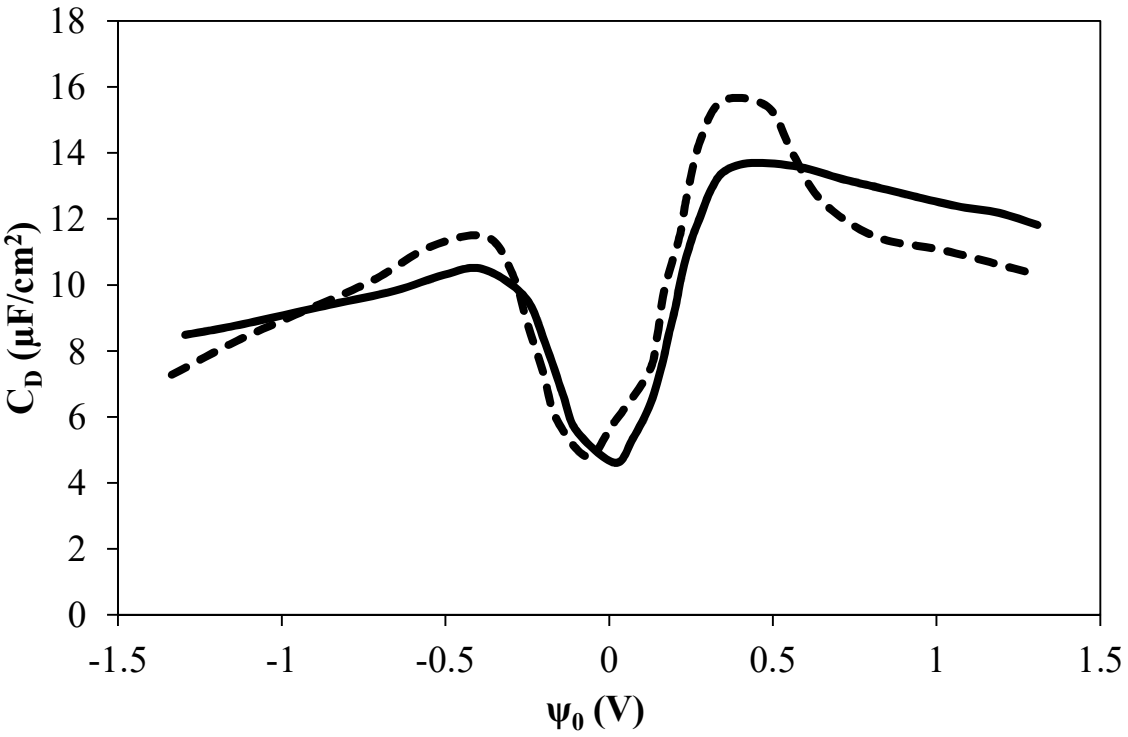

Figure 14 - Comparison of the proposed model to the results obtained by Kornyshev *et al*. [11] (dashed line) with three-bead cation and one-bead anion model for an ionic liquid of $\boldsymbol{\varepsilon = 5}$ at $\boldsymbol{100℃}$. The parameters obtained for this system are $\boldsymbol{l_c = 25.554}$ **Å** , $\boldsymbol{\gamma = 0.0034}$, $\boldsymbol{\xi = 0.272}$, and fixed $\boldsymbol{C_{stern} = 125}$.

We also compared the differential capacitance of ionic liquids from our model to the results obtained by Jiang *et al*. [17] who used a density functional theory approach. In their work they analyzed the impact of different ionic densities on the shape of the differential capacitance curve. In Figure 15 we present the differential capacitance curves (dashed lines) for two different reduced packing fractions, according to the methodology presented by Jiang *et al*. [17], one equal to 0.5 that represents a very dense ionic liquid, and one equal to 0.01, which is a less denser system. Then in our simulation we aimed to adjust the parameter γ that describes the compressibility of the ionic liquid in order to verify how it varies for different conditions of packing of the ionic liquid.

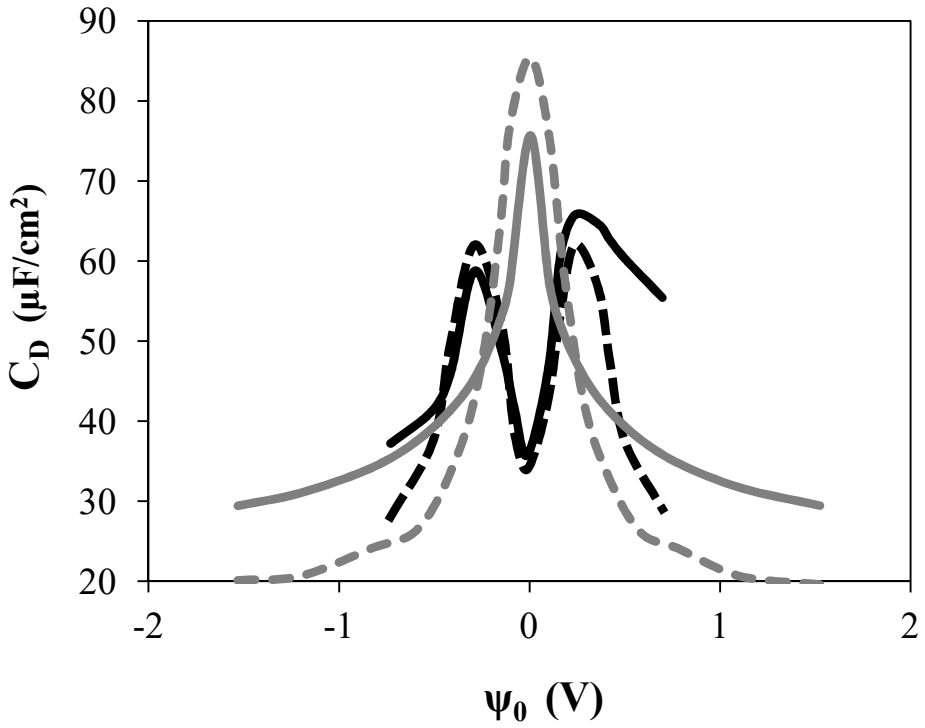

Figure 15 - Comparison of the proposed model (continuous lines) to the results obtained by Jiang *et al*. [17] using DFT calculation (dashed lines) for an ionic liquid with reduced ionic density equal to 0.5 (gray dashed line) and equal to 0.01 (black dashed line). The parameters are: for gray continuous line: $\boldsymbol{l_c = 5.0}$ Å , $\boldsymbol{\gamma = 0.9}$, $\boldsymbol{\xi = 1}$, and $\boldsymbol{C_{stern} = 125}$, and for black continuous line: $\boldsymbol{l_c = 5.0}$ Å , $\boldsymbol{\gamma = 0.002}$, $\boldsymbol{\xi = 0.9}$. The temperature is fixed at $\boldsymbol{T = 25}$℃, and the dielectric constant of the ionic liquid is $\boldsymbol{\varepsilon = 12.5}$.

As we can observe, our model is able to predict fairly well the differential capacitance obtained by Jiang *et al*. [17], and the compressibility (γ) modeled in our work reduces as the density of the ionic liquid is reduced. This reassures the importance of considering the effects of free volume of ionic liquids, and verifies that the compressibility (γ) parameter has a physical meaning and can be used to obtain information about the packing fraction of ionic liquids.

Finally, we compared the C_D calculated from the proposed model with experimental data obtained by Lockett *et al.* [1] for the ionic liquid hmimCl at two different temperatures $100℃$ and $120℃$. As we don't have information about the size of the $hmim^+$ cation, or of the compressibility of this ionic liquid, we adjusted the correlation length (l_c), the compressibility (γ), and the ratio of anion and cation sizes

(ξ). We performed this adjustment for the C_D at $100℃$, and applied the obtained parameters to describe the data at $120℃$.

The model was able to describe well the peaks of differential capacitance with the parameters presented in Figure 16 and Figure 17. However, it was not possible to provide good values of the differential capacitance curve close to the zero electrostatic potential. Kornyshev *et al*. [11] with molecular simulations tried to describe the C_D data for hmimCl at 100ºC. Similar to our model, they were not able to describe the valley of the differential capacitance curve. But when we compare our model to Kornyshev's molecular simulation we have a very good description of the valley observed by them, the same way as our simulations are in accordance with the ones performed by Jiang *et al*. [17] . That might be an indicative that some effects that are important at lower magnitudes of applied potentials are not being considered by our model, and was also not considered on Kornyshev's Monte Carlo simulations, nor Jiang's density functional theory simulations. These effects might be related to long range screening interactions at low applied voltages which are not included in our model.

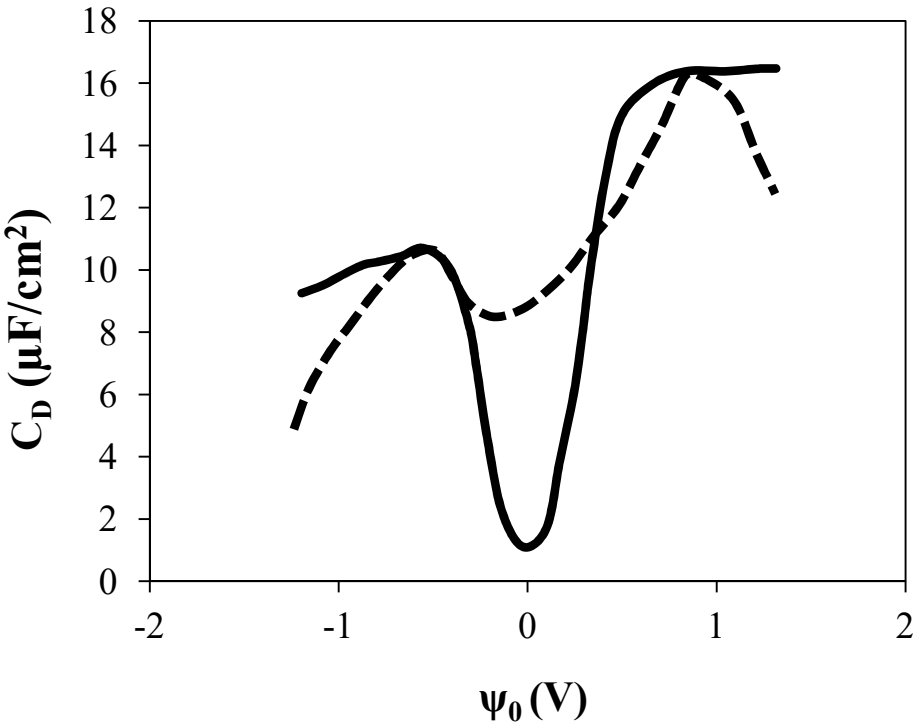

Figure 16 - Comparison of the proposed model (continuous line) to the experimental data obtained by Lockett *et al*. [1] (dashed line) for hmimCl at $\mathbf{100°C}$. The parameters are $\boldsymbol{l_c = 36.429}$ Å , $\boldsymbol{\gamma = 0.005}$, $\boldsymbol{\xi = 0.1}$, and $\boldsymbol{C_{stern} = 125}$. The dielectric constant of the ionic liquid is considered $\boldsymbol{\varepsilon = 5}$.

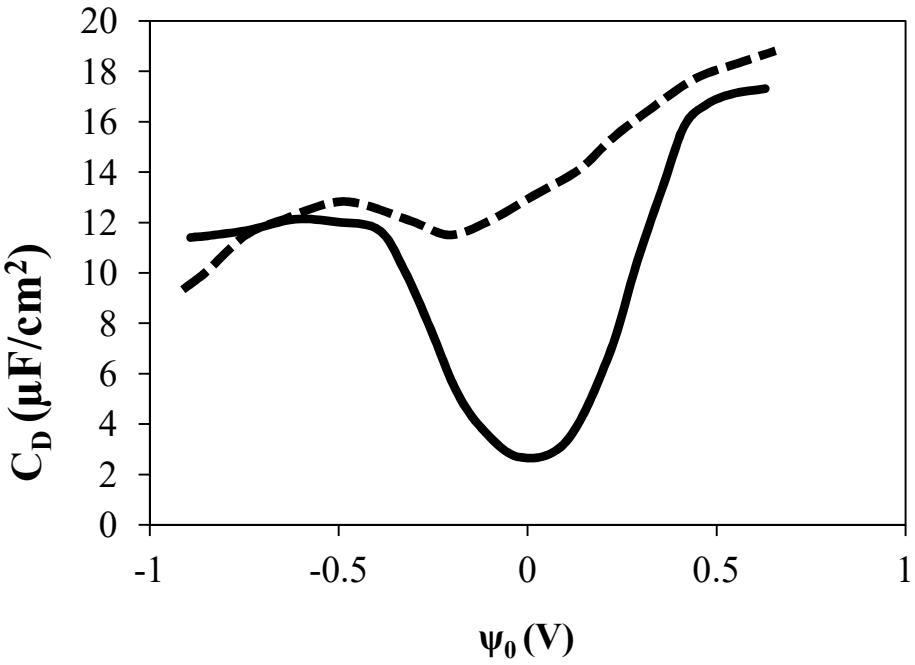

Figure 17 - Comparison of the proposed model (continuous line) to the experimental results obtained by Lockett *et al.* [1] (dashed line) for hmimCl at $\mathbf{120}$℃. The parameters are $\boldsymbol{l_c = 36.4}$ Å, $\boldsymbol{\gamma = 0.005}$, $\boldsymbol{\xi = 0.1}$, and $\boldsymbol{C_{stern} = 125}$. The dielectric constant of the ionic liquid is considered $\boldsymbol{\varepsilon = 5}$.

4.5 Final Remarks

Here, we provide a model to calculate the differential capacitance that takes into account both the electrostatic correlations and the asymmetry in size and shape of ions. Electrostatic correlations play an important role in the differential capacitance, being responsible for the reduction of the magnitude of C_D. Furthermore, the present approach is able to describe very well the differential capacitance of ionic liquids obtained by both molecular simulations and density functional theories. When compared directly to experimental data, the model provides good information of the peaks of the differential capacitance curve, which are directly related to the ion sizes of the ionic liquid. For low applied potentials our model does not predict well the differential capacitance which can be associated to long range screening interactions between the ions that are not included in mean field models.

References

[1] Lockett, V., Sedev, R., Ralston, J., Horne, M., Rodopoulos, T. (2008). Differential capacitance of the electrical double layer in imidazolium-based ionic liquids: Influence of potential, cation size, and temperature. *Journal of Physical Chemistry C*, *112*(19), 7486–7495.

[2] Henderson, D., Lamperski, S., Bari Bhuiyan, L., & Wu, J. (2013). The tail effect on the shape of an electrical double layer differential capacitance curve. *Journal of Chemical Physics*, *138*(14), 1–4.

[3] Trulsson, M., Algotsson, J., Forsman, J., & Woodward, C. E. (2010). Differential capacitance of room temperature ionic liquids: The role of dispersion forces. *Journal of Physical Chemistry Letters*, *1*(8), 1191–1195.

[4] Nakayama, Y., & Andelman, D. (2015). Differential capacitance of the electric double layer: The interplay between ion finite size and dielectric decrement. *Journal of Chemical Physics*, *142* (4).

[5] Li, H., Endres, F., Atkin, R. (2013). Effect of alkyl chain length and anion species on the interfacial nanostructure of ionic liquids at the Au(111)-ionic liquid interface as a function of potential. *Physical Chemistry Chemical Physics: PCCP*, *15*(35), 14624–33.

[6] Costa, R., Pereira, C. M., & Silva, F. (2010). Double layer in room temperature ionic liquids: influence of temperature and ionic size on the differential capacitance and electrocapillary curves. *Physical Chemistry Chemical Physics: PCCP*, *12*(36), 11125–11132.

[7] Ma, K., Woodward, C. E., & Forsman, J. (2014). Classical density functional study on interfacial structure and differential capacitance of ionic liquids near charged surfaces. *Journal of Physical Chemistry C*, *118*(29), 15825–15834.

[8] Breitsprecher, K., Košovan, P., & Holm, C. (2014a). Coarse-grained simulations of an ionic liquid-based capacitor: I. Density, ion size, and valency effects. *Journal of Physics: Condensed Matter*, *26*(28), 284108.

[9] Breitsprecher, K., Košovan, P., & Holm, C. (2014b). Coarse-grained simulations of an ionic liquid-based capacitor: II. Asymmetry in ion shape and charge localization. *Journal of Physics: Condensed Matter*, *26*(28), 284114.

[10] Bedrov, D., Vatamanu, J., & Hu, Z. (2014). Ionic liquids at charged surfaces: Insight from molecular simulations. *Journal of Non-Crystalline Solids*, *407*, 339–348.

[11] Fedorov, M. V., & Kornyshev, A. a. (2008). Ionic liquid near a charged wall: Structure and capacitance of electrical double layer. *Journal of Physical Chemistry B*, *112*(38), 11868–11872.

[12] Georgi, N., Kornyshev, a. a., & Fedorov, M. V. (2010). The anatomy of the double layer and capacitance in ionic liquids with anisotropic ions: Electrostriction vs. lattice saturation. *Journal of Electroanalytical Chemistry*, *649*(1–2), 261–267.

[13] Henderson, D., Lamperski, S., Bari Bhuiyan, L., & Wu, J. (2013). The tail effect on the shape of an electrical double layer differential capacitance curve. *Journal of Chemical Physics*, *138*(14), 1–4.

[14] Merlet, C., Limmer, D. T., Salanne, M., van Roij, R., Madden, P. A., Chandler, D., & Rotenberg, B. (2014). The Electric Double Layer Has a Life of Its Own. *The Journal of Physical Chemistry C*, *118*(32), 140606072147007.

[15] Vatamanu, J., Borodin, O., Bedrov, D., & Smith, G. D. (2012). Molecular Dynamics Simulation Study of the Interfacial Structure and Differential Capacitance of Alkylimidazolium Bis(trifluoromethanesulfonyl)imide [Cnmim][TFSI] Ionic Liquids at Graphite Electrodes. *The Journal of Physical Chemistry C*, *116*(14), 7940–7951.

[16] Lockett, V., Horne, M., Sedev, R., Rodopoulos, T., & Ralston, J. (2010). Differential capacitance of the double layer at the electrode/ionic liquids interface. *Physical Chemistry Chemical Physics: PCCP*, *12*(39), 12499–12512.

[17] Jiang, D. E., Meng, D., & Wu, J. (2011). Density functional theory for differential capacitance of planar electrical double layers in ionic liquids. *Chemical Physics Letters*, *504*(4-6), 153–158.

[18] Kornyshev, A. A. (2007). Double-layer in ionic liquids: paradigm change? *The Journal of Physical Chemistry. B*, *111*(20), 5545–57.

[19] Han, Y., Huang, S., & Yan, T. (2014). A mean-field theory on the differential capacitance of asymmetric ionic liquid electrolytes. *Journal of Physics. Condensed Matter*, *26*(28), 284103.

[20] Bresme, F., & Alejandro, J. (2003). Cavities in ionic liquids. *Journal of Chemical Physics*, 118, 4134.

[21] Bazant, M. Z., Storey, B. D., & Kornyshev, A. A. (2011). Double Layer in Ionic Liquids : Overscreening versus Crowding. *Physical Review Letters*, *106*, 46102.

[22] Storey, B. D., & Bazant, M. Z. (2012). Effects of electrostatic correlations on electrokinetic phenomena. *Physical Review E*, *86*, 56303.

[23] Alijó, P. H. R., Tavares, F. W., Biscaia Jr., E. C., & Secchi, A. R. (2015). Effects of electrostatic correlations on ion dynamics in alternating current voltages. *Electrochimica Acta*, *152*, 84–92.

Chapter 5: Analytical solution for the electrochemical impedance considering electrostatic correlation effects

Electrochemical impedance is a key property on the description and analysis of the phenomena involved on systems under an applied alternated voltage. With the advent of ionic liquids – which nowadays have been widely studied for several applications including taylor-made electrolyte for electrochemical devices – the electrochemical impedance spectroscopy can be important aid on the better understanding of the behavior of ionic liquids close to charged surfaces. In this present work, we aimed to analyze the effects of electrostatic correlations on a system composed of blocking electrodes and an ionic liquid as electrolyte under an AC voltage. Here, we obtained an analytical expression for the electrochemical impedance which showed that electrostatic correlations can expressively change the behavior of the electrochemical impedance, mainly caused by the overscrenning of the electrolytes close to a charged surface.

Keywords: electrochemical impedance, ionic liquids, electrostatic correlations.

5.1 Introduction

Impedance, similarly as the resistance, represents the ability of a circuit to resist the passage of current through itself. It is a very useful measurement as it reflects different phenomena occurring in electrochemical devices (*e.g.* diffusion, faradic reactions, adsorption, and the formation of electrical double layers, among others) [1-5]. Impedance spectroscopy has been widely used to describe a variety of systems containing electrolytes. For example, impedance is used to obtain information about the corrosion process of metallic structures and formation of oxide films [6-9], mass transport and charge transfer on the surface of electrodes [10], and supported ionic liquid membranes [11,12].

The electrochemical impedance can also be a tool to understand the behavior and properties of room temperature ionic liquids (RTIL). Nowadays there is an increasing interest on the use of ionic liquids. This can be attributed to their special ensemble of properties which makes them suitable for different applications: batteries, supercapacitors, chromatography, solar cells, and others [13]. Modeling the impedance of ionic liquids can be a helpful way to understand the phenomena involved in the double layer formed close to charged surfaces and to better understand the behavior observed experimentally.

In the literature we find works where the impedance is modeled on a phenomenological basis, however none of them have a deep description of the electrostatic behavior of the system. For example, Ferrari *et al*. [14] presented an analysis of the influence of the radial and normal contributions of local current density to local electrochemical impedance. For that they performed an experimental analysis of a system with tri-electrode probe and compared their results with mathematical models, both for blocking electrodes and electrodes with Faradic reactions using cylindrical coordinates to take into account the shape of the disk electrodes. To describe the electrostatic potential on that system they used the Laplace equation, not considering any non-electrostatic effects neither electrostatic correlation.

Previous works from Huang *et al*. [15-17] have mathematically analyzed the global and local impedance for blocking electrodes, and for electrodes with faradaic reactions. Even though they didn't consider any electrostatic correlation or non-electrostatic effects on the description of the electrostatic potential, they were able to observe a constant-phase-element behavior on disk electrodes. The same way as ref. [14], they considered only the Laplace equation to describe the behavior of the electrostatic potential. More recently Michel & Montella [18] developed a very detailed computational approach to model the admittance and impedance of disk blocking electrodes. For that, they considered a non-uniform current through the electrodes and used an infinite series solution method. This made possible to them to observe the effect of ohmic and interfacial contributions to impedance, however once again considering only Laplace's equation to describe the behavior of the electrical potential.

For modeling ionic liquids it is necessary to describe the system as molten salts at low temperature, which present special features. As they are basically electrolytes

with no solvent, the interactions between the ions are much stronger than the ones observed in dilute solutions. Therefore, traditional approaches that are used to model dilute electrolyte solutions are not adequate to describe ionic liquids. One of the main effects that must be taken into account when modeling ionic liquids is the ionic electrostatic correlations which have been shown by Bazant *et al*. [19] on the so called BSK model, to play a key role on the behavior of ionic liquids close to charged surfaces. The BSK model was obtained through a gradient approximation for nonlocal electrostatics between different interacting ions. In this model the permittivity is a differential operator that is a function of a correlation length. With this approach it was possible to capture aspects of the behavior of electrolytes described by molecular dynamics and, at the same time, be simple enough to be used on the description of complex systems, as for example, electrokinect flows [22]. Molecular dynamics simulations [21] had also been used to verify the effects of electrostatic correlations in dense ionic solutions, showing that the correlation length tends to increase with the increase of the ionic strength, with its limit being for ionic liquids.

The BSK model does well for large voltage when compared to molecular dynamics simulation [19,22] and also helps to describe electrokinetic phenomena [20,23]. However it does not describe the very long range (many times larger than the Debye length) for electrostatic screening with charge oscillations in ionic liquids and concentrated electrolytes, although it predicts a slightly increase on the screening length with the same scaling as predicted by Smith *et al*. [24].

Recently, Jiang *et al*. [25] applied the BSK model to describe the behavior of room temperature ionic liquids inside conical pores. This model made possible to predict the occurrence of rectification for different surface charges densities of the pores, a behavior that was only experimentally observed before. This motivates and supports the application of the BSK model to describe complex systems, especially the transport of ions of ionic liquids in non-equilibrium conditions. Also Lee *et al*. [26] performed a dynamical analysis of the transport of ions considering a mobility matrix and obtained the same expression for the modified Poisson-Boltzmann equation as the one in the BSK model. Furthermore, electrostatic correlations had shown to be directly related to the osmotic pressure of ionic liquids close to charged surface [27]. Yochelis [28,29] have also shown that electrostatic correlations are a key on understanding and

describing nomonotonic and monotonic decays on the diffuse layer of ionic liquids under confinement.

It is important to notice, that the BSK model, up to now, has been applied mostly to systems under direct current, the only exception is the work of Alijó *et al*. [30] which showed that electrostatic correlations play an important role in the transient behavior of charging and discharging processes. Then developing a model for electrochemical impedance considering electrostatic correlations also contributes to a better treatment of AC systems.

The consideration of electrostatic correlations is also important on the description of the behavior of highly concentrate electrolyte solutions, being applied to aqueous electrolyte solutions in biological ion channels, describing very well experimental data of single channel current [31], ion exchanging mechanisms [32], activity of single ions in strong electrolyte solutions [33], and as well to describe biological calcium channels such as heart muscles [34].

The goal of this work is to obtain an analytical expression for the electrochemical impedance of blocking electrodes considering the effects of ionic electrostatic correlations using the mean field approach by the BSK model. Here, we consider a symmetric electrolyte under an AC voltage in order to obtain an analytical expression. This analytical expression allows us to observe features of the equivalent circuit of the electrode for monovalent electrolyte solutions and monovalent ionic liquids.

5.2 Mathematical Approach

Impedance is a measurement of the ability of a circuit to resist the passage of current through itself, as a function of the frequency of the voltage applied to it. Analogously to the Ohm's Law for the resistance we can obtain an expression for the impedance (Z) as a function of the voltage (ϕ) and the current (I) at a time t [35].

$$Z = \frac{\phi}{I} \tag{5.1}$$

In this work we analyzed the effects of electrostatic correlations on the electrochemical impedance of blocking electrodes (Figure 18). As the roughness of the electrodes is important on the behavior of the electrochemical impedance [36], we considered that the modeled electrode has a smooth surface, so we could observe solely the influence of electrostatic correlations. Then to obtain the analytical expression of Z we need an expression for the electrostatic potential (ϕ) and for the transient capacitive current (J) acting over the circuit. In order to obtain them, we modeled a symmetric, binary electrolyte solution or ionic liquid, considering the effect of electrostatic correlation using the Fourth Order Poisson Equation. Figure 18 presents the scheme of the modeled system.

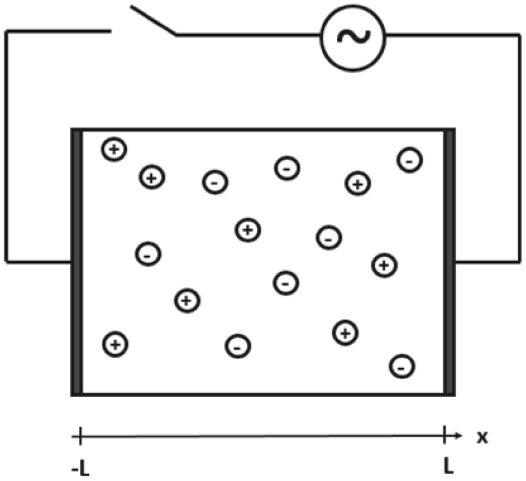

Figure 18 - Blocking electrodes configuration, separated by a distance of $\mathbf{2}\boldsymbol{L}$.

The electrodes are subject to an applied AC voltage and we consider a linear response in a neutral solution, which means that the sum of the concentrations of cations and anions are approximately constant at any position and time $[c_+(x,t) + c_-(x,t) \approx 2c_0 = constant]$. This approximation is valid for low concentrated solutions and/or low applied potential. In order to obtain an analytical solution we considered that both ions have the same valency $\left(\left|z_\pm\right| = z\right)$ and the same constant ionic diffusivity $(D_\pm = D)$.

To model this system we start describing the conservation law through the Nernst-Planck equations for the anion and the cation, as follows:

$$\frac{\partial c_{\pm}}{\partial t} = D\left(\frac{\partial^2 c_{\pm}}{\partial x^2} \pm \frac{\partial}{\partial x}\frac{zec_{\pm}}{kT}\frac{\partial \phi}{\partial x}\right), \tag{5.2}$$

where e is the elementary charge, k is the Boltzmann constant, D is the diffusivity, considered equal for both ions, and T is the temperature.

We subtract one equation from the other and consider the expression of the charge density $\rho = \frac{ze}{\varepsilon}(c_+ - c_-)$ (for symmetric electrolytes) and the neutral solution assumption $c_+(x,t) + c_-(x,t) \approx 2c_0$ so that we can obtain the following expression:

$$\varepsilon\frac{\partial \rho}{\partial t} = D\left(\varepsilon\frac{\partial^2 \rho}{\partial x^2} + \frac{(ze)^2 2c_0}{kT}\frac{\partial^2 \phi}{\partial x^2}\right). \tag{5.3}$$

Identifying the square of the Debye length (λ_D^2).

$$\lambda_D^2 = \frac{kT\varepsilon}{(ze)^2 2c_0} \tag{5.4}$$

Now it is necessary to define the expression that describes the electrostatic potential (ϕ). For that, we use the fourth order Poisson equation which takes into account the effect of electrostatic correlations by considering that the permittivity can be described as linear differential operator, as a function of the correlation length (l_c) (Bazant *et al*., 2010).

$$l_c^2\frac{\partial^4 \phi}{\partial x^4} - \frac{\partial^2 \phi}{\partial x^2} = \rho \tag{5.5}$$

The blocking electrodes are subject to an AC voltage, and for that, we want to express the dependent variables ρ and ϕ on the frequency domain:

$$\rho(x,t) = \mathrm{Re}\hat{\rho}(x)e^{i\omega t}, \tag{5.6}$$

$$\phi(x,t) = \mathrm{Re}\hat{\phi}(x)e^{i\omega t}. \tag{5.7}$$

It is convenient to work with dimensionless variables, so we define:

$$\tilde{\rho} = \frac{\rho}{2zec_0}, \tag{5.8}$$

$$\tilde{x} = \frac{x}{\lambda_D}, \tag{5.9}$$

$$\tilde{l}_c = \frac{l_c}{\lambda_D}, \tag{5.10}$$

$$\tilde{\phi} = \frac{ze\phi}{k_B T}, \tag{5.11}$$

$$\tilde{\omega} = \omega\tau, \tag{5.12}$$

where $\tau = {\lambda_D}^2/D$.

Rewriting equations 3 and 5 on dimensionless form and on the frequency domain we obtain the set of equations that must be solved:

$$\tilde{\tilde{\rho}} \cdot i \cdot \tilde{\omega} = \frac{\partial^2 \tilde{\tilde{\rho}}}{\partial \tilde{x}^2} + \frac{\partial^2 \tilde{\tilde{\phi}}}{\partial \tilde{x}^2}, \tag{5.13}$$

$$\tilde{l}_c^2 \frac{\partial^4 \tilde{\tilde{\phi}}}{\partial \tilde{x}^4} - \frac{\partial^2 \tilde{\tilde{\phi}}}{\partial \tilde{x}^2} = \tilde{\tilde{\rho}}. \tag{5.14}$$

This problem is subject to a couple of symmetry restrictions:

$$\tilde{\tilde{\rho}}(0) = 0, \qquad \tilde{\tilde{\phi}}(0) = 0. \tag{5.15}$$

Furthermore, the potential over each surface $(\tilde{\phi}_0)$ is known, which implies that:

$$\tilde{\tilde{\phi}}_s = \tilde{\phi}_0. \tag{5.16}$$

Also, as we are modeling blocking electrodes we considered that there is no Faradaic current (J_F) passing through the surface of each electrode. The Faradaic current can be expressed as:

$$J_F(\pm L, t) = ze(F_+ \pm F_-), \tag{5.17}$$

where the ionic fluxes ($F_\pm$) are defined as follows:

$$F_\pm = -D\left(\nabla c_\pm \pm c_0 \nabla\tilde{\phi}\right), \tag{5.18}$$

and these statements lead us to the following relation at surfaces ($S = L$ and $S = -L$):

$$\left.\frac{\partial\tilde{\tilde{\rho}}}{\partial\tilde{x}}\right|_S + \left.\frac{\partial\tilde{\tilde{\phi}}}{\partial\tilde{x}}\right|_S = 0. \tag{5.19}$$

To complete the set of boundaries conditions to solve the problem we assume that there is no electrostatic correlation effects taking place on the electrode surfaces, and for that we have:

$$\left.\frac{\partial^3\tilde{\tilde{\phi}}}{\partial\tilde{x}^3}\right|_S = 0. \tag{5.20}$$

We solved analytically equations 13 and 14 and the result obtained was expressed in terms of hyperbolic functions instead of the exponential form, and from the symmetry conditions we can rewrite the equations in terms of hyperbolic sine.

$$\tilde{\tilde{\rho}}(\tilde{x}) = \frac{1}{4\tilde{l}_c^2}\left[A_1\,({a_3}^2 - 2a_3)\sinh(a_1\,\tilde{x}) + A_2\,({a_4}^2 - 2a_4)\sinh(a_2\,\tilde{x})\right] \tag{5.21}$$

$$\tilde{\tilde{\phi}}(\tilde{x}) = A_1\sinh(a_1\,\tilde{x}) + A_2\sinh(a_2\,\tilde{x}) + A_3\,\tilde{x} \tag{5.22}$$

where the parameters a_1, a_2, a_3, and a_4 are functions of the dimensionless electrostatic correlation length $\left(\tilde{l}_c\right)$ and the frequency ($\tilde{\omega}$).

$$a_1 = \frac{\sqrt{2a_3}}{2\tilde{l}_c} \tag{5.23}$$

$$a_2 = \frac{\sqrt{2a_4}}{2\tilde{l}_c} \tag{5.24}$$

$$a_3 = i\,\tilde{l}_c^2\,\tilde{\omega} + 1 - \sqrt{\gamma} \tag{5.25}$$

$$a_4 = i\,\tilde{l}_c^2\,\tilde{\omega} + 1 + \sqrt{\gamma} \tag{5.26}$$

$$\gamma = -\tilde{\omega}^2\,\tilde{l}_c^4 - 2\,i\,\tilde{\omega}\,\tilde{l}_c^2 - 4\,\tilde{l}_c^2 + 1 \tag{5.27}$$

The constants A_1, A_2, and A_3 were obtained by applying the boundary and symmetry conditions, and they are presented in the appendix.

Even though there is no charge transfer on the surface of the blocking electrodes there is still a transient capacitive current which can be obtained from the Maxwell displacement current per area (J):

$$J = -\frac{\partial D}{\partial t} = \varepsilon \frac{\partial}{\partial t}\frac{\partial \phi}{\partial x}. \tag{5.28}$$

This current expressed in the frequency domain $(\hat{J})$ allows us to obtain the expression for the electrochemical impedance over the surface of the blocking electrode $(x = L)$ based on the definition of equation 1.

$$Z = \frac{\hat{\phi}(L)}{-\hat{J}} \tag{5.29}$$

That, in the dimensionless form, can be written as:

$$\tilde{Z} = \frac{\varepsilon D Z}{L\lambda_D^2} = \frac{\hat{\tilde{\phi}}(\tilde{L})}{i\tilde{\omega}\tilde{L}\dfrac{\partial \hat{\tilde{\phi}}(\tilde{L})}{\partial \tilde{x}}}. \tag{5.30}$$

Applying equation 22 to equation 28 and 29 we can obtain the analytical expression for the electrochemical impedance taking into account the electrostatic correlations.

$$\tilde{Z} = \frac{1}{i\tilde{\omega}+1} + \alpha\frac{\tanh(a_1\tilde{L})}{i\tilde{\omega}\tilde{L}} + \beta\frac{\tanh(a_2\tilde{L})}{i\tilde{\omega}\tilde{L}} \tag{5.31}$$

where the coefficients α and β are:

$$\alpha = \tilde{l}_c\frac{\sqrt{2}}{2}\frac{i\tilde{\omega}\tilde{l}_c^2 + 1 + \sqrt{\gamma}}{\sqrt{i\tilde{\omega}\tilde{l}_c^2 + 1 - \sqrt{\gamma}}\,\sqrt{\gamma}\,(i\tilde{\omega}+1)}, \tag{5.32}$$

$$\beta = \tilde{l}_c\frac{\sqrt{2}}{2}\frac{-i\tilde{\omega}\tilde{l}_c^2 - 1 + \sqrt{\gamma}}{\sqrt{i\tilde{\omega}\tilde{l}_c^2 + 1 + \sqrt{\gamma}}\,\sqrt{\gamma}\,(i\tilde{\omega}+1)}. \tag{5.33}$$

5.2.1 Validation of the analytical solution

If we take the limit of the dimensionless correlation length $(\tilde{l}_c)$ going to zero we can derive the impedance expression for the traditional approach, where the electrostatic potential is described by the classical Poisson-Boltzmann equation.

$$\tilde{Z} = \frac{1}{i\tilde{\omega}+1} - \frac{i\cdot\tanh\left(\frac{\sqrt{2i\tilde{\omega}+4}}{2}\,\tilde{L}\right)}{(i\tilde{\omega}+1)^{3/2}\;\tilde{\omega}\tilde{L}} \tag{5.34}$$

As expected, the proposed expression shows a consistent limit when $\tilde{l}_c \to 0$.

The analytical expression was also validated by the reduction of the AC problem to a system were a DC voltage is applied. For that, we take the limit of the frequency going to zero ($\tilde{\omega} \to 0$). Now we are able to define the capacitance on the surface of the electrodes, and this result was compared to the one presented by Storey & Bazant (2012).

$$\frac{C}{C_{DH}} = \frac{\sqrt{8\left(-4\,\tilde{l}_c^2 + 1\right)}}{\tilde{l}_c\left[{a_3}^{3/2}\,\tanh(a_2\,\tilde{L}) - d^{3/2}\,\tanh(a_1\,\tilde{L})\right]} \tag{5.35}$$

Where the parameters are:

$$a_1 = \frac{\sqrt{2}}{2}\frac{\sqrt{a_3}}{\tilde{l}_c}, \tag{5.36}$$

$$a_2 = \frac{\sqrt{2}}{2}\frac{\sqrt{a_4}}{\tilde{l}_c}, \tag{5.37}$$

$$a_3 = 1 - \sqrt{-4\,\tilde{l}_c^2 + 1}, \tag{5.38}$$

$$a_4 = 1 + \sqrt{-4\,\tilde{l}_c^2 + 1}. \tag{5.39}$$

Then equation 36 was compared with Equations 44 and 47 from the article of Storey & Bazant (2012), obtaining the same numerical values. Therefore, the proposed expression shows correct limits when $\tilde{l}_c \to 0$ and $\tilde{\omega} \to 0$.

5.3 Results and discussion

The behavior of the electrochemical impedance as a function of the electrostatic correlation effects is shown by the Nyquist plot of the dimensionless impedance for different values of the dimensionless electrostatic correlation length $(\tilde{l}_c)$. The Nyquist plot relates the real part of the impedance $(\tilde{Z}_R)$ with the negative of its imaginary part $(-\tilde{Z}_I)$ for several values of the frequency $(\tilde{\omega})$. In Figure 19 we varied the frequency from 0.01 to 1000 and steps of 0.001. The effect of the electrostatic correlations was analyzed for six different values of $\tilde{l}_c$: $0, 10, 30, 50, 70$, and 100. The same results are presented in Figure 20 on the form of Bode plots where the absolute value of the impedance and its argument are plotted as a function of the frequency. The parameters used on these simulations are presented in Table 4. All the variables presented in Figures 2 and 3 are on their dimensionless form.

Table 4 - Parameters used on the impedance model (S.I.).

$T = 298.15$ K	$\varepsilon = 4.427093585 \times 10^{-11}$ C^2/J m
$e = 1.602 \times 10^{-19}$ C	$k_B = 1.38065 \times 10^{-23}$ J/K

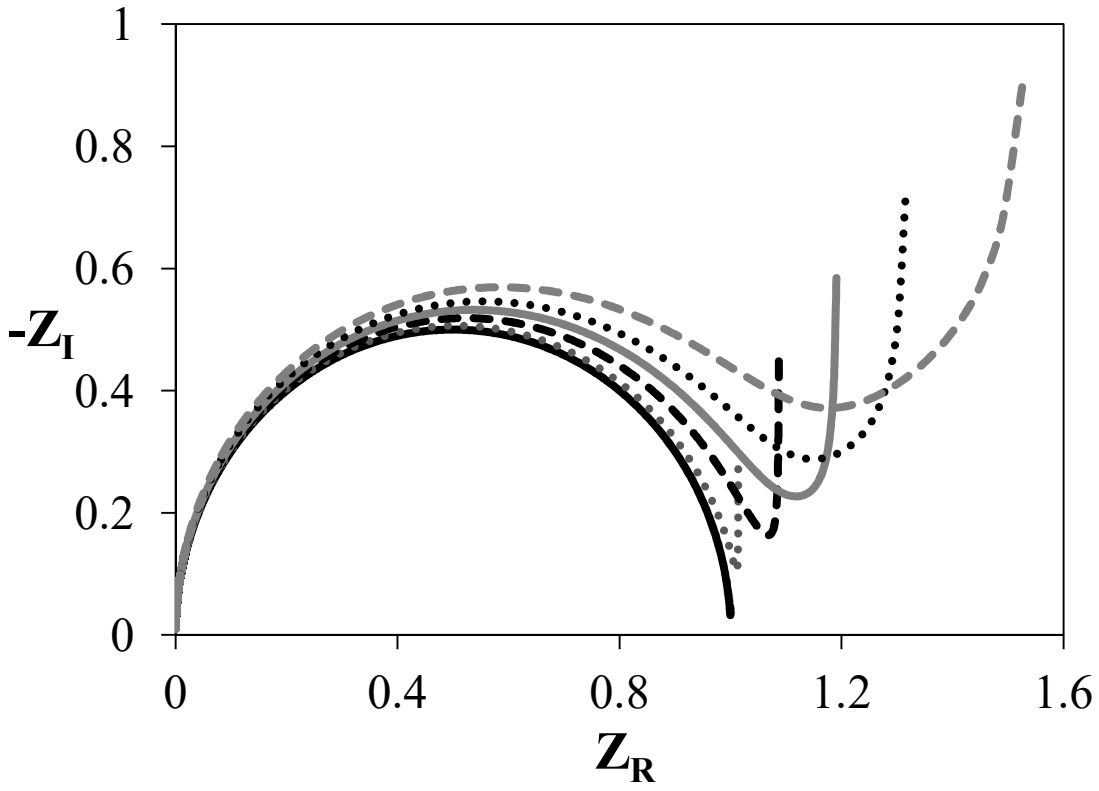

Figure 19 - Nyquist plot of the electrochemical impedance of a symmetric electrolyte, considering different values of the dimensionless correlation length $(\tilde{\boldsymbol{l}}_{\boldsymbol{c}})$. The continuos black line is the case where no electrostatic correlation is considered $\tilde{\boldsymbol{l}}_{\boldsymbol{c}} = \mathbf{0}$, the gray dotted line is $\tilde{\boldsymbol{l}}_{\boldsymbol{c}} = \mathbf{10}$, the dashed black line is $\tilde{\boldsymbol{l}}_{\boldsymbol{c}} = \mathbf{30}$, the gray continuous line is $\tilde{\boldsymbol{l}}_{\boldsymbol{c}} = \mathbf{50}$, the black dotted line is $\tilde{\boldsymbol{l}}_{\boldsymbol{c}} = \mathbf{70}$, and the gray dashed line is $\tilde{\boldsymbol{l}}_{\boldsymbol{c}} = \mathbf{100}$.

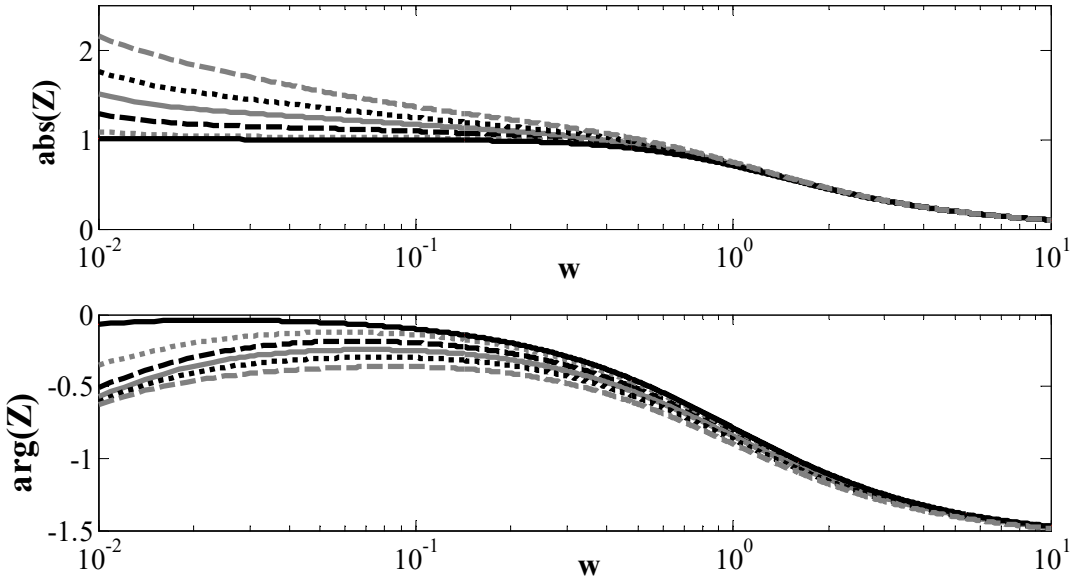

Figure 20 - Bode plot of the electrochemical impedance of a symmetric electrolyte, considering different values of the dimensionless correlation length $(\tilde{\boldsymbol{l}}_{\boldsymbol{c}})$. The continuous black line is the case where no electrostatic correlation is considered $\tilde{\boldsymbol{l}}_{\boldsymbol{c}} = \mathbf{0}$, the gray dotted line is $\tilde{\boldsymbol{l}}_{\boldsymbol{c}} = \mathbf{10}$, the dashed black line is $\tilde{\boldsymbol{l}}_{\boldsymbol{c}} = \mathbf{30}$, the gray continuous line is $\tilde{\boldsymbol{l}}_{\boldsymbol{c}} = \mathbf{50}$, the black dotted line is $\tilde{\boldsymbol{l}}_{\boldsymbol{c}} = \mathbf{70}$, and the gray dashed line is $\tilde{\boldsymbol{l}}_{\boldsymbol{c}} = \mathbf{100}$.

We observe that the electrostatic correlation effects cause a main change on the shape of the impedance curve for values of dimensionless frequency $(\widetilde{\omega})$ lower than one. For values of $\widetilde{\omega}$ higher than one the electrochemical impedance presents similar behavior to the one described by the classic theory, where the electrochemical potential is given by the Poisson-Boltzmann Equation. The change of the shape of the electrochemical impedance curve can be associated with the change on the structure of the electrical double layer. The increase of electrostatic correlation effects is related to the growth of the overcrowding effects (which is explained in details by Bazant *et al*. work from 2010). Analyzing the influence of the overcrowding effects on an equivalent circuit model, it could appear as a series association of the capacitance of double layer, which could be represented by the last two terms of the analytical expression of the electrochemical impedance obtained here (Equation 31). The first term of that equation is equivalent to the contribution of the bulk resistance of the system studied.

5.4 Final Remarks

We proposed an analytical expression for the electrochemical impedance taking into account electrostatic correlations which can play a lead role on the performance of electronic devices containing ionic liquids or concentrated electrolytes. The expression obtained shows that the electrochemical impedance is largely affected by electrostatic correlations especially at low frequencies. This fact is related to the increase of the overscreening close to electrode surfaces for electrolytes highly correlated. Electrostatic correlation effects are relevant to the description of ionic liquids, because of their highly charged nature. When a large electrostatic potential is applied to the system, or/and multivalent ions are involved, electrostatic correlations cannot be neglected, and then the proposed approach to describe the electrochemical impedance here is recommended. Because the impedance is a linear response to a small perturbation, the long range screening effects at low voltages may be important and missing in the BSK model, but the analysis presented in this work are aimed to observe the trend predicted by the BSK model that is a signature of electrostatic correlations. Finally, we would like to highlight that the present analytical expression for the electrochemical impedance is valid not only for ionic liquids, but rather to any symmetric electrolyte solution, with only the appropriate use of the parameters marking the difference between these two kind of systems.

Appendix

The coefficients $A_1, A_2,$ and A_3 from the analytical solutions from equations 5.21 and 5.22 are presented bellow as follows:

$$\begin{aligned} A_1 = {} & 4\,{a_2}^3\tilde{l}_c^2\cosh\left(b\tilde{L}\right)\tilde{\phi}_0 \\ & / \left(\tilde{L}\cosh\left(a_1\,\tilde{L}\right)\cosh\left(a_2\,\tilde{L}\right)a_1\,a_2\left[{a_1}^2\left({a_4}^2+4\tilde{l}_c^2-2a_4\right)\right.\right. \\ & \left.\left.-{a_2}^2\left({a_3}^2+4\tilde{l}_c^2-2\,a_3\right)\right]+4{a_2}^3\tilde{l}_c^2\sinh\left(a_1\,\tilde{L}\right)\cosh\left(a_2\,\tilde{L}\right)\right. \\ & \left.-4{a_1}^3\tilde{l}_c^2\cosh\left(a_1\,\tilde{L}\right)\sinh\left(a_2\,\tilde{L}\right),\right. \end{aligned} \tag{5.40}$$

$$A_2 = 4{a_1}^3\tilde{l}_c^2\cosh(a_1\tilde{L})\,\tilde{\phi}_0 /(\tilde{L}\cosh(a_1\tilde{L})\cosh(a_2\tilde{L})\,a_1a_2[{a_1}^2({a_4}^2+4\tilde{l}_c^2-2a_4) - {a_2}^2({a_3}^2+4\tilde{l}_c^2-2a_3)] + 4\,{a_2}^3\tilde{l}_c^2\sinh(a_1\tilde{L})\cosh(a_2\tilde{L}) - 4{a_1}^3\tilde{l}_c^2\cosh(a_1\tilde{L})\sinh(a_2\,\tilde{L}), \quad (5.41)$$

$$A_3 = ({a_1}^2{a_4}^2+4{a_1}^2\tilde{l}_c^2-{a_2}^2{a_3}^2-4{a_2}^2\tilde{l}_c^2-2{a_1}^2a_4 + 2a_2{a_3}^2)a_2a_1\cosh(a_2\tilde{L})\cosh(a_1\tilde{L})\,\tilde{\phi}_0 /(\tilde{L}\cosh(a_1\tilde{L})\cosh(a_2\tilde{L})\,a_1a_2[{a_1}^2({a_4}^2+4\tilde{l}_c^2-2a_4) - {a_2}^2({a_3}^2+4\tilde{l}_c^2-2a_3)] + 4a_2\,{a_2}^3\tilde{l}_c^2\sinh(a_1\tilde{L})\cosh(a_2\,\tilde{L}) - 4{a_1}^3\tilde{l}_c^2\cosh(a_1\tilde{L})\sinh(a_2\,\tilde{L}). \quad (5.42)$$

where $\tilde{\phi}_0$ is the potential applied at the surface.

References

[1] Harrington, D. A., Conway, B. E. (1987). AC Impedance of Faradaic reactions involving electrosorbed intermediates Kinetic theory. *Electrochimica Acta*, *32*(12), 1703–1712.

[2] MacDonald, M. A., Andreas, H. A. (2014). Method for equivalent circuit determination for electrochemical impedance spectroscopy data of protein adsorption on solid surfaces. *Electrochimica Acta*, *129*, 290–299.

[3] da Silva, D. J. R., Diniz, F. B. (2014). Electrochemical impedance spectroscopy study of concanavalin a adsorption on glassy carbon electrode: An analysis of capacitance dispersion. *Electrochimica Acta*, *119*, 99–105.

[4] Shrikrishnan, S., Sankaran, K., & Lakshminarayanan, V. (2012). Electrochemical impedance analysis of adsorption and enzyme kinetics of calf intestine alkaline phosphatase on SAM-modified gold electrode. *Journal of Physical Chemistry C*, *116*(30), 16030–16037.

[5] Anastopoulos, A. G., Papoutsis, A. D., & Papaderakis, A. A. (2015). Differential capacitance and electrochemical impedance study of surfactant adsorption on polycrystalline Ni electrode. *Journal of Solid State Electrochemistry*, *19*(8), 2369–2377.

[6] Dauphin-Ducharme, P., Mauzeroll, J. (2015). Surface Analytical Methods Applied to Magnesium Corrosion. *Analytical Chemistry*. 87, 7499−7509.

[7] Hamdy, A. S., El-Shenavy, E., El-Bitar, T. (2006). Electrochemical Impedance Spectroscopy Study of the Corrosion Behavior of Some Niobium Bearing Stainless Steels in 3.5% of NaCl. *International Journal of Electrochemical Science*. 1, 171–180.

[8] Bueno, G. V, Taqueda, M. E., Melo, H. G., Guedes, I. C. (2015). Using a DOE and EIS to evaluate the synergistic effects of low toxicity inhibitors for mild steel. *Brazilian Journal of Chemical Engineering*. 32(01), 167–177.

[9] Hamadou, L., Aïnouche, L., Kadri, A., Yahia, S. A. A., Benbrahim, N. (2013). Electrochemical impedance spectroscopy study of thermally grown oxides exhibiting constant phase element behaviour. *Electrochimica Acta*. 113, 99–108.

[10] Torresi, R. M., Lodovico, L., Benedetti, T. M., Alcântara, M. R., Debiemme-Chouvy, C., & Deslouis, C. (2013). Convective mass transport in ionic liquids studied by electrochemical and electrohydrodynamic impedance spectroscopy. *Electrochimica Acta*, *93*, 32–43.

[11] Fortunato, R., Branco, L. C., Afonso, C. A. M., Benavente, J., & Crespo, J. G. (2006). Electrical impedance spectroscopy characterisation of supported ionic liquid membranes. *Journal of Membrane Science*, *270*(1–2), 42–49.

[12] Salar-García, M. J., Ortiz-Martínez, V. M., de los Ríos, A. P., & Hernández-Fernández, F. J. (2015). A method based on impedance spectroscopy for predicting the

behavior of novel ionic liquid-polymer inclusion membranes in microbial fuel cells. *Energy*, *89*, 648–654.

[13] Fedorov, M. V., Kornyshev, A. A. (2014). Ionic Liquids at Electrified Interfaces. *Chemical Review*. 114, 2978−3036.

[14] Ferrari, J. V., Melo, H. G., Keddam, M., Orazem, M. E., Pébère, N., Tribollet, B., Vivier, V. (2012). Influence of normal and radial contributions of local current density on local electrochemical impedance spectroscopy. *Electrochimica Acta*. 60, 244–252.

[15] Huang, V. M.-W., Vivier, V., Frateur, I., Orazem, M. E., Tribollet, B. (2007a). The Global and Local Impedance Response of a Blocking Disk Electrode with Local Constant-Phase-Element Behavior. *Journal of the Electrochemical Society*. 154(2), C89.

[16] Huang, V. M.-W., Vivier, V., Orazem, M. E., Pébère, N., Tribollet, B. (2007b). The Apparent Constant-Phase-Element Behavior of a Disk Electrode with Faradaic Reactions. *Journal of the Electrochemical Society*. 154(2), C99.

[17] Huang, V. M.-W., Vivier, V., Orazem, M. E., Pébère, N., Tribollet, B. (2007c). The Apparent Constant-Phase-Element Behavior of an Ideally Polarized Blocking Electrode. *Journal of the Electrochemical Society*. 154(2), C81.

[18] Michel, R., & Montella, C. (2015). Local/global admittance of blocking disk electrode. Computation and discussion. 1-Infinite series solution. *Journal of Electroanalytical Chemistry*. 751, 90–104.

[19] Bazant, M. Z., Storey, B. D., Kornyshev, A. A. (2011). Double layer in ionic liquids: Overscreening vs . crowding. *Physical Review Letters.* (10), 3–6.

[20] Storey, B. D., & Bazant, M. Z. (2012). Effects of electrostatic correlations on electrokinetic phenomena, *56303*, 1–11.

[21] Uralcan, B., Aksay, I. A., Debenedetti, P. G., & Limmer, D. T. (2016). Concentration Fluctuations and Capacitive Response in Dense Ionic Solutions. *Journal of Physical Chemistry Letters*, *7*(13), 2333–2338.

[22] Jiang, X., Huang, J., Zhao, H., Sumpter, B. G., & Qiao, R. (2014). Dynamics of electrical double layer formation in room-temperature ionic liquids under constant-current charging conditions. *J Phys Condens Matter*, *26*(28), 284109.

[23] Stout, R. F., & Khair, A. S. (2014). A continuum approach to predicting electrophoretic mobility reversals. *Journal of Fluid Mechanics*, *752*, R1.

[24] Smith, A. M., Lee, A. A., & Perkin, S. (2016). The Electrostatic Screening Length in Concentrated Electrolytes Increases with Concentration. *The Journal of Physical Chemistry Letters*, 2157–2163.

[25] Jiang, X., Liu, Y., & Qiao, R. (2016). Current Rectification for Transport of Room-Temperature Ionic Liquids through Conical Nanopores. *Journal of Physical Chemistry C*, *120*(8), 4629–4637.

[26] Lee, A. A., Kondrat, S., Vella, D., & Goriely, A. (2015). Dynamics of Ion Transport in Ionic Liquids. *Physical Review Letters*, *115*(10), 1–5.

[27] Moon, G. J., Ahn, M. M., & Kang, I. S. (2015). Osmotic pressure of ionic liquids in an electric double layer: Prediction based on a continuum model. *Physical Review E*, *92*(6), 63020.

[28] Yochelis, A. (2014). Transition from non-monotonic to monotonic electrical diffuse layers: impact of confinement on ionic liquids. *Physical Chemistry Chemical Physics: PCCP*, *16*(7), 2836–41.

[29] Yochelis, A. (2014). Spatial Structure of Electrical Diffuse Layers in Highly Concentrated Electrolytes: A Modified Poisson-Nernst-Planck Approach. *The Journal of Physical Chemistry C*, *118*(11), 5716–5724.

[30] Alijó, P. H. R., Tavares, F. W., Biscaia Jr., E. C., & Secchi, A. R. (2015). Effects of electrostatic correlations on ion dynamics in alternating current voltages. *Electrochimica Acta*, *152*, 84–92.

[31] Liu, J. L., Eisenberg, B. (2015). Numerical methods for a Poisson-Nernst-Planck-Fermi model of biological ion channels. *Physical Review E - Statistical, Nonlinear, and Soft Matter Physics*, *92*(1), 1–16.

[32] Liu, J.-L., Hsieh, H., & Eisenberg, B. (2016). Poisson–Fermi Modeling of the Ion Exchange Mechanism of the Sodium/Calcium Exchanger. *J. Phys. Chem. B*, *120*(10), 2658–2669.

[33] Liu, J.-L., & Eisenberg, B. (2015). Poisson–Fermi model of single ion activities in aqueous solutions. *Chemical Physics Letters*, *637*, 1–6.

[34] Liu, J. L., & Eisenberg, B. (2013). Correlated ions in a calcium channel model: A poisson-fermi theory. *Journal of Physical Chemistry B*, *117*(40), 12051–12058.

[35] Huang, V. M., Wu, S.-L., Orazem, M. E., Pébère, N., Tribollet, B., Vivier, V. (2011). Local electrochemical impedance spectroscopy: A review and some recent developments. *Electrochimica Acta*. 56(23), 8048–8057.

[36] Jänsch, T., Wallauer, J., & Roling, B. (2015). Influence of Electrode Roughness on Double Layer Formation in Ionic Liquids. *The Journal of Physical Chemistry C*, 150225115226001.

Chapter 6. Final Remarks and Future Works

In this thesis we analyzed the effect of electrostatic ionic correlations in different systems. As these correlations are relevant for a large variety of systems, we focused on the description of the following cases: the micellization phenomena of ionic and zwitterionc surfactants in the presence of monovalent and multivalent electrolytes; the differential capacitance of asymmetric ionic liquids; and the electrochemical impedance of ionic liquids. For that, the modified version of the Poisson-Boltzmann equation (BSK model) is used.

For the micellization phenomena, the inclusion of electrostatic correlations made it possible to obtain a good description of experimental behavior of surfactant solutions containing highly concentrated electrolytes and/or multivalent electrolytes. We also proposed a new approach to calculate the free energy of micellization of zwitterionic surfactants. We considered that micelles formed by zwitterionic surfactants can have both cations and anions binding to its surface, and it directly impacts on the behavior of the surfactant solution. Our model was able to correctly predict experimental observations of ion binding for zwitterionic surfactants. Most importantly, all calculations for the micellization phenomena are predictive, *i.e.* did not use any fitting parameter to experimental data. Comparison results confirm the importance of ionic electrostatic correlations for micelle formation in solutions with high salt concentrations and multivalent electrolytes.

Regarding the differential capacitance (C_D) of ionic liquids, we observed that electrostatic correlations play an important role in the differential capacitance, being responsible for the reduction of the C_D magnitude. The asymmetry of ion sizes is also relevant when describing ionic liquids due to the large difference between their cations and anions. Furthermore, the present approach was able to predict very well the differential capacitance of ionic liquids from molecular simulations and density functional theories. For differential capacitance experimental data of ionic liquids we obtained a fair description for elevated applied potentials. Conditions of large applied voltage can induce a large accumulation of ions close to the electrode surface, which makes electrostatic ionic correlations the dominant effect in these conditions, justifying our model.

When used in simpler calculations, we presented here an analytical expression for the electrochemical impedance taking into account electrostatic correlations, which can play an important role in the performance of electronic devices containing ionic liquids or concentrated electrolytes. The expression obtained shows that the electrochemical impedance is largely affected by electrostatic correlations, especially at low applied frequencies. This fact is related to the increase of the overscreening close to electrode surfaces observed experimentally.

The work presented here can be useful for several applications. One promising use of the approaches proposed here is for the description of complex electrochemical devices and processes in which the dynamics of electrolytes are relevant; for example, electrodialysis, electroactuators, batteries, among others. In Appendix C we present a brief analysis of the dynamical problem for electrolyte solutions considering the effect of the solvent size together with electrostatic correlation effects. The analysis performed and the methodology presented can be useful for future developments in the aforementioned areas.

Electrostatic correlations are also fundamental to the description of biological systems, which usually contain multivalent electrolytes. One example of a biological system where electrostatic correlations are important is the adsorption of proteins for separation processes. The description of interactions between different proteins and between proteins and charged surfaces as a function of salt type, salt concentration, temperature, and pH is essential for modeling the adsorption process. In Appendix E we present the calculation of the adsorption of spherical proteins using an approach based on a modified Poisson-Boltzmann equation. Even though that work only considered the effects of van der Waals interactions, it can be extended to include the effects of electrostatic correlations. For that, in Appendix D we present a numerical methodology to solve the BSK model in bispherical coordinates.

Finally, the methodology presented here for the micellization phenomena of ionic and zwitterionic surfactants can be extended to the description of microemulsions and to the process of selection and design of surfactants.

Appendix A

Brazilian Journal
of Chemical
Engineering

ISSN 0104-6632
Printed in Brazil
www.abeq.org.br/bjche

Vol. 33, No. 03, pp. 515 - 523, July - September, 2016
dx.doi.org/10.1590/0104-6632.20160333s20150129

MOLECULAR THERMODYNAMICS OF MICELLIZATION: MICELLE SIZE DISTRIBUTIONS AND GEOMETRY TRANSITIONS

M. S. Santos[1], F. W. Tavares[1,2*] and E. C. Biscaia Jr[1]

[1]Programa de Engenharia Química/COPPE, Universidade Federal do Rio de Janeiro,
C.P. 68502, CEP: 21941-972, Rio de Janeiro, RJ - Brazil.
E-mail: tavares@eq.ufrj.br
[2]Escola de Química, Universidade Federal do Rio de Janeiro, CEP: 21941-909,
Rio de Janeiro - RJ, Brazil.

(Submitted: February 26, 2015 ; Revised: June 10, 2015 ; Accepted: June 18, 2015)

Abstract - Surfactants are amphiphilic molecules that can spontaneously self-assemble in solution, forming structures known as micelles. Variations in temperature, pH, and electrolyte concentration imply changes in the interactions between surfactants and micelle stability conditions, including micelle size distribution and micelle shape. Here, molecular thermodynamics is used to describe and predict conditions of micelle formation in surfactant solutions by directly calculating the minimum Gibbs free energy of the system, corresponding to the most stable condition of the surfactant solution. In order to find it, the proposed methodology takes into account the micelle size distribution and two possible geometries (spherical and spherocylindrical). We propose a numerical optimization methodology where the minimum free energy can be reached faster and in a more reliable way. The proposed models predict the critical micelle concentration well when compared to experimental data, and also predict the effect of salt on micelle geometry transitions.
Keywords: Micellization; Molecular thermodynamics.

INTRODUCTION

Self-assembly is a broad term applied to spontaneous organization of substances under appropriate conditions and proportions. It is a reversible process and represents a condition of thermodynamic equilibrium, which is relevant to a large variety of phenomena and systems, such as crystal formation, colloidal systems, lipid bilayers, among others (Whitesides and Boncheva, 2002). When surfactants self-assemble, the structures formed are called micelles. Micellization phenomena have been of great interest to both the academic community and industry. It is involved in several applications and processes. We can mention its application in personal care products, paints, processed food, and separations in the petrochemical industry. Intensification of studies in this field is reinforced by the accessibility of critical micelle concentration data and its great importance for the physicochemical behavior of surfactant solutions. Furthermore, several thermodynamic and transport properties of surfactant solutions are affected by the size and shape of micelles (Iyer and Blankschtein, 2012). For example, the solubility of micelles increase with their size (Rusanov, 2014), and micelle shape transitions significantly affect the viscosity of the solution (Kamranfar and Jamialahmadi, 2014). All these facts contribute to the development of models that can predict the behavior of surfactant solutions and also can be used as a tool for designing new surfactants.

*To whom correspondence should be addressed
This is an extended version of the work presented at the 20th Brazilian Congress of Chemical Engineering, COBEQ-2014, Florianópolis, Brazil.

The molecular thermodynamics approach to describe the micellization phenomena was first proposed by Tanford (Tanford, 1974). Tanford analyzed the adequacy of the Gibbs thermodynamic equilibrium to describe the self-assembly of amphiphilic molecules. In Tanford's work, the equilibrium state is calculated by imposing the necessary condition of a stoichiometric linear relation of chemical potential of all species. That implies that the sum of the Gibbs free energies of reactants (amphiphilic molecules) must be the equal to the sum of the Gibbs free energies of products (micelles).

Molecular thermodynamic models aim to be completely predictive. They describe the micellization phenomena only based on information about the molecular characteristics of substances and conditions of the medium, such as, for example, temperature, surfactant concentration, and ionic strength (Goldsipe and Blankschtein, 2007). Nagarajan and collaborators made important contributions to the development of molecular thermodynamic models used to describe the self-assembly of surfactant solutions. In their models (Nagarajan and Ruckenstein, 1991; Nagarajan, 1993; Nagarajan, 2002) they analyzed small and monodisperse micelles and also the transition between two micelle geometries. However, in those works, only the necessary condition for equilibrium is considered. The Nagarajan model was improved by Moreira and Firoozabadi (2009) when they started considering the minimum of Gibbs free energy as a condition for the thermodynamic equilibrium of the solution. However, Moreira and Firoozabadi (2009) used the maximum term approach, which assumes that the micelle size distribution can be represented by one characteristic micelle size and a single number of micelles formed. Therefore, Moreira and Firoozabadi (2009) did not take into account the fact that micelles can be formed with a large distribution of sizes. They also assumed that only small micelles could be formed, with either a spherical or globular shape. In their subsequent works (Moreira and Firoozabadi, 2010; Moreira and Firoozabadi, 2012; Lukanov and Firoozabadi, 2014) those aspects were kept the same. Therefore, to the best of our knowledge, the present work is the only one that considers the minimum Gibbs free energy as the most stable state together with the micelles' size distributions and also analyzes the transition between small (spherical) and rod-like (spherocylindrical) micelles as a function of temperature and salt concentration.

In this work we present an approach where the minimum of total Gibbs free energy is obtained for aqueous surfactant solutions (with and without electrolytes) considering the micelle size distributions and the more stable geometry (spherical and spherocylindrical) of micelles. Here, the stable state for a given set of temperature (T), pressure (P) and composition (N), obtained by the minimization of total Gibbs free energy of the system, gives us information about the most stable micelle geometry, micelles sizes and the critical micelle concentration (CMC) of the solution.

MODEL

The model used to calculate the total Gibbs free energy of the system is similar to the one proposed by Nagarajan and Ruckenstein (1991) and Moreira and Firoozabadi (2009). Given a global specification of T (temperature), P (pressure), N_{SA} (total number of surfactant molecules in the solution) and N_w (number of water molecules), the Gibbs free energy is calculated as a sum of two contributions: free energy of formation and free energy of mixture.

$$G = N_w\mu_w^o + N_{sA}\mu_{1A}^o + \sum_{g=2}^{\infty} N_g g\Delta\mu_g^o + kT\left[N_w \ln X_w + N_{1A}\ln X_4 + \sum_{g=2}^{\infty} N_g \ln X_g\right] \quad (1)$$

where μ_w^o, μ_{1A}^o and μ_g^o are the standard chemical potentials of water, free surfactant and micelle with aggregation number g, N_g is the number of micelles, k is the Boltzmann constant, and X_w, X_{1A} and X_g are the mole fractions of water, free surfactant and micelles.

It is possible to reorganize the previous expression by separating the terms that depend only on fixed variables: T, P, N_{SA}, and N_w, and dividing the expression by kT:

$$\frac{G'}{kT} = \sum_{g=2}^{\infty} N_g g\frac{\Delta\mu_g^o}{kT} + N_w \ln X_w + N_{1A}\ln X_{1A} + \sum_{g=2}^{\infty} N_g \ln X_g \quad (2)$$

Equation (2) represents the expression to be minimized to predict the most stable state of the system. The free energy of micellization $\left(\frac{\Delta\mu_g^o}{kT}\right)$ is defined as a sum of different contributions. These contributions are detailed elsewhere by Nagarajan and Ruckenstein

(1991) and Moreira and Firoozabadi (2009).

When the micelles size distribution is narrow enough, it is common to use the Maximum Term approximation. when the Maximum Term approximation is used, Equation (2) becomes:

$$\frac{G'}{kT} = N_g g \frac{\Delta\mu_g^o}{kT} + N_w \ln X_w + N_{1A} \ln X_{1A} + N_g \ln X_g \quad (3)$$

METHODOLOGY

Critical Micelle Concentration (CMC)

Experimentally, the critical micelle concentration (CMC) is defined as the concentration of surfactant where a sharp change in any property of the solution is observed. This information is available in the literature for a wide variety of surfactants. Therefore we decided to validate our model by comparing our predictive calculations with experimental CMC data. To obtain the CMC, we perform different simulations of a solution containing an increasing amount of surfactant. Then, for each solution with a different amount of surfactant added we performed the minimization of the Gibbs free energy. This procedure permits one to relate the total number of surfactant molecules added (N_{SA}) with the number of free surfactant molecules in the solution (N_{1A}), as is graphically presented in Figure 1. The CMC is then defined as the concentration of surfactant added (N_{SA}) where an inflexion of the curve is observed. To obtain this point automatically, a regularization function is used which relates N_{1A} as a function of N_{SA}, according to Equation (4).

$$N_{1a}(N_{SA}) = a \cdot N_{SA} + b - c \cdot \left(N_{SA} - N_{SA}^*\right) \cdot \left[1 + \frac{\left(N_{SA} - N_{SA}^*\right)}{\sqrt{\left(N_{SA} - N_{SA}^*\right)^2 + \xi^2}}\right] \quad (4)$$

where N_{SA}^*, determined by non-linear regression, corresponds to the critical number of surfactant molecules added to the solution under the conditions T and P, and ξ is the regularization parameter, where $1 > \xi >>> 0$. The parameters a, b, and c are obtained from the fitting of the data to the regularization function.

To perform the parameter fitting we used the deterministic method Sequential Quadratic Programming (SQP). After obtaining the concentration of surfactant added (N_{SA}), we can calculate the critical micelle concentration using the number of water molecules assumed in the simulation (N_W).

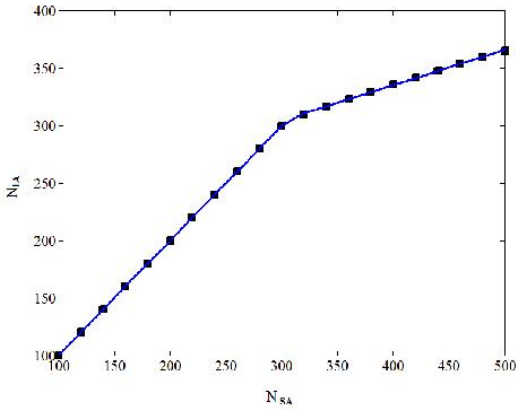

Figure 1: Determination of the CMC. Each point represents one minimization process of the Gibbs free energy and the continuous line is the adjusted regulation function. CMC is obtained by parameter fitting of the regularization function represented by Equation (4).

Micelle Size Distribution

To develop the methodology for the micelle size distributions, first we verify what kind of behavior this distribution can have. For that, we consider a set of optimization variables, where it is assumed that we could obtain micelles with an aggregation number from 2 to 100. To construct the next figure, we define as optimization variables the vector of the number of micelles formed for each aggregation number g. Thus, for this specific case we did not pre-set any shape for the micelle size distribution. Figure 2 shows the tendency obtained for the micelle size distribution for an aqueous solution of sodium dodecyl sulfate (SDS) at a concentration ten times higher than its critical micelle concentration. It is interesting to observe that the problem converges to a micelle size distribution with a behavior similar to a Gaussian distribution.

From now on in this work, a Gaussian shape is assumed for all the micelle size distributions. Therefore, it is possible to define the total number of micelles formed, the mean (or expectation) aggregation number of the distribution and its standard deviation as important variables for calculating the minimum free energy of the system.

To validate our methodology for the micelle size

distribution, first we compared it with the maximum term approach, both considering the minimum Gibbs free energy to define the most stable state. Because we calculate the critical micelle concentration, only small micelles are considered (spherical and globular shapes only). The geometrical relations used for this section are similar to those presented by Nagarajan and Ruckenstein (1991). Using our methodology, three optimization variables, as mentioned before, are used to calculate each minimum of Gibbs energy. Using the Maximum Term Approximation, we have two optimization variables: the number of micelles formed, N_g, and the specific aggregation number, g.

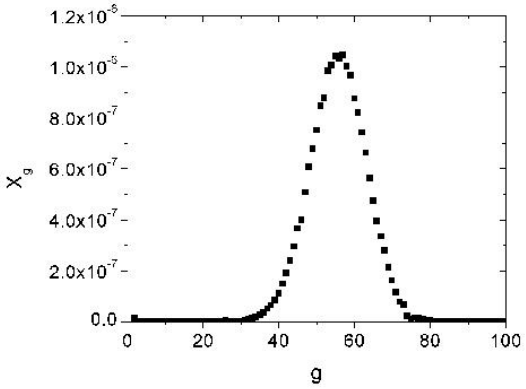

Figure 2: Micelle size distribution for a solution of sodium dodecyl sulfate (SDS) at a concentration ten times its critical micelle concentration. X_g is the mole fraction of micelles with the aggregation number g. T = 25 °C, P = 1 atm, and N_w = 3400000. The micelle size distribution converges to a Gaussian-like distribution after the optimization procedure.

Geometry Optimization

As in all optimization problems, we must pay attention to the correct definition of the optimization variables to be used in the numerical algorithm. The incorrect selection of variables, if they do not satisfy some constraints or correspond to an over specification, may lead to erroneous results and misinterpretations. It is even more important when using nondeterministic algorithms because the analyticity of the functions and equality constraints are not taken into account. This can result in objective functions with several local minima.

Analyzing the geometric relations presented in Table 1, we can observe that, if the length of the cylindrical part of the micelle (L_c) is zero, the geometry reduces to a spherical micelle. For cases where the geometric transition is considered, we define as optimization variables the number of micelles formed (N_g), the number of surfactant molecules in the cylindrical part of the micelle (g_{cyl}), the radius of the spherical ends of the micelles (R_s), and the length of the cylindrical part (L_c). The number of surfactant molecules in the spherical ends of the micelle is then obtained from the geometric relations presented in Table 1, which assumes the form of:

$$g_{sph} = \frac{1}{\upsilon_s} \cdot \left[\frac{8\pi}{3} \cdot R_s{}^3 - \frac{2\pi}{3} \cdot H^2 \cdot (3R_s - H) \right] \qquad (5)$$

To reduce the optimization search region, we defined limits for the optimization variables. The maximum value of the radius, R_s, is assumed to be equal to the extended length of the surfactant tail, ensuring that there is no empty space inside the micelle. Besides that, R_s must be equal to or greater than the radius of the cylindrical part of the micelle to ensure that the amount of surfactant molecules in the spherical ends is positive. Figure 3 presents a surface of the Gibbs energy, to be minimized, fixing values for L_c and R_s. We can observe that the function has a smooth behavior and a well-defined global minimum.

Numerical Method

As presented in the previous section, calculating the critical micelle concentration involves repeating the Gibbs energy minimization several times for different surfactant concentrations. To reduce the computational time to perform these calculations, we propose the following optimization procedure. First, we define an amount of water to be considered and the temperature of the system. After that, we start our simulations with a small amount of surfactant (to guarantee that we are below the critical micelle concentration). For this first simulation we use the Particle Swarm Optimization method (PSO). The result is then used as an initial guess for the Sequential Quadratic Programming (SQP) deterministic method. Then, we make a small increment in the amount of surfactant and perform the optimization with the deterministic method. The initial guess now, in this case, is the optimum value of the optimization at the lower surfactant concentration. With this methodology, it is only necessary to use the nondeterministic method once, which largely reduces the computational effort. All simulations were performed with the software *Matlab*® version R2008a. More details about the PSO method can be found elsewhere (Kennedy and Eberhart, 1995) and for the SQP method in Byrd *et al.* (2000).

Table 1: Geometric relations for a spherocylindrical micelle.

Cylindrical part (radius R_c, length L_c)	Spherical part (radius R_s)
$V_g = \pi R_c^2 L_c = g\upsilon_s$	$H = R_s\left[1-\left\{1-\left(\frac{R_c}{R_s}\right)^2\right\}^{1/2}\right]$
$A_g = 2\pi R_c L_c = ga$	$V_g = \left[\frac{8\pi R_s^3}{3} - \frac{2\pi}{3}H^2(3R_s - H)\right] = g\upsilon_s$
$A_{g\delta} = 2\pi(R_c + \delta) = ga_\delta$	$A_g = \left[8\pi R_s^2 - 4\pi R_s H\right] = ga$
$P_f = \frac{V_g}{A_g R_c} = \frac{\upsilon_s}{aR_c} = \frac{1}{2}$	$A_{g\delta} = \left[8\pi(R_s+\delta)^2 - 4\pi(R_s+\delta)(H+\delta)\right] = ga_\delta$
	$P_f = \frac{V_g}{A_g R_s}$

V_g is the volume of the micelle, A_g is its surface area, $A_{g\delta}$ is its area at a distance δ from the surface, P_f is the packing factor, and R is the radius of the micelle (s for the spherical part and c for the cylindrical part). Variable H is a geometrical parameter. The expression of the volume of the surfactant tail (υ_s), as well as molecular parameters for different surfactants are presented elsewhere (Nagarajan and Ruckstein, 1991).

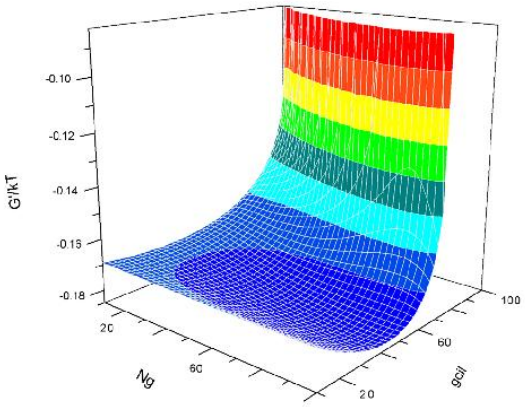

Figure 3: Typical example of the Gibbs energy, G'/kT, as a function of the number of micelles with aggregation number g, N_g, and the number of surfactant molecules in the cylindrical part of the micelle, g_{cyl}. We fixed the values of the length of the cylindrical part of the micelle, L_c, and the radius of the spherical ends of the micelles, R_s, to be equal to 2.89 nm and 1.23 nm, respectively.

RESULTS AND DISCUSSION

Figure 4 presents the critical micelle concentration (CMC) for different surfactants as a function of their tail length. To perform these calculations we assumed that micelles are globular or spherically shaped. The performance of the maximum term method and the micelle size distribution method were compared. We observe that both methodologies are in very good agreement and predict the critical micelle concentrations well. We expect that at low surfactant concentration (close to the CMC) the micelle-size distribution tends to be narrower, compared with high surfactant concentration. For example, in Figure 5 we present the micelle size distribution for different surfactants at different concentrations. We observe relatively wide size distributions for all the cases presented in Figure 5, meaning that, for those cases, the Maximum Term method certainly is not the best approach. We expect wider distributions for high surfactant concentration or for microemulsion systems, in which case the methodology proposed here becomes more adequate to describe those systems. Another aspect that motivates the use of the size distribution approach proposed here is because sizes (mean, variance and other moments of the distribution) are important information for the stability of emulsions. For example, when an electric field is applied to an emulsion, its stability is a function of the diameter of the micelles to the fourth power.

We also proposed a methodology to describe the micelle geometry transitions. The results obtained are presented in Table 2. The surfactant dodecyl trimethylammonium bromide (C_{12}TAB) forms spherical micelles even at high surfactant concentration. However, sodium dodecyl sulfate (SDS) presents a transition from spherical to spherocylindrical as observed experimentally (Victorov and Koroleva, 2014). Another result obtained is that the addition of electrolytes

to the surfactant solution causes the formation of spherocylindrical micelles for tetradecyl trimethylammonium bromide (C_{14}TAB), and hexadecyl trimethylammonium bromide (C_{16}TAB). For the nonionic surfactant, decyl(dimethyl)phosphine oxide (C_{10}PO), the model predicts the formation of spherocylindrical micelles even without electrolytes added to the solution, but at higher surfactant concentrations. In general, we are in good qualitative agreement with the trends observed by experiments.

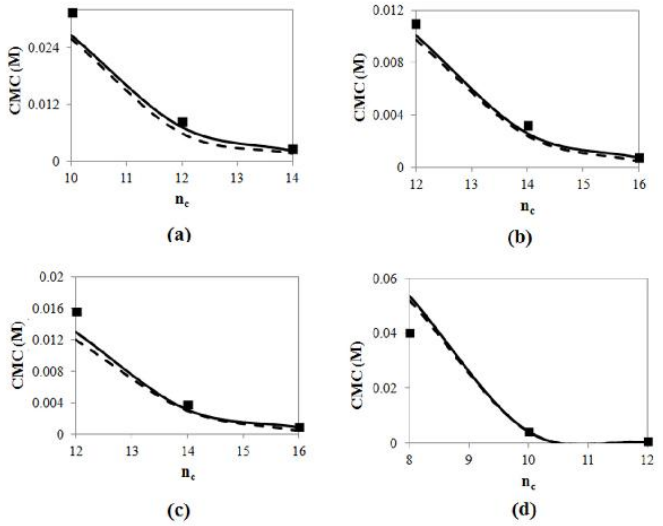

Figure 4: Critical micelle concentration (CMC) for different surfactants in aqueous solutions obtained by the maximum term method (continuous lines), and the size distribution methodology (dashed lines). The squares are experimental data (Khan and Shah, 2008; Neves *et al.*, 2007; Evans, 1956; Zhao *et al.*, 2012, Velázquez and Lopez-Dias, 2007). (a) Sodium n_c-alkyl sulfate, (b) n_c-alkyl pyridinium bromide, (c) n_c-alkyl trimethylammonium bromide, (d) n_c-alkyl(dimethyl)phosphine.

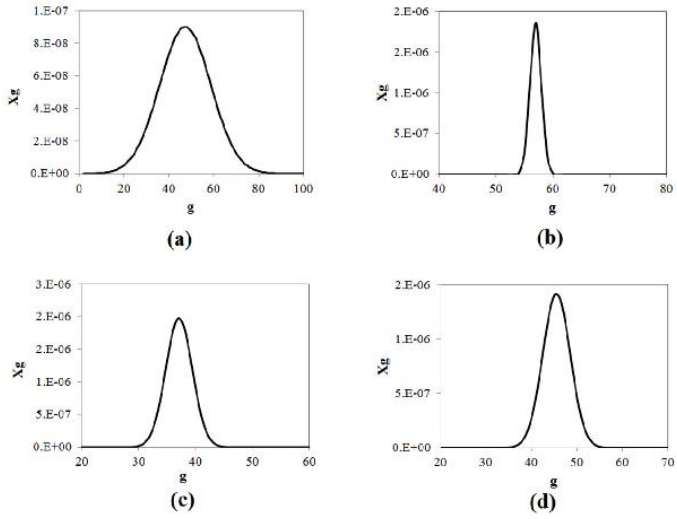

Figure 5: Micelle size distributions for different surfactants obtained by the proposed methodology. X_g is the molar fraction of micelles with aggregation number g: (a) 16.34 mM SDS solution; (b) 81.7 mM C_{12}TAB solution; (c) 32.68 mM C_{14}TAB solution; (d) 32.68 mM C_{16}TAB solution. We defined $T = 25$ °C, $P = 1$ atm, and $N_w = 3400000$.

Table 2: Geometry transition between spherical and spherocylindrical micelles.

	Surfactant concentration (mM)	Electrolyte concentration (M)	N_g	Geometry	R_S	g_{sph}
SDS	49.0	-	31	Spherical	1.54	65
	81.7	-	52	Spherical	1.57	69
	49.0	0.6	7	Spherocylindrical $g_{cyl}=333$, $L_c=17.27$ nm	1.67	92
	81.7	0.6	3	Spherocylindrical $g_{cyl}=1565$, $L_c=81.56$ nm	1.67	92
$C_{12}TAB$	49.0	-	49	Spherical	1.23	34
	81.7	-	92	Spherical	1.25	35
	49.0	0.6	60	Spherical	1.35	46
$C_{14}TAB$	81.7	2.0	14	Spherical	1.59	70
	81.7	4.0	10	Spherocylindrical $g_{cyl}=20$, $L_c=1.56$ nm	1.62	79
$C_{16}TAB$	16.4	0.2	12	Spherical	1.76	82
	81.7	0.2	64	Spherical	1.74	95
	16.4	2.0	6	Spherocylindrical $g_{cyl}=69$, $L_c=4.99$ nm	1.80	97
	81.7	2.0	9	Spherocylindrical $g_{cyl}=457$, $L_c=33.79$ nm	1.80	98
$C_{10}PO$	9.8	-	6	Spherical	1.34	57
	16.4	-	3	Spherocylindrical $g_{cyl}=201$, $L_c=17.56$ nm	1.34	62

CONCLUSIONS

Here we proposed a methodology to consider the micelle size distribution and also an approach to predict micelle shape transitions, both considering the minimum of Gibbs free energy of the system. Comparing the predictive performance of calculated critical micelle concentrations with experimental data validated the model. Good results are obtained. The proposed methodology is able to predict quantitatively the transition between spherocylindrical and spherical in sodium dodecyl sulfate and qualitatively for n-alkyl trimethylammonium bromide, according to experimental data. Furthermore, the methodology used to obtain the critical micelle concentration (CMC) significantly reduces the computational cost involved.

This work pioneers a more detailed description of the micellization phenomena by Molecular Thermodynamics simulation considering the minimum of Gibbs free energy. It can be extended to describe systems where the micelle size distribution is relevant and also where large micelles are formed. For example, the micelle size distribution is important to consider when studying the stability of emulsions, especially when external fields are applied. We suggest, for future work, adapting this model to consider a better description of systems with high electrolyte concentration, where spherocylindrical micelles are expected to be formed, and also to extend this approach by considering equations of state, which is a very promising path.

ACKNOWLEDGEMENTS

We thank the Brazilian Agencies CNPq (*Conselho Nacional de Desenvolvimento Científico e Tecnológico*) and CAPES (*Coordenação de Aperfeiçoamento de Pessoal de Nível Superior*) for providing scholarships and for supporting this work.

NOMENCLATURE

a	Micelle surface area per surfactant (m^2)
a_δ	Micelle surface area per surfactant at a distance δ (m^2)
A_g	Superficial area of the micelle of aggregation number g (m^2)

$A_{g\delta}$	Superficial area of the micelle of aggregation number g at a distance δ (m^2)
a, b, c	Regularization constants
g	Aggregation number
G	Gibbs free energy (J)
H	Geometric constant (m)
k	Boltzmann constant ($J \cdot K^{-1}$)
L_c	Length of the cylindrical part of the micelle (m)
n_c	Number of carbons in the surfactant tail
N_i	Number of molecules of i
P	Pressure (Pa)
P_f	Packing factor
R_c	Radius of the cylindrical part of the micelle (m)
R_s	Radius of the spherical part of the micelle (m)
T	Temperature (K)
V_g	Volume of the micelle of aggregation number g (m^3)
v_s	Volume of the surfactant tail (m^3)
X	Molar fraction

Greek Letters

μ	Chemical potential (J)
$\Delta\mu$	Free energy of micellization (J)

Subscripts

w	Water
SA	Surfactant
$1A$	Free surfactant
g	Micelle of aggregation number g
s, *sph*	Spherical
c, *cyl*	Cylindrical

REFERENCES

Byrd, R. H., Gilbert, J. C. and Nocedal, J., A trust region method based on interior point techniques for nonlinear programming. Mathematical Programing, 89(1), p. 149-185 (2000).

Evans, H. C., Alkyl sulphates. Part I. Critical micelle concentrations of the sodium salts. Journal of Chemical Society, p. 579-586 (1956).

Goldsipe, A. and Blankschtein, D., Molecular-thermodynamic theory of micellization of multicomponent surfactant mixtures: 1. Conventional (pH-Insensitive) surfactants. Langmuir, 23(11), p. 5942-5952 (2007).

Iyer, J. and Blankschtein, D., Are ellipsoids feasible micelle shapes? An answer based on a molecular-thermodynamic model of nonionic surfactant micelles. Journal of Physical Chemistry, B, 116, p. 6443-54 (2012).

Kamranfar, P. and Jamialahmadi M., Effect of surfactant micelle shape transition on the microemulsion viscosity and its application in enhanced oil recovery processes. Journal of Molecular Liquids, 198, p. 286-291 (2014).

Kennedy, J. and Eberhart, R., Particle swarm optimization. Proceedings of IEEE International Conference on Neural Networks IV, p. 1942-1948 (1995).

Khan, A. M. and Shah, S. S., Determination of Critical Micelle Concentration (CMC) of Sodium Dodecyl Sulfate (SDS) and the effect of low concentration of pyrene on its CMC using ORIGIN software. Journal of Chemical Society of Pakistan, 30(2), p. 186-191 (2008).

Lukanov, B. and Firoozabadi, A., Specific ion effects on the self-assembly of ionic surfactants: A molecular thermodynamic theory of micellization with dispersion forces. Langmuir, 30(22), p. 6373-6383 (2014).

Moreira, L. A. and Firoozabadi, A., Thermodynamic modeling of the duality of linear 1-alcohols as co-surfactants and cosolvents in self-assembly of surfactant molecules. Langmuir, 25(20), p. 12101-12113 (2009).

Moreira, L. A. and Firoozabadi, A., Molecular thermodynamic modeling of droplet-type microemulsions. Langmuir, 28(3), p. 1738-1752 (2012).

Moreira, L. A. and Firoozabadi, A., Molecular thermodynamic modeling of specific ion effects on micellization of ionic surfactants. Langmuir, 26(19), p. 15177-15191 (2010).

Nagarajan, R., Modelling solution entropy in the theory of micellization. Colloids and Surfaces A, 71, p. 39-64 (1993).

Nagarajan, R., Self-assembly: The neglected role of the surfactant tail. Langmuir, 18(01), p. 31-38 (2002).

Nagarajan, R. and Ruckenstein, E., Theory of surfactant self -assembly: A predictive molecular thermodynamic approach. Langmuir, 7(3), p. 2934-2969 (1991).

Neves, A. C. S., Valente, A. J. M., Burrows, H. D., Ribeiro, A. C. F., Lobo, V. M. M., Effect of terbium(III) chloride on the micellization properties of sodium decyl and dodecyl-sulfate solutions. Journal of Colloid and Interface Science, 306, p. 166-74 (2007).

Puvvada, S. and Blankschtein, D., Molecular-thermodynamic approach to predict micellization, phase behavior and phase separation of micellar solutions. I. Application to nonionic surfactants. Journal of

Chemical Physics, 92(6), p. 3710-3724 (1990).
Rusanov, A. I., The wonderful world of micelles. Colloidal Journal, 76(2), p. 121-126 (2014).
Tanford, C., Thermodynamics of micelle formation: Prediction of micelle size and size distribution chemistry. Proceedings of the National Academy of Science, 71(5), p. 1811-1815 (1974).
Velázquez, M. M. and López-Díaz, D., Variation of the critical micelle concentration with surfactant structure: A simple method to analyze the role of attractive - repulsive forces on micellar association. The Chemical Educator, 12(5), p. 1-6 (2007).
Victorov, A. I. and Koroleva, S. V., Modeling of the effects of ion specificity on the onset and growth of ionic micelles in a solution of simple salts. Langmuir, 30(12), p. 3387-3396 (2014).
Whitesides, G. M. and Boncheva, M., Beyond molecules: self-assembly of mesoscopic and macroscopic components. Proceedings of the National Academy of Science USA, 99(8), p. 4769-4774 (2002).
Zhao, M., Gao, Y. and Zheng, L., Micelle Formation by N-alkyl-N-methylpiperidinium bromide ionic liquids in aqueous solution. Colloids and Surfaces A: Physicochemical and Engineering Aspects, 412, p. 90-95 (2012).

Appendix B

Algorithm to obtain the critical micelle concentration from molecular thermodynamics simulations

1) Input data: (i) amount of water; (ii) amount, kind and physicochemical properties of the surfactant; (iii) temperature of the solution;

2) Minimization of the Gibbs free energy:

2.1) Calculation of the Gibbs free energy:

2.1.i) Calculate the molar fractions of water, free surfactant, micelles and ions;

2.1.ii) Calculate the free energy of micellization for each geometry;

2.1.iii) Calculate the Gibbs free energy for each geometry;

2.1.iv) Compare the values of the Gibbs free energy for each geometry of the micelles. The lowest one will be assumed to be the most stable state of the surfactant solution.

2.2) Minimize the Gibbs free energy – using a hybrid method of optimization (PSO followed by SQP). From this minimization we can obtain the number of micelles formed, their sizes, their morphology and the number of free surfactants in the solution.

3) Increase the amount of surfactant in the solution and return to step 1. From this stage, step 2.2 uses as an initial guess of the optimization variables the results obtained from the previous optimization, thus only the SQP method is used after the first amount of surfactant is simulated.

4) When the final amount of surfact is simulated, we can relate the number of molecules of free surfactant in the solution with the number of molecules of surfactant added to the solution. This curve is used to obtain the critical micelle concentration using the expression proposed in the work of Santos *et al*. (2016)

References

Santos, M. S.; Tavares, F. W.; Biscaia Jr., E. C. Molecular Thermodynamics of Micellization: Micelle Size Distributions and Geometry Transitions, Braz. J. Chem. Eng., Vol. 33, No. 03, pp. 515 – 523, 2016.

Appendix C

The dynamics of electrolyte solutions considering the ion size asymmetry and the solvent size

Here, we considered the dynamics of electrolyte solutions between charged electrodes. For that, we start considering the Nernst-Planck equation for the ion i.

$$\frac{\partial c_i}{\partial t} + \nabla \Gamma_i = 0$$

Where c_i is the concentration of ion i, t is the time and Γ_i is the ionic flux, which is calculate from the following relation:

$$\Gamma_i = -\frac{D}{kT} c_i \nabla \mu_i$$

With D being the diffusivity of the ions, k the Boltzmann constant, T the temperature and μ_i the electrochemical potential of the ion.

To include the effects of the electrolyte and solvent sizes we used the work developed by Kilic (2008) where, using a lattice approach he took into account steric effects of electrolyte solutions.

$$\mu_{\pm} = ze\psi + kT\left[\ln\left(\frac{c_{\pm}}{c_+ + c_- + c_w}\right) - \frac{a_{\pm}^3}{a_w^3}\ln\left(\frac{c_w}{c_+ + c_- + c_w}\right)\right]$$

In this expression, the index + and – are related to the cation and anion respectively, and w for the solvent, which here we consider to be the water. The parameter a is the hydrated radii of the ions and of the water. To obtain the electrostatic potential (ψ) we coupled the previous equations with the modified Poisson-Boltzmann equation which takes into account electrostatic correlation effects.

$$\varepsilon(l_c^2 \nabla^4 \psi - \nabla^2 \psi) = \rho$$

The parameter l_c is the electrostatic correlation length and on this analysis we considered it to be equal to the hydrated radii of the ion. To enhance the numerical

solution of the equations of this problem we defined dimensionless variables and an auxiliary variable as follows:

$$\chi_i = \frac{c_i}{c_0}$$

$$y = \frac{e\psi}{kT}$$

$$\bar{\Gamma}_i = \frac{\Gamma_i}{Dc_0\kappa}$$

$$\bar{\mu}_i = \frac{\mu_i - \mu_{i0}}{kT}$$

$$\zeta = \frac{x}{L}$$

$$\tau = \frac{t\kappa D}{L}$$

$$\phi = \alpha^2\left(\frac{\partial^2 y}{\partial \zeta^2}\right) - y$$

where L is the distance between the electrodes, and $\kappa = \sqrt{\frac{2N_A e^2 I}{\varepsilon kT}}$ is the Debye length for a given ionic strength (I).

For the boundary conditions we have that there is no ion flux on the surface of the electrodes, which leads to:

$$\bar{\Gamma}_i|_{\zeta=0} = \bar{\Gamma}_i|_{\zeta=1} = 0$$

Furthermore, it is considered that there are no electrostatic correlations on the surface of the electrode:

$$\left(\frac{\partial y}{\partial \zeta} + \frac{\partial \phi}{\partial \zeta}\right)\Big|_{\zeta=0} = \left(\frac{\partial y}{\partial \zeta} + \frac{\partial \phi}{\partial \zeta}\right)\Big|_{\zeta=1} = 0$$

Here we considered two different systems, one where a direct current is applied (DC problem) and one where an alternate current is applied over the electrodes (AC

problem). For the DC problem, we have a specified potential (y_0) applied over both electrodes, which results on the following boundary conditions:

$$y|_{\zeta=0} = -y_0\left[1 - exp\left(-\frac{\tau}{0.1}\right)\right]$$

$$y|_{\zeta=1} = y_0\left[1 - exp\left(-\frac{\tau}{0.1}\right)\right]$$

And for the AC problem:

$$y_s - y|_{\zeta=0} = -\delta\lambda\left.\frac{\partial y}{\partial \zeta}\right|_{\zeta=0}$$

$$y_s - y|_{\zeta=1} = \delta\lambda\left.\frac{\partial y}{\partial \zeta}\right|_{\zeta=1}$$

The parameters $\alpha, \delta,$ and λ can be find on the work of Alijó *et al*., 2015. Lastly, it is also necessary to define the initial condition for both problems, which is assumed that the concentration of the ions at the beginning is equal to the bulk concentration at any place between the electrodes.

$$\chi_i|_{\tau=0} = 1$$

The equations were numerically solved using orthogonal collocation on finite elements on the EMSO software. The distribution of the collocation points was defined to be concentrated on the regions close to the electrodes in order to have a better description of the fast changes on the dependent variables close to the electrodes. All the results here present the independent variable ζ as a function of the collocation points for a better visualization of the behavior of the dependent variables on the electrical double layer.

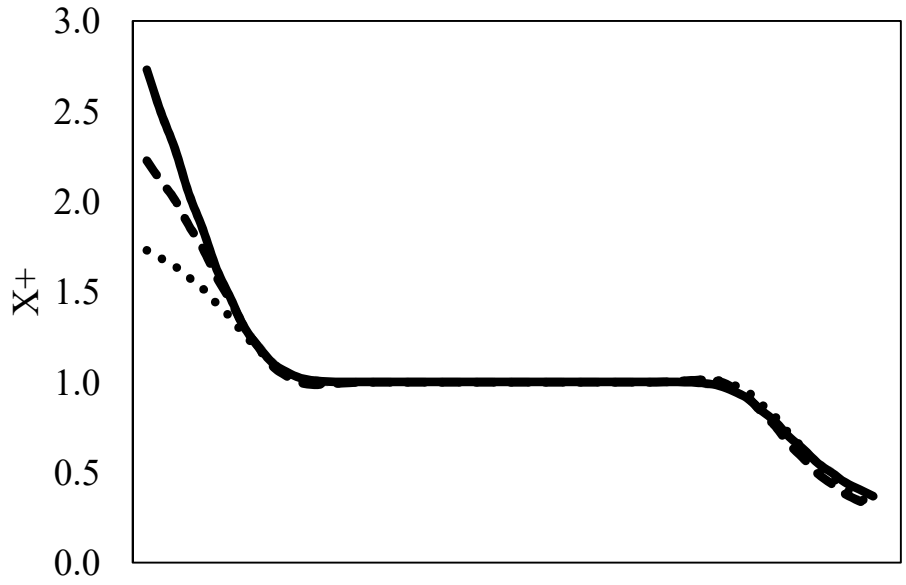

Figure 21 – Variation of the dimensionless cation concentration between the electrodes as a function of the different sizes of the cation, anion, and solvent under a DC voltage. The continuous line is for the case where the anion, the cation and the solvent have radii equal to 0.3nm. The dashed line is for the cation and the anion with the same size radii $\boldsymbol{a_{\pm} = 0.6nm}$ and the solvent $\boldsymbol{a_w = 0.3nm}$. And the dotted line for when the cation is larger than the anion $\boldsymbol{a_+ = 0.8nm}$, $\boldsymbol{a_- = 0.6nm}$, and $\boldsymbol{a_w = 0.3nm}$.

Figure 21 shows how the different size of the ions impact on the concentration of the cation between the electrodes for the DC problem where a dimensionless potential $y_0 = 1$ is applied to the electrodes. As the size of the cation increases the concentration of cations reduces close to the electrode that is charged negatively as a response on the increase of steric effects. From Figure 22 to Figure 24 we present the results obtained for a DC problem with the cation, anion, and the solvent (water in this case) having different sizes. And on Figure 25 to Figure 27 we present the results for the AC problem for an electrolyte solution where anion, cation, and solvent present the same sizes.

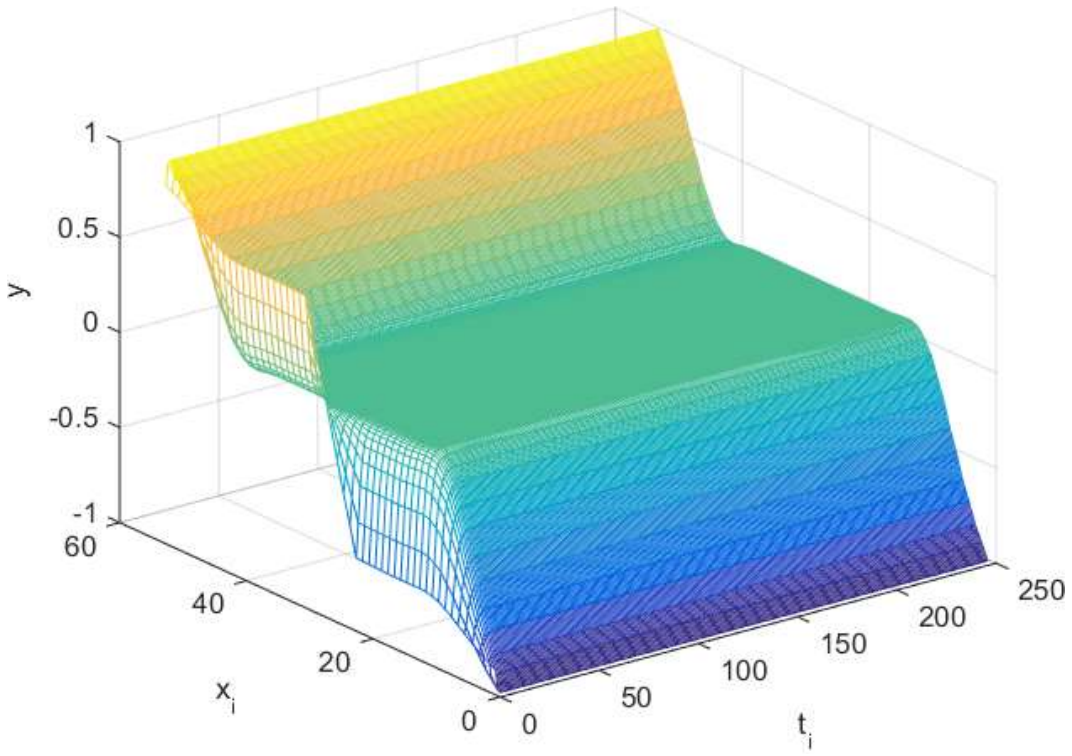

Figure 22 – Variation of the dimensionless electrostatic potential as a function of the dimensionless time $(\boldsymbol{\tau})$ and the collocation points between the electrodes for the DC problem. We considered an ionic strength $\boldsymbol{I = 1M}$, a symmetric electrolyte 1:1, and $\boldsymbol{a_+ = 0.8\ nm}$, $\boldsymbol{a_- = 0.6\ nm}$, and $\boldsymbol{a_w = 0.3\ nm}$.

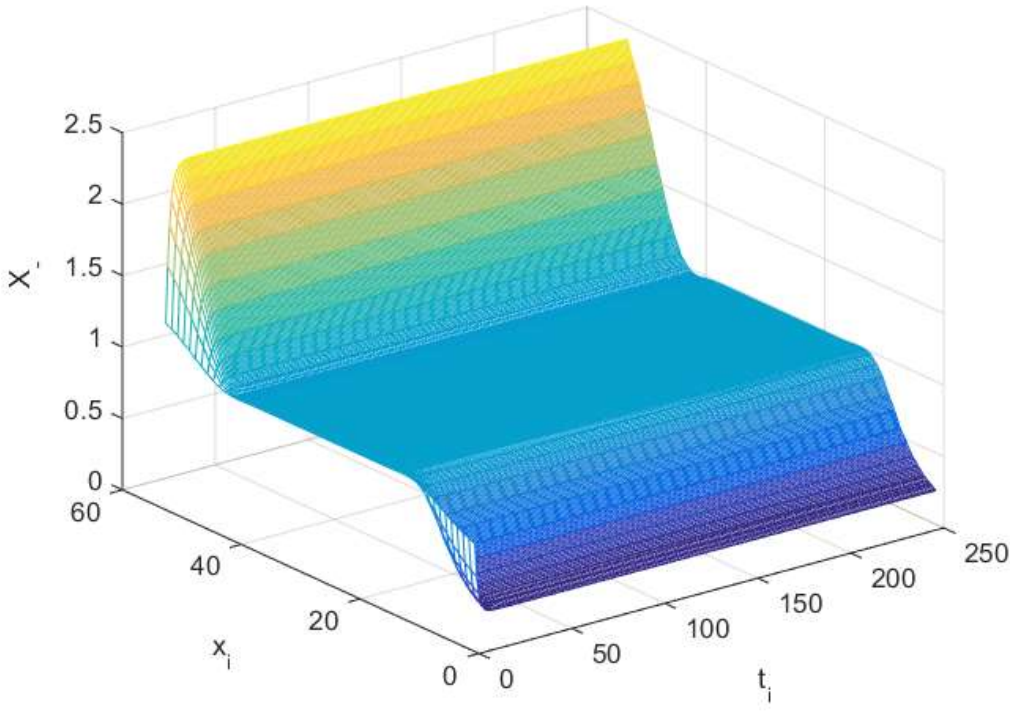

Figure 23 - Variation of the dimensionless anion concentration as a function of the dimensionless time $(\boldsymbol{\tau})$ and the collocation points between the electrodes for the DC problem. We considered an ionic strength $\boldsymbol{I = 1M}$, a symmetric electrolyte 1:1, and $\boldsymbol{a_+ = 0.8\ nm}$, $\boldsymbol{a_- = 0.6\ nm}$, and $\boldsymbol{a_w = 0.3\ nm}$.

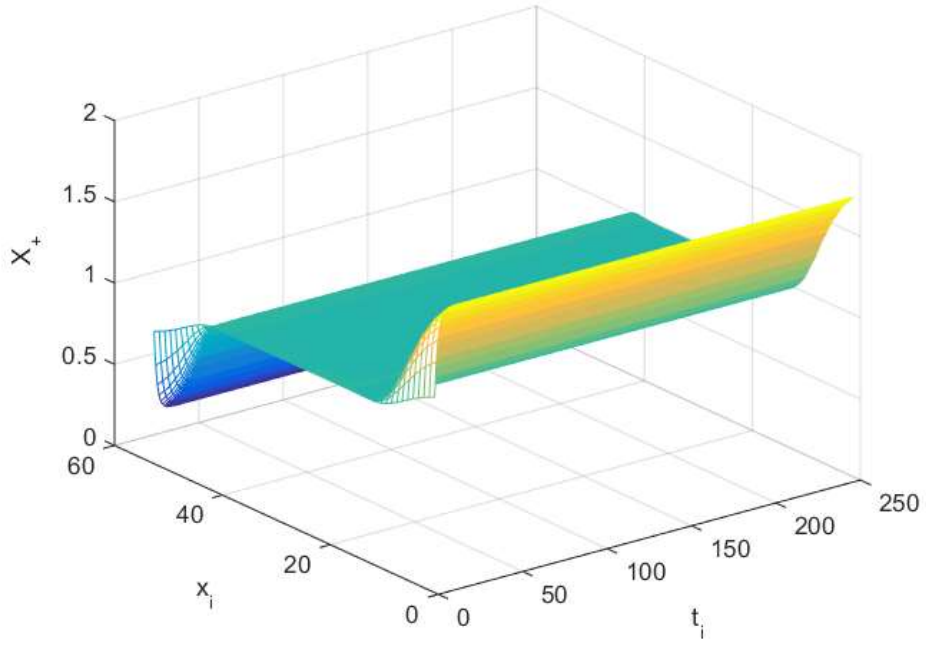

Figure 24 - Variation of the concentration of the cation as a function of the dimensionless time $(\boldsymbol{\tau})$ and the collocation points between the electrodes for the DC problem. We considered an ionic strength $\boldsymbol{I = 1M}$, a symmetric electrolyte 1:1, and $\boldsymbol{a_+ = 0.8\ nm}$, $\boldsymbol{a_- = 0.6\ nm}$, and $\boldsymbol{a_w = 0.3\ nm}$.

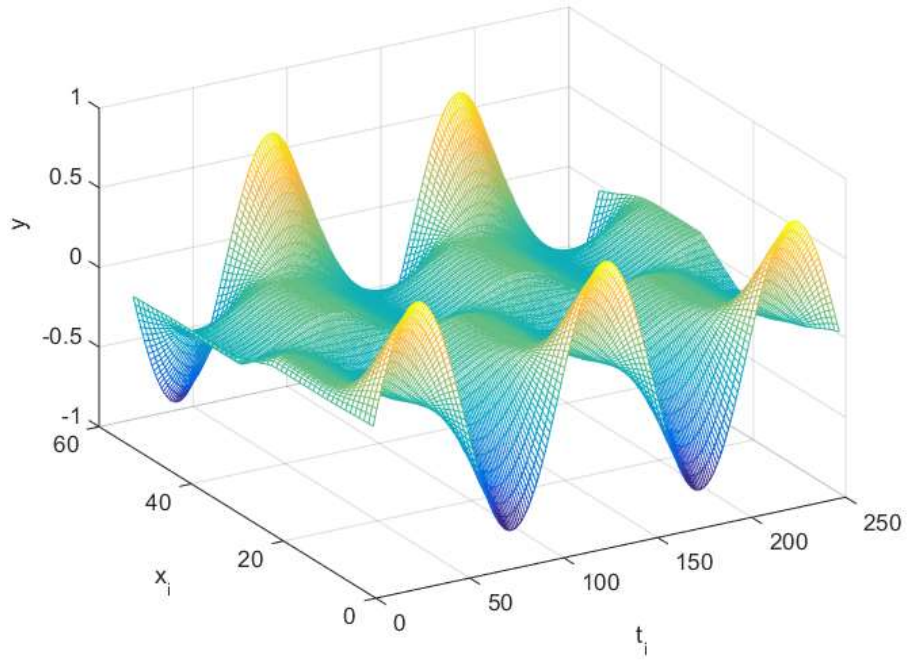

Figure 25 - Variation of the dimensionless electrostatic potential as a function of the dimensionless time $(\boldsymbol{\tau})$ and the collocation points between the electrodes for the AC problem. We considered an ionic strength $\boldsymbol{I = 1M}$, a symmetric electrolyte 1:1, and $\boldsymbol{a_+ = 0.3\ nm}$, $\boldsymbol{a_- = 0.3\ nm}$, and $\boldsymbol{a_w = 0.3\ nm}$ and a dimensionless frequency $\boldsymbol{\omega = 0.3}$.

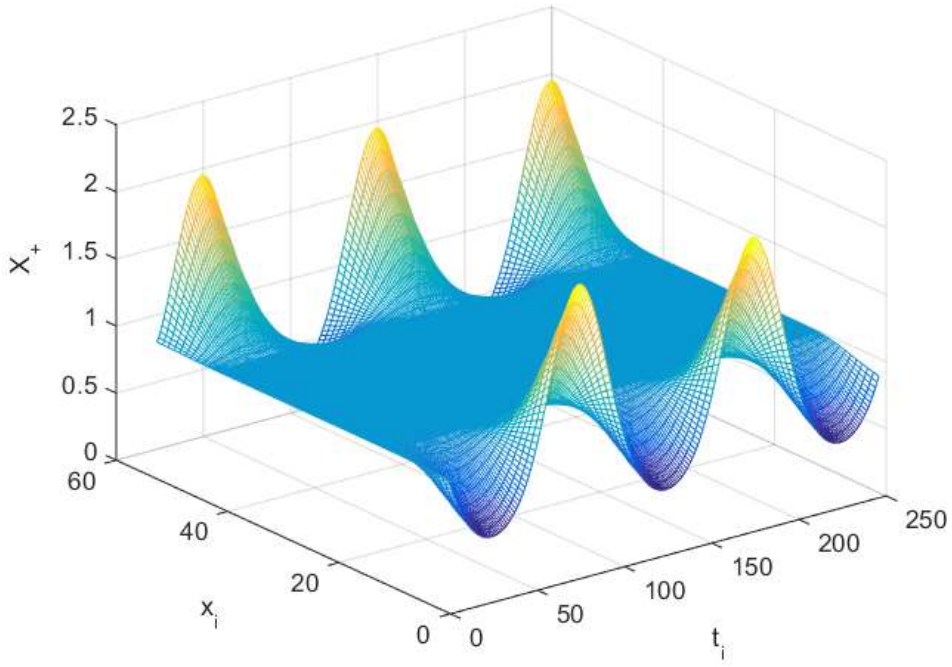

Figure 26 - Variation of the dimensionless anion concentration as a function of the dimensionless time $(\boldsymbol{\tau})$ and the collocation points between the electrodes for the AC problem. We considered an ionic strength $\boldsymbol{I = 1M}$, a symmetric electrolyte 1:1, and $\boldsymbol{a_+ = 0.3\ nm}$, $\boldsymbol{a_- = 0.3\ nm}$, and $\boldsymbol{a_w = 0.3\ nm}$ and a dimensionless frequency $\boldsymbol{\omega = 0.3}$.

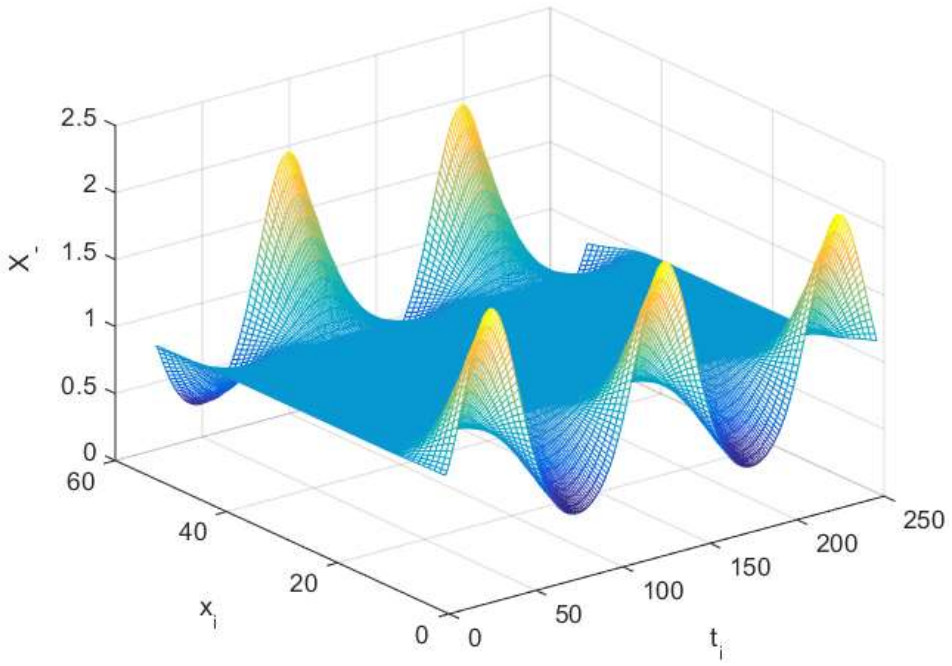

Figure 27 - Variation of the dimensionless cation concentration as a function of the dimensionless time $(\boldsymbol{\tau})$ and the collocation points between the electrodes for the AC problem. We considered an ionic strength $\boldsymbol{I = 1M}$, a symmetric electrolyte 1:1, and $\boldsymbol{a_+ = 0.3\ nm}$, $\boldsymbol{a_- = 0.3\ nm}$, and $\boldsymbol{a_w = 0.3\ nm}$, and a dimensionless frequency $\boldsymbol{\omega = 0.3}$.

Appendix D

To analyze the effect of electrostatic correlations in the interaction between two charged spherical colloidal particles or proteins we can use the BSK model for the modified Poisson equation in bispherical coordinates. In this appendix we present a brief introduction to bispherical coordinate system, how to couple it to the BSK model and finally a proposed numerical method to solve the resulting partial differential equation system.

A convenient way to describe the curvature effect between two spherical colloidal particles is by considering the bispherical coordinate system. This system turns the mash of the region between the two spheres into a rectangular and finite element, which is associated with several numerical advantages.

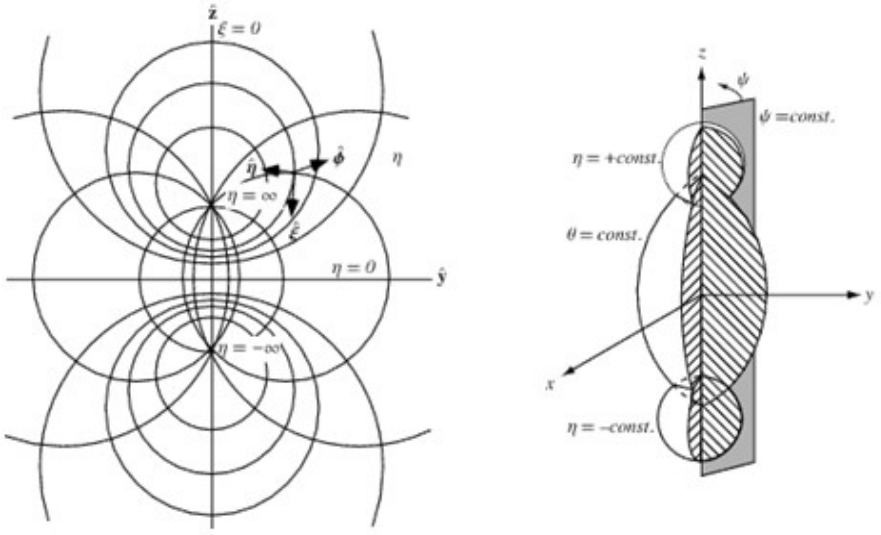

Figure 28 – Bispherical coordinate system. (WEISSTEIN, 2014)

This system is defined in the dimensions η, θ, φ, where surfaces with constant η are spheres, surfaces with constant θ have an apple shape if $\theta < \pi/2$ or lemon-shape if $\theta > \pi/2$, and surfaces with constant φ are semi-planes. (MOON & SPENCER, 1961). Therefore, if we consider that exists symmetry across the z axis, we can express this coordinate system in terms η e θ only. For those cases, the Laplacian operator is given by:

$$\nabla^2\psi = \frac{(\cosh\eta - \cosh\theta)}{a^2 \sin\theta}\left[\frac{\partial}{\partial\theta}\left(\frac{\sin\theta}{\cosh\eta - \cosh\theta}\frac{\partial\psi}{\partial\theta}\right) + \sin\theta\frac{\partial}{\partial\eta}\left(\frac{1}{\cosh\eta - \cosh\theta}\frac{\partial\psi}{\partial\eta}\right)\right] \tag{D.1}$$

The value of η in the surface of the spheres being studied(η_0) is obtained as a function of the radius of the spheres (r) and the distance between them(d).

$$\cosh\eta_0 = \frac{d}{r} \tag{D.2}$$

When describing colloidal and protein particles it is not necessary to study the region inside of this spherical particles, and because of that, the domain of this kind of system is $-\eta_0 \leq \eta \leq \eta_0$ and $0 \leq \theta \leq \pi$. At last, we need to define the variable a which is a function of η in the surface of the sphere (η_0):

$$-\frac{a}{\sinh\eta_0} = r \tag{D.3}$$

To go from the bispherical coordinate system to the Cartesian coordinate system we apply the following relations:

$$\begin{aligned} x &= \frac{a\sin\theta}{\cosh\eta - \sin\theta} \\ y &= \frac{a\cos\theta}{\cosh\eta - \sin\theta} \\ z &= \frac{a\sinh\eta}{\cosh\eta - \sin\theta} \end{aligned} \tag{D.4}$$

Electrostatic correlations (BSK model) in bispherical coordinates

The BKS model in terms of the dimensionless electrostatic potential (y), is defined as follows:

$$l_c^2\,\nabla^4 y - \nabla^2 y = \frac{e^2}{\varepsilon kT}\sum_i z_i c_i \tag{D.5}$$

To avoid the use of the fourth order differential operator, the following variable change is applied:

$$a^2\nabla^2 y = \phi \tag{D.6}$$

Multiplying both sides of the previous equation by a^2 and defining a new dimensionless variable $\hat{l}_c = l_c/a$ we obtain:

$$\hat{l}_c^2\,\nabla^2\phi - \phi = \frac{a^2\,e^2}{\varepsilon kT}\sum_i z_i c_i \tag{D.7}$$

Now we express equations D.6 and D.7 in bispherical coordinates.

$$\frac{(\cosh\eta - \cos\theta)^3}{\sin\theta}\left[\frac{\partial}{\partial\theta}\left(\frac{\sin\theta}{\cosh\eta - \cos\theta}\,\frac{\partial y}{\partial\theta}\right) + \sin\theta\,\frac{\partial}{\partial\eta}\left(\frac{1}{\cosh\eta - \cos\theta}\,\frac{\partial y}{\partial\theta}\right)\right] = \phi \tag{D.8}$$

$$\hat{l}_c^2\frac{(\cosh\eta - \cos\theta)^3}{\sin\theta}\left[\frac{\partial}{\partial\theta}\left(\frac{\sin\theta}{\cosh\eta - \cos\theta}\,\frac{\partial\phi}{\partial\theta}\right) + \sin\theta\,\frac{\partial}{\partial\eta}\left(\frac{1}{\cosh\eta - \cos\theta}\,\frac{\partial\phi}{\partial\theta}\right)\right] = \phi + \frac{a^2\,e^2}{\varepsilon kT}\sum_i z_i c_i \tag{D.9}$$

The boundary conditions for systems containing spherical particles with specified electrostatic potential on their surface is presented below:

$$y(\theta, -\eta_0) = y_{01}$$

$$y(\theta, \eta_0) = y_{02}$$

$$\left(\frac{\partial y}{\partial\theta}\right)\Big|_{\theta=0} = \left(\frac{\partial y}{\partial\theta}\right)\Big|_{\theta=\pi} = 0$$

$$\left(\frac{\partial\phi}{\partial\theta}\right)\Big|_{\theta=0} = \left(\frac{\partial\phi}{\partial\theta}\right)\Big|_{\theta=\pi} = 0$$

$$\left(\frac{\partial\phi}{\partial\eta}\right)\Big|_{\eta=-\eta_0} = \left(\frac{\partial\phi}{\partial\eta}\right)\Big|_{\eta=\eta_0} = 0$$

The domain of the independent variables is defined between $\theta = [0, \pi]$ and $\eta = [-\eta_0, \eta_0]$. It is also important to notice that the ionic concentration (c_i) is a function of the electrostatic potential (y) and because of that the resulting system of equations is coupled.

To solve this system we define two new auxiliary variable $u(\eta)$ and $v(\eta)$:

$$u_j(\eta) = \frac{1}{\cosh \eta - \cos \theta_j} \frac{dy_j(\eta)}{d\eta}$$
$$v_j(\eta) = \frac{1}{\cosh \eta - \cos \theta_j} \frac{d\phi_j(\eta)}{d\eta} \quad \text{(D.10)}$$

We propose a numerical methodology to solve this problem that is based on performing a polynomial approximation over the independent variable θ. This approach is detailed in the following item.

Polynomial approximation

This approach to solve a system of equations in bishperical coordinates consists in approximating the dependent variables y and ϕ as polynomial of degree n in θ, choosing $\theta_j = x_j \, \pi$, where $0 < x_1 < x_2 < \cdots < x_n < 1$ are the n roots of the Legendre polynomial normalized for the interval [0,+1].

With that, we can approximate variables y and ϕ as:

$$y(\theta, \eta) \cong y^{(n+1)}(\theta, \eta) = \sum_{i=0}^{n+1} l_i(\theta) \; y_i(\eta) \quad \text{(D.11)}$$

$$\phi(\theta, \eta) \cong \phi^{(n+1)}(\theta, \eta) = \sum_{i=0}^{n+1} l_i(\theta) \; \phi_i(\eta) \quad \text{(D.12)}$$

where $y_i(\eta) = y^{(n+1)}(\theta_i, \eta)$ and $\phi_i(\eta) = \phi^{(n+1)}(\theta_i, \eta)$.

From the previous definitions we can express the derivatives of the dependent variable related to θ as a function of matrixes A and B. Bellow we exemplify this construction for the dimensionless electrostatic potential y:

$$\left.\frac{\partial y^{(n+1)}(\theta,\eta)}{\partial\theta}\right|_{\theta_j} = \frac{1}{\pi}\left.\frac{\partial y^{(n+1)}(x,\eta)}{\partial x}\right|_{x_j} = \frac{1}{\pi}\sum_{i=0}^{n+1} A_{j,i}(\theta)\ y_i(\eta) \tag{D.13}$$

$$\left.\frac{\partial^2 y^{(n+1)}(\theta,\eta)}{\partial\theta^2}\right|_{\theta_j} = \frac{1}{\pi}\left.\frac{\partial^2 y^{(n+1)}(x,\eta)}{\partial x^2}\right|_{x_j} = \frac{1}{\pi}\sum_{i=0}^{n+1} B_{j,i}(\theta)\ y_i(\eta) \tag{D.14}$$

The system of equations to be solved will assume the form of a system of ordinary differential equations in relation to the independent variable η, and this system is presented here:

$$\frac{dy_j}{d\eta} = \left(\cosh\eta - \cos\theta_j\right) u_j \tag{D.15}$$

$$\begin{aligned}\frac{du_j}{d\eta} = \frac{1}{\left(\cosh\eta - \cos\theta_j\right)^3}\Bigg[&\phi_j(\eta) - \left(\cosh\eta - \cos\theta_j\right)^2 \sum_{i=0}^{n+1} B_{j,i}(\theta)\ y_i(\eta) \\ &- \frac{\left(\cosh\eta - \cos\theta_j\right)\left(\cosh\eta\ \cos\theta_j - 1\right)}{\sin\theta_j}\Bigg]\sum_{i=0}^{n+1} A_{j,i}(\theta)\ y_i(\eta)\end{aligned} \tag{D.16}$$

$$\frac{d\phi_j}{d\eta} = \left(\cosh\eta - \cos\theta_j\right) v_j \tag{D.17}$$

$$\hat{l}_c^2 \frac{dv_j}{d\eta} = \frac{1}{\left(\cosh\eta - \cos\theta_j\right)^3}\left[\phi_j(\eta) + \frac{a^2\, e^2}{\varepsilon kT}\sum_i z_i c_i - \hat{l}_c^2\left(\cosh\eta - \cos\theta_j\right)^2 \sum_{i=0}^{n+1} B_{j,i}\, y_i - \frac{\hat{l}_c^2\left(\cosh\eta - \cos\theta_j\right)\left(\cosh\eta\ \cos\theta_j - 1\right)}{\sin\theta_j} \sum_{i=0}^{n+1} A_{j,i}\, y_i\right] \tag{D.18}$$

For j =1, 2, …, m-1 and $-\eta_0 < \eta <\ \eta_0$.

And the boundary conditions can be written as: $y_j\left(-\eta_0\right) = y_{01}$, $y_j\left(\eta_0\right) = y_{02}$, $v_j\left(-\eta_0\right) = 0$ and e $v_j\left(\eta_0\right) = 0$.

This problem can be defined as a system of differential equations involving values in the boundaries which can be solved considering the search for the values of $u_j\left(-\eta_0\right)$ e $\phi_j\left(-\eta_0\right)$ that will lead to $y_j\left(\eta_0\right) = y_{02}$ e $v_j\left(\eta_0\right) = 0$.

Obtaining matrixes A and B for the polynomial approximation

Proposing $\left.\frac{\partial y}{\partial\theta}\right|_{\theta_j} = \sum_{i=0}^{n+1} A_{j,i}\, y_i$, $\left.\frac{\partial^2 y}{\partial\theta^2}\right|_{\theta_j} = \sum_{i=0}^{n+1} B_{j,i}\, y_i$ for $j = 1,\ 2, \ldots, n$ where $y(\theta,\eta) \cong y^{(n+1)}(\theta,\eta) = \sum_{i=0}^{n+1} q_i(\theta)\ y_i(\eta)$ in which $y_i(\eta) = y^{(n+1)}(\theta_i,\eta)$.

The function $q_i\left(\theta\right)$ is a polynomial function of degree $\left(n+1\right)$ in θ and it satisfies:

$$q_i(\theta_j) = \delta_{i,j} = \begin{cases} 1 \text{ for i = j} \\ 0 \text{ for i} \neq \text{j} \end{cases} \tag{D.19}$$

$$\left.\frac{dq_i(\theta_j)}{d\theta}\right|_{\theta=0} = \left.\frac{dq_i(\theta_j)}{d\theta}\right|_{\theta=1} = 0 \tag{D.20}$$

For i, j = 1, 2, … , n.

Besides that, we select $\theta_j = x_j\,\pi$, where $0 < x_1 < x_2 < \cdots < x_n < 1$ are the n roots of the p Legendre polynomial normalized on the interval [0,+1]. This leads us to:

$$\frac{dq_i(\theta)}{d\theta} = \theta\,(\pi - \theta)\sum_{k=2}^{n} M_{k,i}\theta^{k-2} = \sum_{k=2}^{n} M_{k,i}\left(\pi\,\theta^{k-1} - \theta^{k}\right) \tag{D.21}$$

And then,

$$q_i(\theta) = M_{1,i} + \sum_{k=2}^{n} M_{k,i}\left(\frac{\pi\theta^k}{k} - \frac{\theta^{k+1}}{k+1}\right) \tag{D.22}$$

With the conditions presented in equation D.19, we can obtain the values of the elements $M_{k,i}$:

$$M_{1,i} + \sum_{k=2}^{n} M_{k,i}\left(\frac{\pi\,\theta_j^k}{k} - \frac{\pi\,\theta_j^{k+1}}{k+1}\right) = \delta_{i,j} \tag{D.23}$$

We can also define the expression for $G_{j,k}$:

$$G_{j,k} = \begin{cases} 1 \quad \text{for } k = 1 \\ \dfrac{\pi\,\theta_j^k}{k} - \dfrac{\pi\,\theta_j^{k+1}}{k+1} \quad \text{for } k = 2, \ldots, n \end{cases} \tag{D.24}$$

Where $\boldsymbol{G}\cdot\boldsymbol{M} = \boldsymbol{I} \rightarrow \boldsymbol{M} = \boldsymbol{G}^{-1}$

The first and second derivatives on the points $\theta_i = x_i\,\pi$, are calculated from:

$$A_{i,k} = \left.\frac{dq_i(\theta)}{d\theta}\right|_{\theta_j} \quad and \quad B_{i,k} = \left.\frac{d^2q_i(\theta)}{d\theta^2}\right|_{\theta_j} \tag{D.25}$$

Which lead us to:

$$A_{i,k} = \theta_j \left(\pi - \theta_j\right) \sum_{k=2}^{n} M_{k,i}\, \theta_j^{k-2} \tag{D.26}$$

$$B_{i,k} = \sum_{k=2}^{n} M_{k,i} \left[\pi(k-1)\, \theta_j^{k-2} - k\, \theta_j^{k-1}\right] \tag{D.27}$$

For the boundary conditions, we suggest the use of a Taylor series expansion for the derivatives in θ. For a value of $\theta_0 = 0 < \theta < \theta_1$ we can expresses for the dimensionless electrostatic potential:

$$\frac{\partial y}{\partial \theta} = \left.\frac{\partial y}{\partial \theta}\right|_{\theta_1} + \left.\frac{\partial^2 y}{\partial \theta^2}\right|_{\theta_1} (\theta - \theta_1) \rightarrow \left.\frac{\partial y}{\partial \theta}\right|_{\theta_0 = 0} = \left.\frac{\partial y}{\partial \theta}\right|_{\theta_1} + \left.\frac{\partial^2 y}{\partial \theta^2}\right|_{\theta_1} (\theta_0 - \theta_1) = 0 \tag{D.28}$$

$$\frac{y_2(\eta) - y_0(\eta)}{2\,\Delta\theta} - \Delta\theta\, \frac{y_2(\eta) - 2\, y_1(\eta) + y_0(\eta)}{\Delta\theta^2} \rightarrow y_0(\eta) = \frac{4y_1(\eta) - y_2(\eta)}{3} \tag{D.29}$$

The same is applied for the auxiliary variable ϕ:

$$\phi_0(\eta) = \frac{4\phi_1(\eta) - \phi_2(\eta)}{3} \tag{D.30}$$

We can use the same approach for the second boundary and for $\theta_{m-1} < \theta < \theta_m = \pi$, we have:

$$\begin{aligned} \frac{\partial y}{\partial \theta} = \left.\frac{\partial y}{\partial \theta}\right|_{\theta_{m-1}} + \left.\frac{\partial^2 y}{\partial \theta^2}\right|_{\theta_{m-1}} \cdot (\theta - \theta_{m-1}) \rightarrow \left.\frac{\partial y}{\partial \theta}\right|_{\theta_m = \pi} \\ = \left.\frac{\partial y}{\partial \theta}\right|_{\theta_{m-1}} + \left.\frac{\partial^2 y}{\partial \theta^2}\right|_{\theta_{m-1}} (\theta_m - \theta_{m-1}) = 0 \end{aligned} \tag{D.31}$$

$$\frac{y_m(\eta) - y_{m-2}(\eta)}{2\,\Delta\theta} - \Delta\theta\,\frac{y_m(\eta) - 2\,y_{m-1}(\eta) + y_{m-2}(\eta)}{\Delta\theta^2} \to y_m(\eta) = \frac{4y_{m-1}(\eta) - y_{m-2}(\eta)}{3} \tag{D.32}$$

And the same for the auxiliary variable:

$$\phi_m(\eta) = \frac{4\phi_{m-1}(\eta) - \phi_{m-2}(\eta)}{3} \tag{D.33}$$

Appendix E

THE MODIFIED POISSON-BOLTZMANN EQUATION APPLIED TO CALCULATE PROTEIN ADSORPTION

Marlon de Souza Gama[1]*; Mirella Simões Santos*[2]*; Eduardo Rocha de Almeida Lima*[3]; *Frederico Wanderley Tavares*[1,2]*; Amaro Gomes Barreto Jr*[1†]

[1]Escola de Química, Universidade Federal do Rio de Janeiro, Cidade Universitária, CEP: 21949-900, Rio de Janeiro, RJ, Brazil

[2]Programa de Engenharia Química/COPPE – Universidade Federal do Rio de Janeiro, Cidade Universitária, CEP: 21949-972, Rio de Janeiro, RJ, Brazil

[3]Programa de Pós-graduação em Engenharia Química, Universidade do Estado do Rio de Janeiro, 20550-013, Rio de Janeiro, Brazil

[†] Corresponding author (Phone: +55-21-3938-7638, e-mail: amaro@eq.ufrj.br)

ABSTRACT

Ion-exchange chromatography has been widely used as a standard process in purification and analysis of protein, based on the electrostatic interaction between the surface of the stationary phase and the protein. A variety of models and considerations were made through the years, improving the thermodynamics of colloids but short attempts were applied for direct predict the behavior of proteins. Here, we present an improved methodology for solving the modified Poisson-Boltzmann equation considering bispherical geometry aiming the prediction of the adsorption equilibrium constant. By including the dispersion interaction between ions and protein, and between ions and surface, the modified PB equation is able to describe the Hofmeister effect. We solve the modified Poisson-Boltzmann equation to calculate the potential of mean force protein-surface, treated as spherical colloid-plate system, as a function of process variables. The Henry constants of adsorption, for different protein and surfaces, are shown as function of pH, salt concentration and temperature. In addition, we performed a sensitivity analysis to verify the behavior of different kind of salts and its impact on the Hofmeister effects.

Keywords: Poisson-Boltzmann; Bispherical coordinates; Ion-colloid dispersion; Hamaker.

1. INTRODUCTION

Protein adsorption is the key phenomenon of countless biological process as well of many protein separation and purification technologies. It is mainly governed by electrostatic interactions between the protein surface and the adsorbate and, because of that, it is crucial to have a good description of the electrostatics of the system when modeling this phenomenon. One of the first attempts to model the behavior of colloidal systems came from the Derjaguin-Landau-Verwey-Overbeek theory (DLVO) that considers a electrostatic double layer being formed on the surroundings of a charged surface [1] which could be described by a linearized form of the Poisson-Boltzmann (PB) equation [2]. Later, based on the Hamaker [3] contribution, Verwey [2] and long after Ståhlberg et al. [4], improved this approach by combining the attractive London-van der Waals potential with electrostatic interactions.

When aiming to specifically describe microscopic adsorptive processes, information about the amount of protein adsorbed per area (or per mass) of adsorbent is an essential parameter for the description of this process. It is a function of the pH of the solution and its ionic strength, and it affects the interaction between adsorbent and adsorbate because of the changes in the charge of their surfaces and because of the non-electrostatic effects caused by the kind of salt applied. Recently, a model based on the linearized PB equation was used to correlate adsorption of proteins in Ion-Exchange Chromatography (IEC) by the estimation of the amino acids residue densities [5–7], since they are directly related to the surface charge density of the protein.

Another approach often used to model protein adsorption is the Sterical Mass-Action method (SMA) [8,9]. SMA applies a stoichiometric binding theory and couples, in a set of correlation parameters, all the electrostatic and equilibrium information of the system, not considering important effects like non-electrostatic (NES) and co-ion effects [10], leading to a poor precision at higher salt concentrations or pH values close to the protein isoelectric point (pI) [9]. The same happens to all the models based on the DLVO theory because it does not take into account any non-electrostatic effects. Even though NES effects can be neglected at low ionic strength (0.01 M), they cannot be neglected when modeling highly concentrated electrolyte solutions or multivalent ions. This directly impacts on the need for the improvement of the colloid theory for biological application [11]. Furthermore, it was shown that different ions affect in different ways the behavior of proteins, most of the time their impact follows directly the Hofmeister series. To be able to predict this kind of behavior it is essential to consider dispersion forces in the model [12].

Another way to improve the theoretical description of protein adsorption was suggest by Roth and Lenhoff [15] which takes into account the three-dimensional configuration of the protein, using information of the mesh conformation of lysozyme while interacting with a stationary surface. This approach, though, still uses the linearized form of the Poisson-Boltzmann equation. Because of that, the result from this study showed a good agreement with experimental data for lysozyme at small ionic strength, as expected, but did not obtain a good fit for wide ionic strength range, even considering Hamaker interaction.

When applying the Poisson-Boltzmann equation to describe systems containing protein or any spherical colloids it is important to define correctly the coordinate systems in which this equation will be applied. This helps on a better physical

understanding of the interaction between two colloids or a colloid-surface interaction in contrast with using approximations for a planar geometry such as the Derjaguin approximation to adapt for the spherical-planar geometry [5,16,17]. The PB equation in Bispherical Coordinates was chosen by Lima et al. [13] as a more realistic model that also provides a good computational time and accuracy. This model was able to predict the osmotic second virial coefficient as a function of ionic strength considering the interaction between two charged colloids (globular proteins). The article also reports the application of the Hamaker force and analyzes the effect of the kind of salt arising due to non-electrostatic interactions.

In order to predict the influence of protein adsorption on IEC, here we calculate the Henry constant of a protein modeled as a charged colloid adsorbed on an ion-exchange adsorbent using the PB equation in bispherical coordinates. We consider the dispersion interactions between ions and protein and between ions and adsorbent surface and also the Hamaker potential. With this, we are able to predict the Henry constant as a function of pH, ionic strength, ionic specificity, and temperature.

2. ELECTROSTATIC MODEL FOR DIFFERENT COORDINATE SYSTEMS

An equilibrium model was reported by Ståhlberg et al. [18] showing the relationship between the electrostatic free energy and the retention factor (relative to adsorption equilibrium constant for a diluted system, i.e. Henry constant) for ion-exchange chromatography of protein. To achieve the main goal to predict the adsorption behavior of different mAbs variants on IEC based on their interaction with the charged surface, we need the Henry constant.

Using the equilibrium condition for the chemical potential of protein, we obtain [19]:

$$c = c_0 \exp\left[-\frac{W(I, pH, h)}{k_B T}\right] \tag{1}$$

where c is the concentration of the colloid, c_0 is bulk concentration of the colloid , h is the distance between the protein surface and the surface of the stationary phase, I is the ionic strength of the solution, W is the free energy of interaction between the colloid

and the adsorbate, k_B is the Boltzmann constant, and T the absolute temperature (here 298.15 K).

Knowing that the surface excess concentration can be obtained by:

$$q(pH,I)=\int_0^{\infty}(c-c_0)dh \tag{2}$$

where q is the surface excess concentration of the protein for a given desired pH and ionic strength, I.

The Henry equation is written as a function of the potential of mean force (or the free energy, W) after combining both equations (Eq. 1-2) [5]:

$$K=\frac{q(pH,I)}{c_0}=\int_0^{\infty}\left[\exp\left(-\frac{W(I,pH,h)}{k_BT}\right)-1\right]dh \tag{3}$$

where K is the dimensional Henry constant (m).

The simplification used to calculate the potential of mean force have an effect on the behavior of the K constant in colloid science. The widely used method to obtain electrostatic free energy from the linearized PB equation [17,18] neglects the possibility of including NES effects. In contrast, the solution of the nonlinear PBE in bispherical coordinates permits to add NES terms that convey to be relevant to the system, as discussed in the following sections.

2.1 Modified PBE in Bispherical Coordinates

In face of those previous studies, we presume that a nonlinear model using bispherical coordinates, or a similar way to describe plane-sphere interactions and the contributions of electrostatic, ionic specificity and van der Waals force for a diluted system, provides an acceptable profile behavior without the need of parameter estimation.

Based on those considerations, the Poisson-Boltzmann equation including the ion-protein dispersion is given by the following equation:

$$\nabla^2\psi=\frac{1}{2}\left[\exp(\psi-U_-)-\exp(-\psi-U_+)\right] \tag{9}$$

where ∇^2 is the Laplacian operator in bispherical coordinates [20], given by:

$$\nabla^2\psi = \frac{(\cosh\eta - \cos\theta)^3}{[k_D h \sinh(\eta_0)]^2 \sin\theta}\left[\frac{\partial}{\partial\theta}\left(\frac{\sin\theta}{\cosh\eta - \cos\theta}\frac{\partial\psi}{\partial\theta}\right) + \sin\theta\frac{\partial}{\partial\eta}\left(\frac{1}{\cosh\eta - \cos\theta}\frac{\partial\psi}{\partial\eta}\right)\right] \quad (10)$$

here $U_{\pm}$ is the van der Waals interaction between the ions and the protein, (η , θ) are the independent variables of the bispherical coordinate system where the rotation of symmetry is assumed to be a line orthogonal to the plate passing through the center of the sphere, η_0 is the value of η at the sphere surface. For the evaluation of the plane-sphere force, we perform the integration over the surface at $\eta = \frac{\eta_0}{2}$ for a realistic approach.

The boundary conditions in η are writing as:

$$\left(\frac{\partial\psi}{\partial\eta}\right)_{\eta=0} = -\frac{\sigma_2}{\varepsilon\varepsilon_0}\frac{k_D h \sinh(\eta_0)}{\cosh(\eta_0) - \cos(\theta)}$$
$$\left(\frac{\partial\psi}{\partial\eta}\right)_{\eta=\eta_0} = -\frac{\sigma_1}{\varepsilon\varepsilon_0}\frac{k_D h \sinh(\eta_0)}{\cosh(\eta_0) - \cos(\theta)} \quad (11)$$

Boundary conditions in θ:

$$\left(\frac{\partial\psi}{\partial\theta}\right)_{\theta=0} = \left(\frac{\partial\psi}{\partial\theta}\right)_{\theta=\pi} = 0 \quad (12)$$

The equation for the non-electrostatic term relative to ionic specificity is given by [22]:

$$U_{\pm} = \frac{-B_S \cdot r_{ion}^3}{(r_1 - R_{sphere})^3\left[1 + \frac{(r_1 - R_{sphere})^3}{2R_{sphere}^3}\right]} + \frac{-B_P \cdot r_{ion}^3}{r_2{}^3} \quad (13)$$

Here, R_{sphere} is the hydraulic protein diameter, r_{ion} is the ion radius; the B_S is the ion-sphere and B_P is the ion-plate dispersion constant. We assumed the same surface dielectric propriety on the plate and colloid, thus, $B_S = B_P$; r_1 is the distance between the ion and the center of the colloid equal to $\sqrt{\overline{X}^2 + (D - \overline{Z})^2}$ and r_2 is the distance between the ion and the planar surface equal to $\sqrt{\overline{X}^2 + (D + \overline{Z})^2}$: being $\overline{X}$ and $\overline{Z}$ the

Cartesian coordinates associated with the bispherical variables and *D* is the half center-to-center distance between sphere-plate.

The relationship with Cartesian coordinates and the numerical details are better described by Lima et al. [23], even so it is noteworthy point that the integration is calculated by Composite Simpson's rule and the differential equation is solved using Finite Volume Method linked with the Thomas algorithm.

Here we treat sodium chloride as the main salt in solution accounting for ionic strength, so the following values are taken in consideration for the dispersion constant [24]: $0.138\,k_B T$ for sodium ion and $1.086\,k_B T$ for chloride ion. For sensitivity analysis, different kinds of ions are studied: bromide ($1.348\,k_B T$), iodide ($1.735\,k_B T$), potassium ($0.574\,k_B T$) and strontium ($0.575\,k_B T$) (same reference as above). A cutoff radius of 2 Å was assumed for the ions to secure the potential convergence at the interfaces [11].

The expression for the nondimensional force in bispherical coordinates is given by [25], which is obtained by the integration of the stress tensor over a suitable surface, as a function of the electric field and the difference in the osmotic pressure [26].

$$f(\eta)=2\pi\int_0^{\pi}\left\{\left[\frac{[k_D h\sinh(\eta_0)]^2(\cosh\psi-1)}{(\cosh\eta-\cos\theta)^2}+\frac{1}{2}\left(\left(\frac{\partial\psi}{\partial\theta}\right)^2-\left(\frac{\partial\psi}{\partial\eta}\right)^2\right)\times(1-\cosh\eta\cdot\cos\theta)\right]+\frac{\partial\psi}{\partial\theta}\frac{\partial\psi}{\partial\eta}\sinh\eta\cdot\sin\theta\right\}\frac{\sin\theta}{\cosh\eta-\cos\theta}\cdot d\theta \tag{14}$$

The free energy can be calculated in two different ways: (1) through an equation using information of the potential with respect to the volume control and surface integrals and (2) using an expression for integration of the force as a function of the distance between the colloid and the plane surface. For a plane-surface case, the first method may lead to a poor accuracy [25], so the second method was select as the most efficient way to find the potential of mean force:

$$\frac{W^{PB}(k_D h)}{\kappa_B T}=-\varepsilon_R\varepsilon_0\left(\frac{\kappa_B T}{e^2}\right)\int_{\infty}^{k_D h} f(h)d(h) \tag{15}$$

Where W^{PB} is the electrostatic contribution from the PBE equation to the interaction potential of mean force between the protein and the adsorbent for a given distance ($k_D h$). This potential of mean force takes into account temperature, charge densities of

protein and adsorbend (related with pH), salt concentration (related with PB equation) and salt type (related with dispersion interaction between ions and protein and ions and adsorbent surface).

The total potential of mean force between the protein and adsorbent is given by three contributions:

$$W = W^{PB} + W^{Ham} + W^{hs} \tag{16}$$

where W^{hs} is the hard-sphere contribution: (1) $W^{hs} = \infty$ for $h < 0$ and (2) $W^{hs} = 0$ for $h \geq 0$. W^{Ham} is related to the non-Coloumbic potential between the protein and the surface of the adsorbent, known as the Hamaker dispersion. The method for calculating W^{Ham} is resumed as follows [13,27]:

$$W^{Ham} = \begin{cases} -\dfrac{H}{6}\left(\dfrac{r_p}{r_p + r_H}\right) & \text{for } h \leq r_p + r_H \\ -\dfrac{2H}{9}\left(\dfrac{r_p}{h}\right)^3 & \text{for } h > r_p + r_H \end{cases} \tag{17}$$

where r_H corresponds to the protein hydration-layer thickness, 1.5 Å [13]. The parameter H represents the Hamaker constants, which are different for each pair of colloid-adsorbent. For the interaction between mAbs and YMC BioPro SP, the Hamaker constant is established as $2k_BT$ [6]. It is assumed $H = 5\,k_B\,T$ for the interaction with Fractogel EMD SE HiCap as a frequent value for protein interaction in aqueous solution [24].

2.2 Charge density calculation

Equations including direct information of the potential at the surfaces are used to find the resolution of the free energy, but for IEC it is more effective to represent the model as a function of the charge density [21] since the information of the surface amino acid groups can be found by simple experimental titrations.

The surface charge density was writing as suggested by Ehrl et al. [28] and also applied by Guélat et al. [5] to determinate the charge of amino e histidine density groups:

$$\sigma_{+} = \frac{+F\rho_i}{1+\left(Ka_{i+}/c_{H^+}\right)+c_{anion}\gamma \cdot Ks_{iCl}} \tag{18}$$

where F is the Faraday constant (96,485 C mol^{-1}), i denote the amino or histidine groups, ρ_i represent the density of ionizable surface groups i (mol m^{-2}), Ka_{i+} is the effective dissociation constant of the acid grupos i (mol L^{-1}), γ is the activity coefficient of the chosen salt, Ks_{iCl} is the effective association constant of the groups i (L mol^{-1}) and c_{anion} is the concentration of salt anion (mol L^{-1}).

Moreover, a similar equation describes the density of carboxyl and sulfonate groups:

$$\sigma_{-} = \frac{-F\rho_j}{1+\left(c_{H^+}/Ka_{j^-}\right)+c_{cation}\gamma \cdot Ks_{jNa}} \tag{19}$$

where j denote the carboxyl or sulfonate groups, ρ_j represent the density of ionizable surface groups j (mol m^{-2}), Ka_{j^-} is the effective dissociation constant of the basic grupos j (mol L^{-1}), Ks_{jNa} is the effective association constant of the groups j (L mol^{-1}) and c_{anion} is the concentration of salt cation (mol L^{-1}). The values of the effective dissociation and association constant is found elsewhere [5].

c_{H^+} refers to the concentration of ions H^+ at the region between the IEC surface interface and the solution. We applied the charge regulation calculation for high pH (above pH 5.0) to correlate the ion surface concentration. For lower pH, deviations appears when compared with experimental data probably by the surface model simplicity, which works with a general DLVO approach. Here we used instead the bulk concentration as an approximation for the H^+ concentration at the interface surface at the region where the charge regulation is insufficient to give the potential prediction (pH < 5.0).

3. PROTEIN AND STATIONARY SURFACE DATA

The study of the adsorption phenomenon of monoclonal antibodies (mAbs) reported by Guélat et al. [5] and Guélat et al. [6] (change the reference) showed that a linearized PB equation is suitable to describe the behavior of the Henry constant, defined as a function of pH and ionic strength in IEC for different stationary phases: Fractogel EMD SE HiCap (binding group $-(CH_2)_2SO_3^-$) and YMC BioPro SP (10 μm) (binding group $-(CH_2)_3SO_3^-$) for interaction with mAb1; and YMC BioPro SP (5 μm) for Bevacizumab and Trastuzumab adsorption. However, in both studies, it was necessary to re-estimate the ionizable amino acid surface groups to obtain an agreement with the experimental data.

The data analyzed here comes from those papers. The density of amino, histidine and carboxylic component groups are calculated by the ratio between the number of ionic groups (obtained by the references after the proper counting of amino acid sequence available at Protein Data Bank and DrugBank online database) and the protein surface area.

The hydrodynamic radius of mAb1 was defined as 5 nm [5], and the same value was specified for Trastuzumab [7,29]. For Bevacizumab, the radius of 6.3 nm was measured by Wen et al. [30] using dynamic light scattering and applied here for the calculation the density of groups. The main parameters used are resumed in Table 1.

Table 1. Parameters considered on the model. Other parameters, as the effective association constants or acid-base dissociation constants of each component, can be found at the cited references. (rever o valor! Estao no arquivo em FORTRAN. PS: temos 3 fases estacionarias.)

	The density of groups (mol m^{-2})			Reference
Protein	Amino	Histidine	Carboxyl	
mAb1	$6.872 \cdot 10^{-7}$	$1.374 \cdot 10^{-7}$	$6.237 \cdot 10^{-7}$	[5]
Bevacizumab	$5.844 \cdot 10^{-7}$	$8.938 \cdot 10^{-8}$	$4.194 \cdot 10^{-7}$	[31]
Trastuzumab	$8.034 \cdot 10^{-7}$	$1.480 \cdot 10^{-7}$	$6.343 \cdot 10^{-7}$	
Stationary phase	Sulfonate groups			
Fractogel EMD SE HiCap	$5.64 \cdot 10^{-6}$			[5]
YMC BioPro SP	$1.90 \cdot 10^{-6}$			

4. RESULTS AND DISCUSSION

Before the model analysis, we need to first acknowledge the charge at the surfaces and assure that we are observing an ion-exchange process at the range of pH studied. Fig. 2 was obtained using the method described by Ehlr et al. [28] for the computation of the surface charge density via the activity of the salt [32], solution pH and information about effective association constants and acid-base dissociation constants:

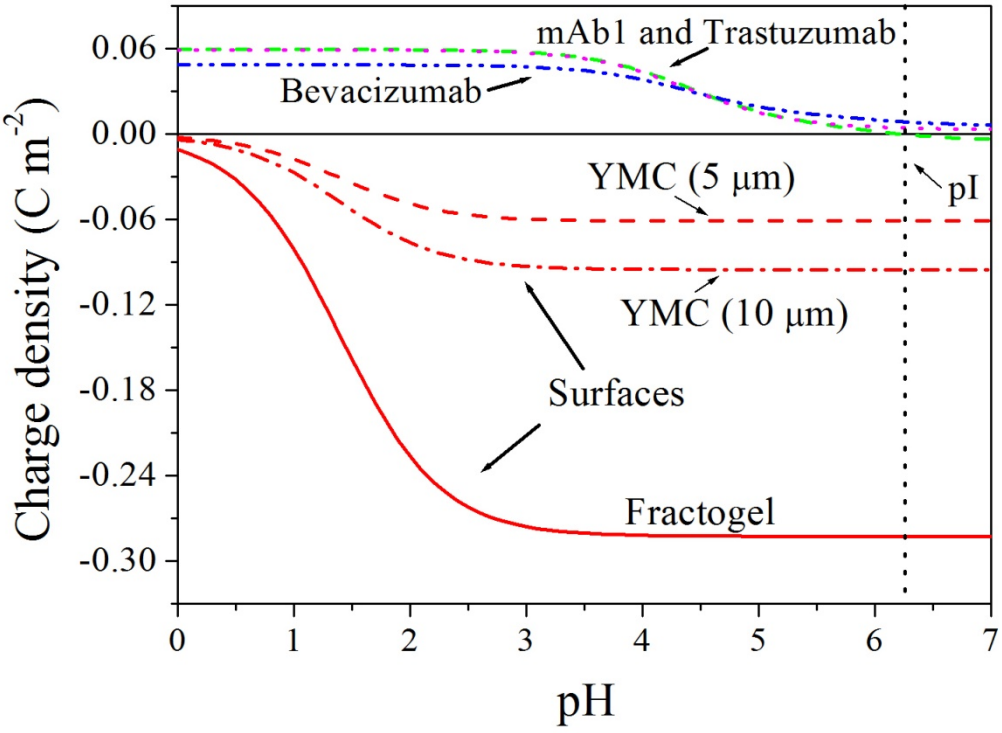

Figure 2. Surface charge density of proteins and stationary phase throughout the pH for a NaCl concentration of 0.3 mol L^{-1}: (–) represents the behavior of Fractogel EMD SE HiCap; (– –) is for YMC BioPro SP (5 µm) and (· – ·) is for YMC BioPro SP (10 µm); (– · ·) is the Bevacizumab charge density and the profile of mAb1 (–) and Trastuzumab (···) overlap almost over all the pH range. Only after the mAb1 pI (approximately 6.3), the Trastuzumab shows a slight increase on the charge density.

As noted, on the range of 4.4 to 7.0, all the proteins have a prevailing positive charge and the stationary phase surfaces have a constant negative charge, making the adsorption process purely electrostatic. Thus, since at the pI the colloid has a null net charge, it is expected that the addition of salt disturb the adsorption in a negative way.

We can see more clearly this result after solving the potential of mean force with respect to the pH at a fixed NaCl concentration (0.3 mol L^{-1}) for mAb1. In Fig. 3, for pH close to the pI (approximately 6.3), the protein shows a repulsive behavior; whereas, for the lower pH region the protein exhibits positive characteristics, leading to the IEC adsorption.

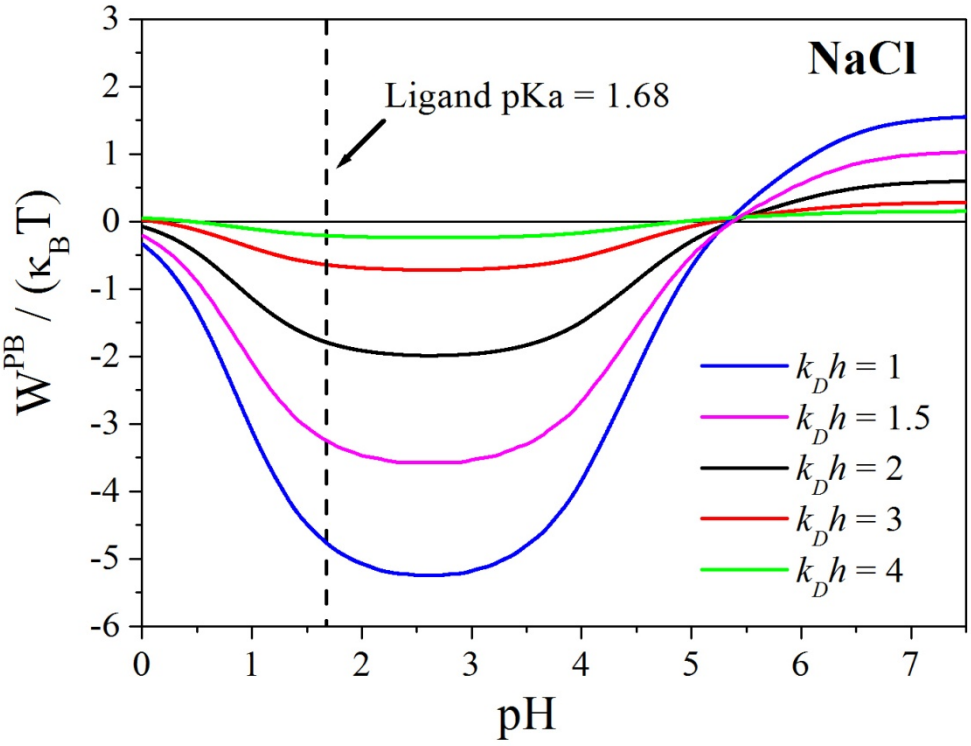

Figure 3 Effect of pH on the potential of mean force from the PBE for different dimensionless distances between the surfaces of plane-sphere system. NaCl concentration is equal to 0.3 mol L^{-1} (Fractogel EMD SE HiCap).

In addition to this study, Stankovich and Carnie [25] suggested that the force integration range relies between 0.1 and 2 $k_D h$, however, as showed in Fig. 4, the bulk condition is achieved after 7 $k_D h$ and a loss of information occurs at any integration before this point.

As mentioned earlier, $k_D h$ represent the dimensionless separation distance between a spherical surface, representing the colloid, and the stationary phase, defined as a plane surface. For a short distance, the potential of mean force will display a significant attraction and a repulsive behavior for points after the isoelectric point. As the sphere is separated from the plane surface, the intensity of the potential of mean force is reduced as shown in Fig. 3. The region where pH is lower than 1.68 represents the region where the ionic groups, from the plane surface, become more positive (Fig. 2) affecting the IEC, even with no apparent modification on the protein charge.

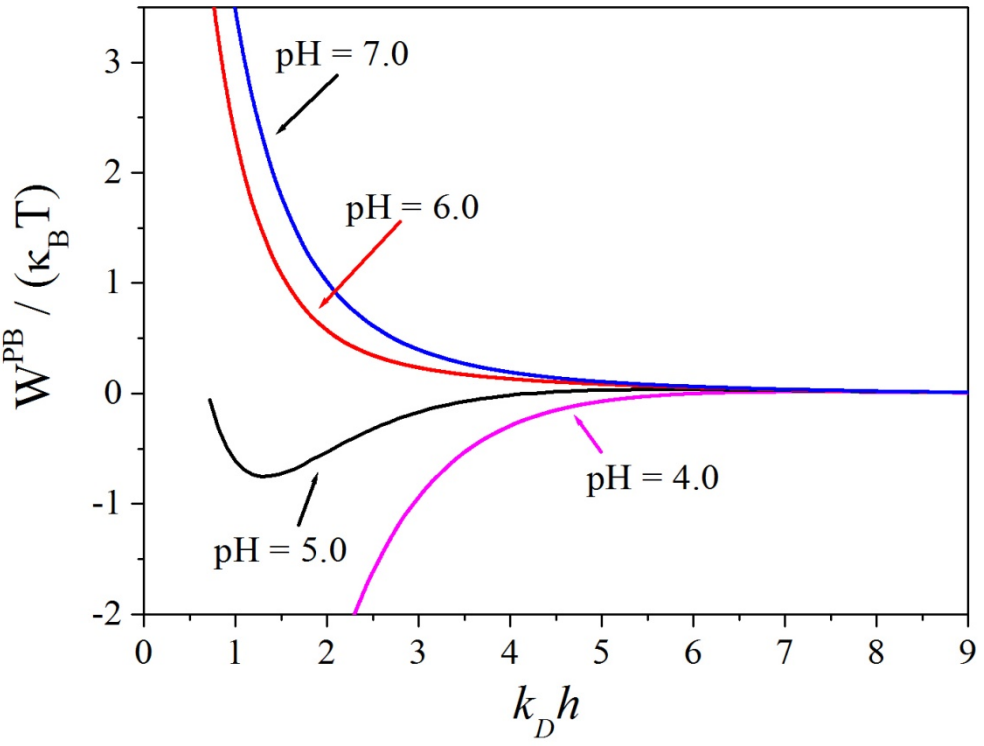

Figure 4. Potential of mean force from the PBE over the distance between the protein surface and the plane with a salt concentration of 0.3 mol L^{-1} NaCl (Fractogel EMD SE HiCap).

In order to acknowledge the Hofmeister effect, we solved the PBE potential of mean force for four different kinds of salts: NaBr and NaI to analysis the influence of the anion; and KCl and $SrCl_2$ for the cations. As we can see, NaCl keeps the major contribution in W^{PB} and its aftereffects are discussed along with the Henry constant results.

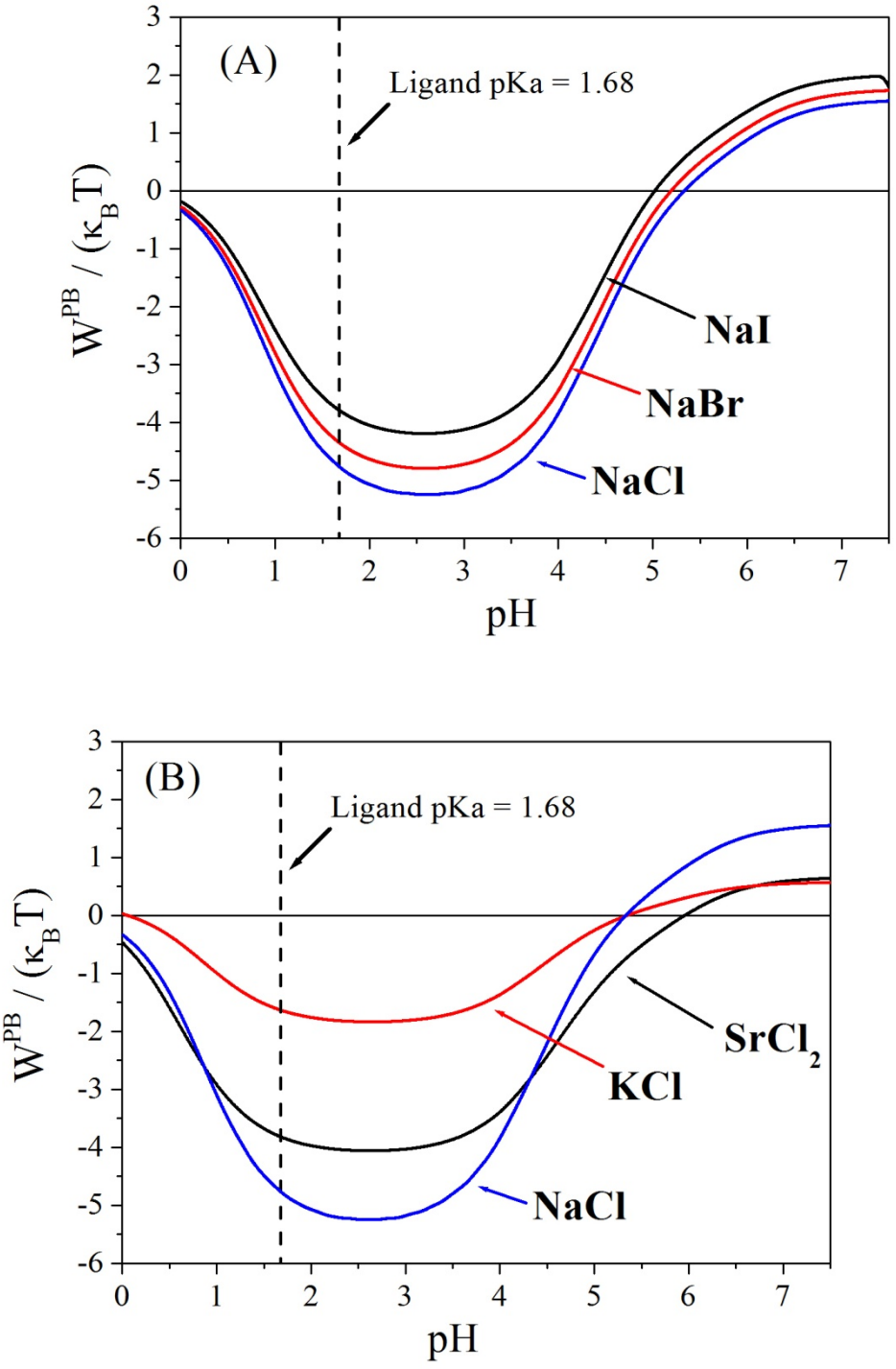

Figure 5. Comparison between the dimensionless potential of mean of three different type of (A) anions and (B) cations. The sphere-plate distante is fixed at κh =1, for the analysis purpose with ionic strength equal to 0.3 mol L^{-1} (Fractogel EMD SE HiCap).

Finally, Fig. 6 shows the Henry constant solved using Eq. 3 integrated with the total potential of mean force given by Eq. 16, for bispherical coordinates, considering the ion-colloid dispersion and van der Waals force, compared to experimental data.

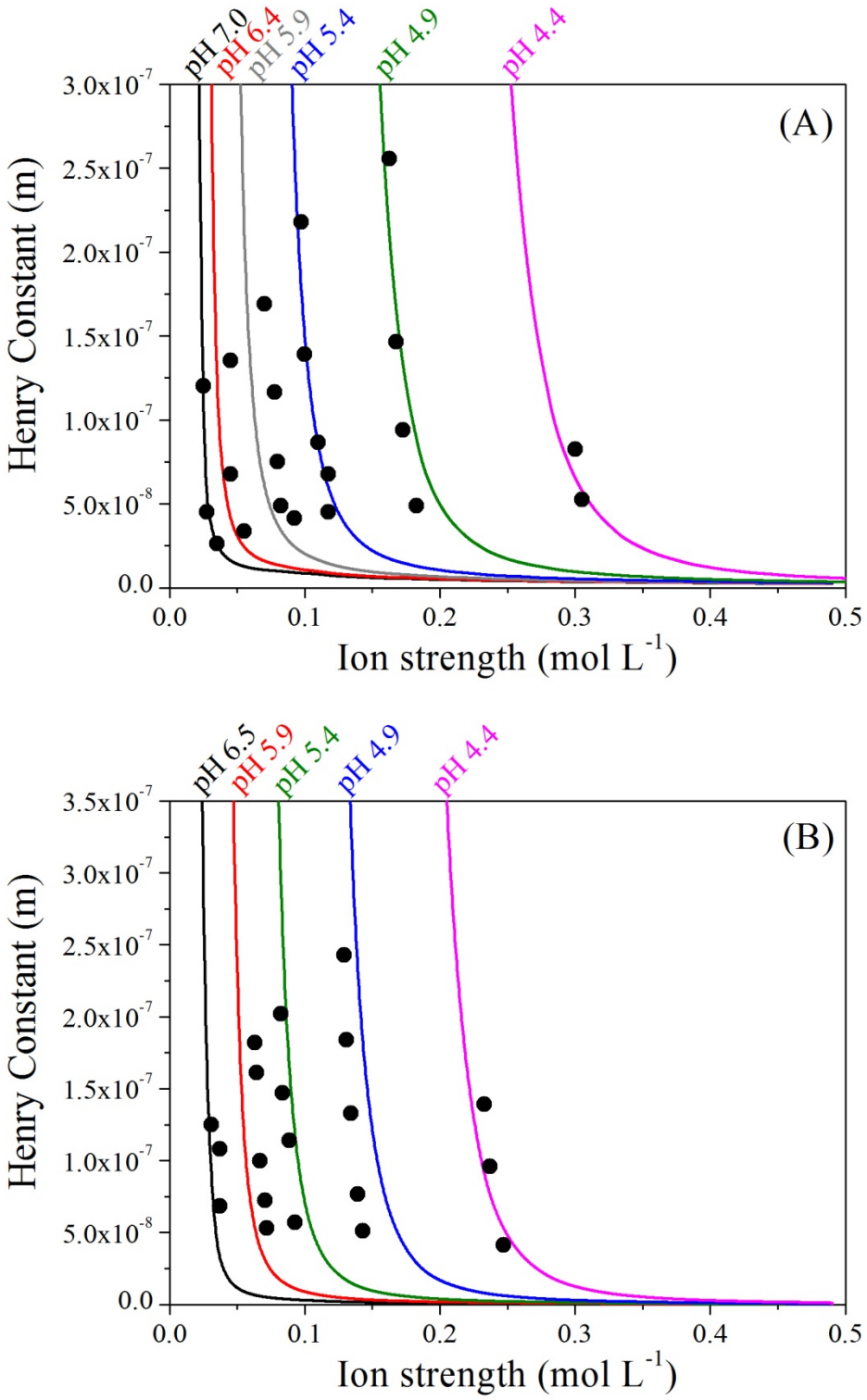

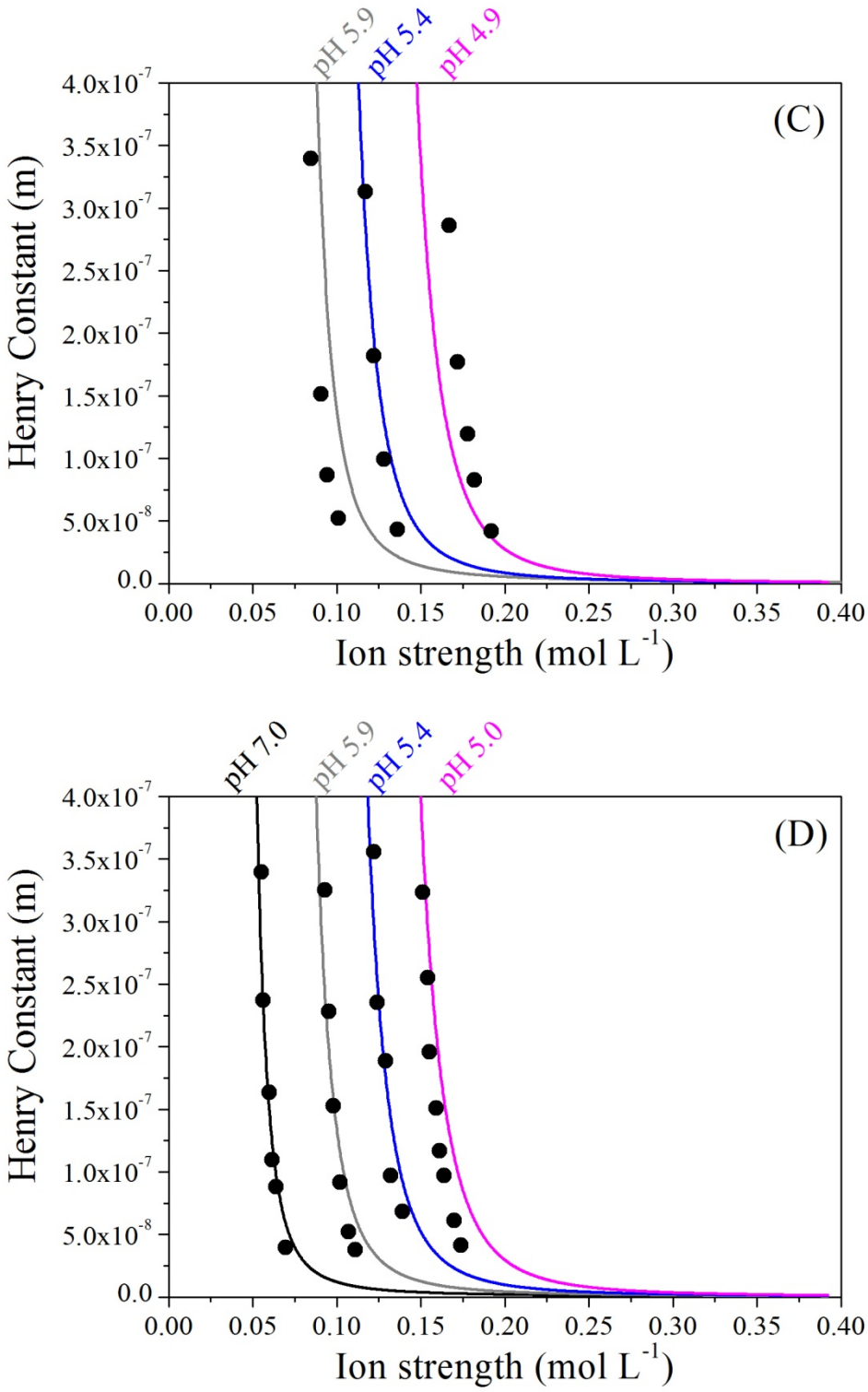

Figure 6. Henry constant behavior for protein adsorption process: mAb1 on (A) Fractogel EMD SE HiCap and (B) YMC BioPro SP; Bevacizumab (C) and Trastuzumab (D) on YMC BioPro SP as a function of salt concentration and pH. The filled curves are related to the theoretical results without parameter estimation and the circles are experimental data from [5,20].

As we can see, the model was able to predict with a good agreement the adsorption behavior for two different adsorbent on ion-exchange chromatography. Fractogel EMD SE and YMC BioPro SP are both considered strong anion-exchangers, even though Fractogel had almost three times more ionic groups on the surface (Tab. 1). For pH equal to 4.4, where the system is strongly electrostatic, the curve decays gradually with the salt concentration, while at pH 7.0 the effect is substantial.

The selection of the Hamaker constant was consistent with the set of assumptions made in this work, thus for a better agreement with experimental data, this parameter could be re-estimated for each protein taking into consideration the entire set of pH curves.

In addition, the type of salt also alters the adsorption performance (Fig. 7) as noted before by the variation in the PBE free energy contribution (Fig. 5), where the anion has a bigger influence on the value of the Henry constant. The Hofmeister series is followed for both cation and anion in study, with the higher Henry constant corresponding to the system containing NaCl. The co-ion effect tends to be minor in contrast with the counterion behavior, as is resumed by the KCl and NaCl profiles. However, the impact of Sr^{2+} calculated shows a considerable reduction in the Henry constant in Fig. 7 and a singular profile in Fig. 5b. The difference of valence (2:1) leads to a rapid decay of the adsorption due the sites competition, and also by the different ionic polarizability between the analyzed ions.

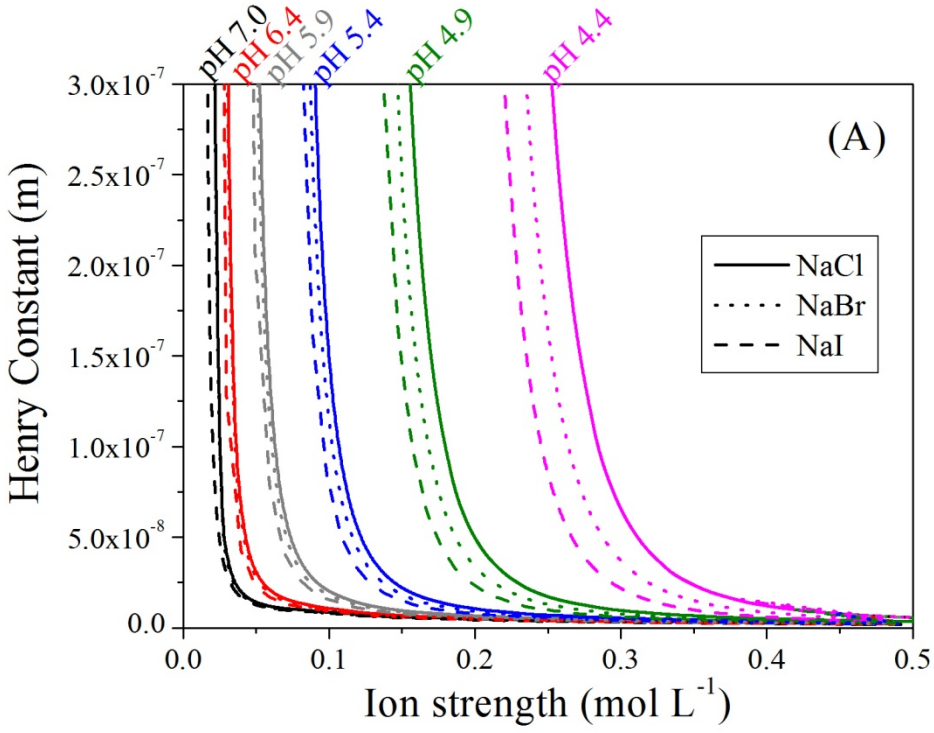

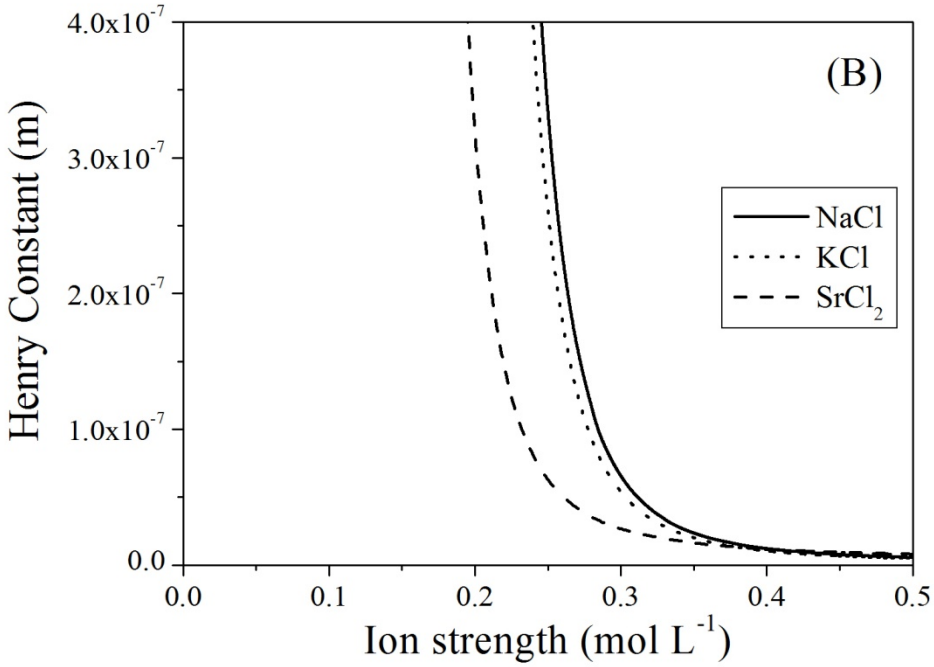

Figure 7. Theoretical effect of the influence of three different types of (A) anion and (B) cation types on Henry's constant for mAb adsorption.

The results presented in this work demonstrate that no parameter adjustment is necessary after the inclusion of van der Waals force and ion specificity and a more realistic geometry structure to have a good description of experimental Henry constants, reassuring the importance of those effects on the description of systems with the adsorption of proteins.

5. CONCLUSIONS AND PERSPECTIVE

This work applied the Poisson-Boltzmann equation in bispherical coordinates with the inclusion of ionic dispersion parameters and Hamaker force for IEC study. The results show a very good prediction with the monoclonal antibodies adsorption behavior as a function of pH and ionic strength for two different stationary phases, without any fitted parameters, then the model presented here is fully predictive. In addition, a sensibility study was performed where we observed that the effects of ions on the system follows with the Hofmeister anionic series for different values of pH. The prediction of the electrostatic response represents an important step in colloidal science, making possible to improve the simulation of complex systems that present Coulombic forces as, for example, the multimodal chromatography. This work can be extended with the inclusion of ion size effects and of electrostatic correlations, which can be relevant for systems containing concentrated electrolyte solutions.

ACKNOWLEDGMENTS

For financial support, we are grateful to the Brazilian Agencies, Coordenação de Aperfeiçoamento de Pessoal de Nível Superior (CAPES), Fundação Carlos Chagas Filho de Amparo à Pesquisa do Estado do Rio de Janeiro (FAPERJ) and Conselho Nacional de Desenvolvimento Científico e Tecnológico (CNPq).

SYMBOLS

B_S Ion-sphere dispersion constant

B_P Ion-plate dispersion constant

c Concentration of the colloid

c_0 Bulk concentration of the colloid

D Half center-to-center distance between sphere-plate.

e Elementary charge of the electron

f Nondimensional force

I Ionic strength

h Distance protein surface and the stationary phase surface

H	Represents the Hamaker constants
K	Dimensional Henry constant
k_B	The Boltzmann constant
k_D	Inverse Debye length
n_i^0	Number of ions *i* per cm^3 in the bulk
q	Surface excess concentration
q^*	Characteristic charge of the ion
$\underline{r}_i$	Distance between the ion and the center of the two spheres
r_1	Distance between the ion and the center of the colloid
r_2	Distance between the ion and the planar surface
r_{ion}	Ion radius
r_H	Protein hydration-layer thickness
R_{sphere}	Hydraulic protein diameter
T	Absolute temperature (298.15 K)
u	Free energy of the system
$U_{\pm}$	van der Waals interaction ion-protein
W	Potential of the mean force of sphere-plate interaction
W^{PB}	Contribution of the electrostatic free energy
W^{hs}	Hard-sphere contribution of free energy
W^{Ham}	Non-Coloumbic potential
x	Charged region between the surfaces
$\overline{X}$	Cartesian coordinate associated with the bispherical variables
$\overline{Z}$	Cartesian coordinate associated with the bispherical variables
z_i	Ions valence

Greek symbols

ε_0	Vacuum permittivity
ε_R	Dielectric constant of the medium

(η, θ) Independent variables of the bispherical coordinate system

σ_1 Colloid charge density

σ_2 Stationary phase charge density

ϕ Electrostatic potential

ψ Dimensionless electrostatic potential $\left(e\phi/k_B T\right)$

REFERENCES

[1] J.T.G. Verwey, E. J. W., Overbeek, Theory of the Stability of Lyophobic Colloids, 1948.

[2] E.J.W. Verwey, Theory of the Stability of Lyophobic Colloids., J. Phys. Colloid Chem. 51 (1947) 631–636. doi:10.1021/j150453a001.

[3] H.C. Hamaker, The London—van der Waals attraction between spherical particles, Physica. 4 (1937) 1058–1072. doi:10.1016/S0031-8914(37)80203-7.

[4] J. Ståhlberg, B. Jönsson, C. Horváth, Combined effect of coulombic and van der Waals interactions in the chromatography of proteins., Anal. Chem. 64 (1992) 3118–24. doi:10.1021/ac00048a009.

[5] B. Guélat, G. Ströhlein, M. Lattuada, M. Morbidelli, Electrostatic model for protein adsorption in ion-exchange chromatography and application to monoclonal antibodies, lysozyme and chymotrypsinogen A, J. Chromatogr. A. 1217 (2010) 5610–5621. doi:10.1016/j.chroma.2010.06.064.

[6] B. Guélat, G. Ströhlein, M. Lattuada, L. Delegrange, P. Valax, M. Morbidelli, Simulation model for overloaded monoclonal antibody variants separations in ion-exchange chromatography, J. Chromatogr. A. 1253 (2012) 32–43. doi:10.1016/j.chroma.2012.06.081.

[7] M. Salvalaglio, M. Paloni, B. Guelat, M. Morbidelli, C. Cavallotti, A two level hierarchical model of protein retention in ion exchange chromatography, J. Chromatogr. A. 1411 (2015) 50–62. doi:10.1016/j.chroma.2015.07.101.

[8] H. Iyer, S. Tapper, P. Lester, B. Wolk, R. Van Reis, Use of the steric mass action model in ion-exchange chromatographic process development, J. Chromatogr. A. 832 (1999) 1–9. doi:10.1016/S0021-9673(98)01002-4.

[9] W.D. Chen, H.H. Hu, Y.D. Wang, Analysis of steric mass-action model for protein adsorption equilibrium onto porous anion-exchange adsorbent, Chem. Eng. Sci. 61 (2006) 7068–7076. doi:10.1016/j.ces.2006.07.036.

[10] C. a Brooks, S.M. Cramer, Steric mass-action ion exchange: Displacement profiles and induced salt gradients, AIChE J. 38 (1992) 1969–1978. doi:10.1002/aic.690381212.

[11] M. Boström, D.R.M. Williams, B.W. Ninham, Specific Ion Effects: Why DLVO Theory Fails for Biology and Colloid Systems, Phys. Rev. Lett. 87 (2001) 168103. doi:10.1103/PhysRevLett.87.168103.

[12] Y. Zhang, P. Cremer, Interactions between macromolecules and ions: the Hofmeister series, Curr. Opin. Chem. Biol. 10 (2006) 658–663. doi:10.1016/j.cbpa.2006.09.020.

[13] E.R.A. Lima, E.C. Biscaia, M. Boström, F.W. Tavares, J.M. Prausnitz, Osmotic Second Virial Coefficients and Phase Diagrams for Aqueous Proteins from a Much-Improved Poisson−Boltzmann Equation †, J. Phys. Chem. C. 111 (2007) 16055–16059. doi:10.1021/jp074807q.

[14] L.A. Moreira, M. Boström, B.W. Ninham, E.C. Biscaia, F.W. Tavares, Effect of the ion-protein dispersion interactions on the protein-surface and protein-protein interactions, J. Braz. Chem. Soc. 18 (2007) 223–230. doi:10.1590/S0103-50532007000100026.

[15] C.M. Roth, A.M. Lenhoff, Electrostatic and van der Waals contributions to protein adsorption: computation of equilibrium constants, Langmuir. 9 (1993) 962–972. doi:10.1021/la00028a015.

[16] Z. Adamczyk, P. Weroński, Application of the DLVO theory for particle deposition problems, Adv. Colloid Interface Sci. 83 (1999) 137–226. doi:10.1016/S0001-8686(99)00009-3.

[17] B. Jönsson, J. Ståhlberg, The electrostatic interaction between a charged sphere and an oppositely charged planar surface and its application to protein adsorption, Colloids Surfaces B Biointerfaces. 14 (1999) 67–75. doi:10.1016/S0927-7765(99)00025-9.

[18] J. Ståhlberg, B. Jönsson, C. Horváth, Theory for electrostatic interaction chromatography of proteins., Anal. Chem. 63 (1991) 1867–74. doi:10.1021/ac00017a036.

[19] L.A. Moreira, M. Boström, B.W. Ninham, E.C. Biscaia, F.W. Tavares, Hofmeister effects: Why protein charge, pH titration and protein precipitation depend on the choice of background salt solution, Colloids Surfaces A Physicochem. Eng. Asp. 282-283 (2006) 457–463.

doi:10.1016/j.colsurfa.2005.11.021.

[20] P. Moon, D.E. Spencer, Field Theory Handbook, Springer Berlin Heidelberg, Berlin, Heidelberg, 1961. doi:10.1007/978-3-642-53060-9.

[21] J.A. Asenjo, B.A. Andrews, Protein purification using chromatography: selection of type, modelling and optimization of operating conditions, J. Mol. Recognit. 22 (2009) 65–76. doi:10.1002/jmr.898.

[22] E.R.A. Lima, E.C. Biscaia, M. Boström, F.W. Tavares, Ion-Specific Forces between a Colloidal Nanoprobe and a Charged Surface, Langmuir. 23 (2007) 7456–7458. doi:10.1021/la700690g.

[23] E.R.A. Lima, F.W. Tavares, E.C.J. Biscaia, Finite volume solution of the modified Poisson-Boltzmann equation for two colloidal particles., Phys. Chem. Chem. Phys. 9 (2007) 3174–3180. doi:10.1039/b701170a.

[24] F.W. Tavares, D. Bratko, H.W. Blanch, J.M. Prausnitz, Ion-Specific Effects in the Colloid−Colloid or Protein−Protein Potential of Mean Force: Role of Salt−Macroion van der Waals Interactions, J. Phys. Chem. B. 108 (2004) 9228–9235. doi:10.1021/jp037809t.

[25] J. Stankovich, S.L. Carnie, Electrical Double Layer Interaction between Dissimilar Spherical Colloidal Particles and between a Sphere and a Plate: Nonlinear Poisson−Boltzmann Theory, Langmuir. 12 (1996) 1453–1461. doi:10.1021/la950384k.

[26] S.L. Carnie, D.Y.C. Chan, J. Stankovich, Computation of Forces between Spherical Colloidal Particles: Nonlinear Possion-Boltzman Theory, J. Colloid Interface Sci. 165 (1994) 116–128. doi:10.1006/jcis.1994.1212.

[27] V.A. Parsegian, Van der Waals Forces, Cambridge University Press, Cambridge, 2005. doi:10.1017/CBO9780511614606.

[28] L. Ehrl, Z. Jia, H. Wu, M. Lattuada, M. Soos, M. Morbidelli, Role of counterion association in colloidal stability, Langmuir. 25 (2009) 2696–2702. doi:10.1021/la803445y.

[29] J.M. Scheer, W. Sandoval, J.M. Elliott, L. Shao, E. Luis, S.-C. Lewin-Koh, G. Schaefer, R. Vandlen, Reorienting the Fab Domains of Trastuzumab Results in

Potent HER2 Activators, PLoS One. 7 (2012) e51817. doi:10.1371/journal.pone.0051817.

[30] H. Wen, J. Hao, S.K. Li, Characterization of Human Sclera Barrier Properties for Transscleral Delivery of Bevacizumab and Ranibizumab, J. Pharm. Sci. 102 (2013) 892–903. doi:10.1002/jps.23387.

[31] B. Guélat, L. Delegrange, P. Valax, M. Morbidelli, Model-based prediction of monoclonal antibody retention in ion-exchange chromatography, J. Chromatogr. A. 1298 (2013) 17–25. doi:10.1016/j.chroma.2013.04.048.

[32] J.-Y. Lee, I. Han, A Semi-empirical Equation for Activity Coefficients of Ions with One Parameter, Bull. Korean Chem. Soc. 34 (2013) 3709–3714. doi:10.5012/bkcs.2013.34.12.3709.